ISSN 2507-9174

De La Salle University

Journal of Computational Innovations and Engineering Applications

Vol. 2 No. 1

July 2017

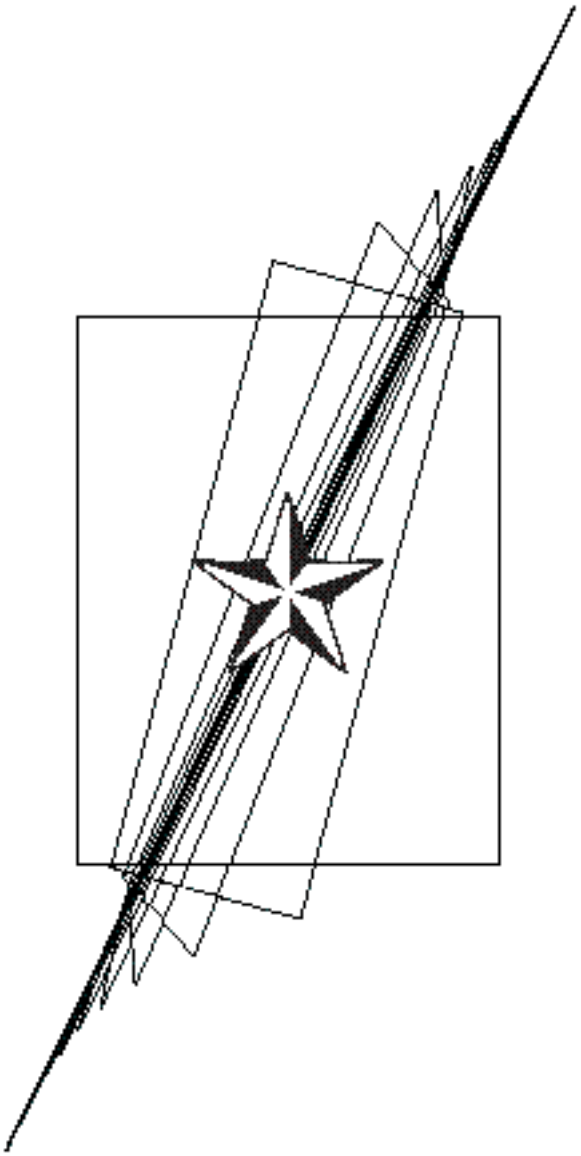

JOURNAL OF COMPUTATIONAL INNOVATIONS AND ENGINEERING APPLICATIONS

Volume 2 Number 1
JULY 2017

The **Journal of Computational Innovations and Engineering Applications (JCIEA)** is a peer-reviewed, open access journal of De La Salle University, Manila. The JCIEA aims to promote the development of new and creative ideas on the use of technology in solving different problems in different fields of our daily lives. The JCIEA solicits high quality papers containing original contributions in all areas of theory and applications of Engineering and Computing including but not limited to: Computational Applications, Computational Intelligence, Electronics and Information and Communications Technology (ICT), Manufacturing Engineering, Energy and Environment, Robotics, Control and Automation, and all their related fields. The JCIEA editorial board is comprised of experts from around the world who are proactively pushing for the development of research in these fields.

Annual Subscription Rates: Foreign libraries and institutions: US$60 (airmail). Individuals: US$50 (airmail). Philippine domestic subscription rates for libraries and institutions: Php1,800, individuals: Php1,300. Please contact Ms. Joanne Castañares for subscription details: telefax: (632) 523-4281, e-mail: dlsupublishinghouse@dlsu.edu.ph

ISSN 2507-9174

Published by De La Salle University Publishing House
2401 Taft Avenue, Manila 0922 Philippines
Telephone: (63 2) 523-4281 / 524-2611 loc 271
Fax: (63 2) 523-4281
Email: dlsupublishinghouse@dlsu.edu.ph
Website: http://www.dlsu.edu.ph/offices/publishing-house/journals.asp
http://www.jciea.com

The De La Salle University Publishing House is the publications office of De La Salle University, Manila, Philippines.

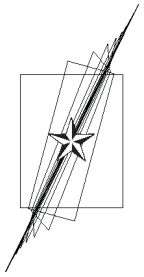

JOURNAL OF COMPUTATIONAL INNOVATIONS AND ENGINEERING APPLICATIONS

Table of Contents

From the Editor

The *Journal of Computational Innovations and Engineering Applications* (JCIEA) is a peer-reviewed and abstracted journal published twice a year by De La Salle University, Manila, Philippines. JCIEA aims to promote and facilitate the dissemination of quality research outputs that can push for the growth of the nation's research productivity. In its second volume first issue, six articles were selected to provide valuable references for researchers and practitioners in the field of environmental engineering, microalgal cultivation for food, pharmaceuticals, and fuel source, aeronautical engineering and design, swarm and computational intelligence, and self-adaptive systems for network performance optimization.

The first article is "*A Survey on Management of Upstream Land Use and its Impact on Downstream Water Quality Parameters*." This paper introduces the various upstream land use activities that are major contributors of downstream water pollution. The proposed measures to reduce the pollution of downstream water bodies such as sustainable agricultural activities, systematic land allocation and managemenat are discussed in the paper. It presents the analysis of upstream land use against the water quality parameters measured at different water management facilities to identify the most significant land use factors for optimization.

The second article is "*Foraging Behaviors – Pheromone, Task Allocation, and Trophallaxis - A Relative Comparison for Robotic Swarm Foraging*." A group of algorithms enhancing such collective behavior is inspired by the animals working together as a group such as ants, bees, and etc. In connection, swarm is defined as a set of two or more independent homogenous or heterogeneous agents acting upon a common environment in a coherent fashion which generates emergent behavior. The development of artificial swarms or robotic swarms has attracted a lot of researchers in the last two decades including pheromone, trophallaxis and task allocation algorithms. However, among these swarm based algorithms, the most efficient in terms of group performance, efficiency and interference in collecting the dusts or objects in an environment with variable terrains. With this, the researchers see the need to develop a swarm simulation platform that would compare the swarm- behavior-based algorithms for an ideal use of robots in different environments in dust collection.

The third article is "*Lift Enhancement of the LRN 1015 Airfoil using a Gurney Flap: A Computational Fluid Dynamics Investigation*." A Gurney flap is a small tab installed at the trailing edge of a wing to enhance the lift of an airfoil. The LRN 1015 airfoil has a high lift-to-drag ratio but is not considered to be a high-lift airfoil. If its lift is improved, additional benefits such as reduced take-off and landing roll, reduced stalling velocity, and increased payload capacity, among others, can be gained. In this light, the effects of the integration of the flap into the airfoil were investigated using a computational fluid dynamics approach. Part of this study is the

validation of the computational fluid dynamics model used through investigation of the unflapped airfoil using ANSYS CFX with a Shear Stress Transport *k*-ω turbulence model, and comparison of the results with wind tunnel data.

The fourth article, "*Development of a microalgal automated cultivation system on Tetradesmus obliquus*," proposed an automated monitoring system for a closed microalgae photobioreactor. Microalgae have been a potential source of food, cosmetics, pharmaceutical, and fuel. However, monitoring the growth parameters of microalgae such as the pH level, salinity, dissolved oxygen, and its color density over time has not yet been achieved in previous studies. The set-up includes a vision system to monitor the changes in the color of the solution, corresponding to the population growth of the microalgae cells. Optical density readings are also done to characterize the growth of the microalgae organisms to serve as a benchmark for the experiment results. The system is employed and tested on *Tetradesmus obliquus* (Turpin) M.J.Wynne species, also known as [syn. *Scenedesmus obliquus* (Turpin) Kützing].

The fifth article, "*Portable Water Purification System using Electrodialysis Reversal*," discussed the development of a water purification system using electrodialysis reversal that can be carried in remote or rural areas and can be powered either by AC supply or solar energy. This system provides an easy way to treat brackish water by using electrodes and current to mitigate the impurities, including the bacteria present in the contaminated water. Three (3) microbiological tests are performed to determine the quality of water produced namely: fecal coliform, total coliform test and heterotrophic plate count test. Through a series of experiments with the support of an accredited Department of Health (DOH) water testing laboratory, it is proven that an hour of treatment is enough to produce five (5) gallons of potable water.

The sixth article is "*Self-Adaptive WLAN Access Point for Optimizing Network Performance Using Multi-Objective Genetic Algorithm (MOGA)*." The current deployment of WLAN access points (AP) require manual configuration of wireless parameters. Wireless parameters are commonly set haphazardly without being aware of the basic wireless conditions. This paper proposes a self-adaptive AP based on genetic algorithms (GA). The AP adapts to interference and link quality of client stations. Interference is mitigated and client link quality is improved or optimized. A chromosome consists of genes of parameters such as frequency channel, channel width, maximum data rate, maximum transmit power, and guard interval. Often competing objectives such as mitigating interference, maximizing the data rate, and minimizing the error rates necessitate that the GA be multi-objective. The MOGA comes up with the fittest candidates by running them through a fitness function which scores the genes based on the survey scan of other interferer AP and the wireless performance statistics of client devices. The GA's chosen configuration is applied and its effect is continuously assessed.

The JCIEA editorial board expresses their warmest thanks and deepest gratitude to the distinguished authors for their outstanding contribution to JCIEA second volume first issue. They likewise express profound appreciation to the peer reviewers for their assistance and cooperation.

Original research outputs are most welcome to JCIEA. There is no publication fee in this journal, and the research papers are assured of fair and fast peer review process. For further information, please visit www.dlsu.edu.ph/offices/publishinghouse/journals.asp. and www.jciea.com

Prof. Elmer P. Dadios, PhD
Editor-in-Chief, JCIEA

A Survey on Management of Upstream Land Use and its Impact on Downstream Water Quality Parameters

Wada Patella, Rodrigo S. Jamisola Jr., Moathodi W. Letshwenyo, and Analene Montesines Nagayo

***Abstract*—This paper introduces the various upstream land use activities that are major contributors of downstream water pollution. The proposed measures to reduce the pollution of downstream water bodies such as sustainable agricultural activities, systematic land allocation and management are discussed in the paper. It presents the analysis of upstream land use against the water quality parameters measured at different water management facilities to identify the most significant land use factors for optimization. Recommendations on how to optimize land use allocation and formulate policies for the purpose of protecting downstream water bodies, as well as reducing the cost associated with water purification, are mentioned.**

Keywords: **land management; water pollution; upstream activities; downstream catchment, agricultural sustainability**

I. Introduction

ANTHROPOGENIC activities are the principal threat to river water quality [1]. Without well-established management policies on land use, upstream human activities will continue to cause the deterioration of downstream water quality. Thus, it is necessary to improve the way people utilize and manage land use activities for the preservation of downstream water quality. Studies on technical interventions and policy formulation are continually being explored in an effort to reduce the pollution of water sources. [2] proposed acceleration of policy and institutional reforms to rescue the water pollution resulting from industrial activity in China. This is supported by another study [3] in which they identified policy formulation as one way of supporting the available environmental laws towards reducing water pollution from anthropogenic activities. On the technical side, the benefit of having adequate infrastructure to scale down the land use-related impacts on the downstream water quality has particularly been realised in Germany and Europe. During the last three decades fo r example, the chemical quality of many watercourses improved because of development and enhancement of sewage treatment systems [4].

There is a positive correlation between water quality and land use, land cover and type, and intensity of use [5] [6] [7] [8] [9]. For example, [10] and [8] stated that surface water quality deterioration is highly correlated with poor human practices and vegetation cover degradation. The rate at which land use dynamics are changing therefore requires proper land management and proactive land allocation planning in order to minimize the associated downstream pollution. Available literature focuses mainly on lack of policies, urbanization, poor planning, industrialization and agriculture as the leading contributors to water quality deterioration. These are discussed in the following sub-sections:

A. Policies

The lack of policies or the inadequacy of their implementation are some well-known factors that are stifling the efforts aimed towards water quality

Wada Patella and Moathodi W. Letshwenyo are affiliated with Department of Civil and Environmental Engineering, Botswana International University of Science and Technology, Palapye, Botswana. (e-mail: patellaw@biust.ac.bw)

Rodrigo S. Jamisola Jr. is affiliated with Department of Mechanical, Energy and Industrial Engineering, Botswana International University of Science and Technology, Palapye, Botswana. (e-mail: jamisolar@biust.ac.bw)

Analene Montesines Nagayo is affiliated with Department of Mechanical, Energy and Industrial Engineering, Botswana International University of Science and Technology, Palapye, Botswana; Electrical and Electronics Section, Department of Engineering, Al Musanna College of Technology, Muladdah, Sultanate of Oman (e-mail: Analene@act.edu.om)

preservation. These resulted to the introduction of regulations aimed at protecting natural water resources [11]. In Europe, there are some documented policies that have been implemented for the preservation of water quality. Some examples are the Dutch nutrient policies for agriculture which came as a result of European environmental directives. The objective of the Nitrates Directive is to reduce water pollution resulting from agricultural activities [12]. Its implementation decreased nutrient surpluses and improved downstream water quality [13].The National Emission Ceilings Directive also resulted in the reduction of ammonia emissions, with downstream benefits of the water sources. The adoption and implementation of relevant policies could therefore benefit the downstream water sources.

B. Urbanization

In 1960, 23% of the Ghanaian population live in urban areas, which increased to about 51% in 2010 as a result of urbanization [14]. This resulted in an uncontrolled conversion of land from agricultural to residential use. Compared to Botswana, a similar trend on rural to urban migration is observed, but at a much higher rate. For the years 1971, 1981, 1991, 2001 and 2011, percentage urban population increased from 9%, 17.7%, 45.7%, 54.2% and 64.1% of the total population, respectively [15]. These values are higher than the world average population that are living in urban areas which was estimated to be 54% of the total population in 2014 [16]. [2] concluded that both population increase and industrial development in the 1950s and 1980s respectively have increased water demand despite the limited available sources. It is also found that such changes always result in high food demand and hence, more agricultural land requirements, resulting in downstream water pollution.

Some effects of urbanization on the water quality include sedimentation transport into water bodies. Altering the drainage patterns and expansion of impermeable cover through roads and pavements increases the amount of runoff, which in turn accelerates soil erosion [17]. The response to rural-urban migration is an increase in construction activities. Construction sites are known sources of water pollution [18]. From construction sites, sediments are the largest water pollutant, and they account for 10% of the sediment load to water bodies in the US [19].

C. Land Allocation and Planning

Improper land use planning and allocation accelerates non-point source pollution [20] [21]. In Ghana, traditional authorities play a lead role in the land allocation and planning process [14]. Given the challenges associated with this type of planning, poor sanitation can be expected, and hence pollution of neighbouring water sources is anticipated. To prevent this from happening, land authorities need to take the lead in land allocation and planning [22]. This can be achieved by using scientifically tested and accepted practices. These include, but are not limited to, reduction of overgrazing, overstocking, and zoning [23]. [24] observed that rational land use and its distribution can improve the consumption of water resources. This consequently reduces the chances of downstream water pollution. In an effort to minimise mismanagement of land and the associated downstream pollution effects, land allocation models have been developed to help address land allocation problems in different sectors of the economy [24]. Some sectors that have benefited from these models include agriculture and transportation [25] [26] [27].

D. Industrialization

Industrialization has been found to play a significant role in contributing to water pollution through the discharge of highly polluted wastewaters [28]. In one study [29], it was proven that industrialization has resulted in the increase of heavy metal addition into the pedoshere. A study by [30] identifies paper industry as one area that has not been significantly studied, particularly the chemical constituents of the effluent. Given the pollution potential of similar industries, and the reported chemical usage, more studies need to be conducted to quantify their contribution to downstream environments.

[2] identified the scale, intensity and speed of industrialization as one factor that led to the acceleration of water quality deterioration in China. Also identified in the study is the type of raw material and technology used in industrial processes that has a bearing on the pollution impacts downstream. In studies that seek to identify a relationship between urban land use and downstream water quality, authors found a positive correlation between the two. A study by [7] discovered out that industrial land use is next in the line after urbanization with respect to the deterioration of downstream water quality. With industrial land use, the impacts were significant within

a 100m buffer, beyond which the impact on water quality decreased [7].

E. Agriculture

Even though there are some agricultural activities that can improve water quality, the effect is far less than the rate at which it causes pollution to the downstream water sources. Most studies conclude that agricultural activities are very common non-point pollution sources [7] [31], mainly due to nutrient losses into water bodies [32]. In England and Wales, agriculture is the main source of fine sediment loss into watersheds [33]. Similarly, sediments are listed as the most common pollutant of water bodies in the United States [34], which originate from agriculture-related sources [35] [36]. With this, efforts are made through the implementation of policies aimed at reducing pollution from agricultural activities. One of the legislative policies aimed at reducing nitrogen emissions from agriculture is the Nitrates Directive [37].

II. Land use activities and their parameters

Figure 1 is a pictorial representation of some common land use activities that contribute to downstream water pollution. The different land use activities in Figure 1 have specific water quality parameters that add to the receiving water bodies. The effect of each parameter on the downstream water quality varies in magnitude and significance. Table I summarizes the land use activities, the associated parameters, as well as their respective impacts on downstream water quality.

Table I showed that even though natural activities have a contribution to water quality degradation, anthropogenic activities are dominant, and vary in complexity. Water sources that are related to human activity receive the highest pollution load [42]. Pollutants resulting from each land use activity vary significantly, and are used as water quality parameters. As shown in Table II below, these parameters are classified as physical, chemical or biological [42]. Examples of each parameters are presented in Table II. Their levels in water give an indication of whether the water is safe for consumption or not. If not, water needs to be treated to acceptable standards by reducing them to levels determined by regulatory authorities. Highly polluted water samples may require Advanced Treatment Technologies (ATTs) because conventional treatment methods may be insufficient. However, ATTs are expensive because they are energy intensive.

The most appropriate water purification method can only be determined when the raw water quality is fully understood. The choice of which water quality parameters to check before treatment has a bearing on the treatment efficiency and the quality of the final water. By checking a few parameters before treatment, the final water quality is likely to be compromised.

Fig. 1. Some common land use activities that contribute to downstream water pollution [38]

TABLE I
FINDINGS ON LAND USE ACTIVITIES AND THE CORRESPONDING PARAMETERS WITH RESPECT TO WATER QUALITY

Land use activity	Land use parameter	Findings	Reference (s)
Agriculture	Stocking rate	Stocking rates show a correlation in total phosphorus, ammonium and total nitrogen.	Buck et al. (2004) [5]
	Land cover/ vegetation	Watersheds with higher vegetation cover have lower turbidity. High pasture cover results in higher values of electrical conductivity (EC) and Total Nitrogen concentrations.	Gu et al. (2008) [6]; Moschini et al. (2016) [9]; Rickson (2014) [39]
	Amount of fertiliser used	Agriculture is the largest source (15% contribution) of Nitrogen in the atmosphere. Approximately 23% of it applied in watersheds is lost to river flow.	Schlesinger (2008) [40]; Billen et al. (2002) [41]
	Area of agricultural use	There is positive correlation between area cultivated and downstream pollutants	Buck et al. (2004) [5]; Meneses et al (2015) [8]
Industrialization	Distance of industrial land to water body	When distance from industrial land use increases, the correlation between water quality and industrial land use decreases.	Lin et al. (2015) [7]
	Type of industry	Effluent depends on the raw materials and technical production steps.	Bosowski et al. (2015) [30]
Urbanization	Area of urbanization	A larger area of activity increases the pollution potential to water courses.	Meneses et al. (2015) [8]
	Population density	Suspended Particle Matter (SMP), nitrogen and Dissolved Phosphorus increase with population.	Gu et al. (2008) [6]
	Availability & Effectiveness of WWTP	Addition of a WWTP elevates the Nitrogen levels in receiving water bodies downstream.	Ahearn et al. (2005) [10]

TABLE II
COMMON WATER QUALITY PARAMETERS [42]

Physical	Chemical		Biological
	Inorganic	Organic	
Colour	Ammonia	Total Organic Carbon	Total Coliform
Turbidity	Calcium	Total trihalomethanes	E-coli
Dissolved Solids	Chloride	Phenols	Thermotolerant (faecal) Coliform bacteria
Odour	Chlorine Residual	Chloroform	Faecal streptococci
Conductivity	Fluoride	Aldrin	Clostrodium perfringens
pH	Magnesium	Dieldrin	Cryptosporidium
Taste	Nitrate	Chlordane	Giardia
Temperature	Nitrite	DDT	
	Potassium	Endrin	
	Sodium	Heptachlor	
	Sulfate	Heptachlor epoxide	
	Zinc	Methoxychlor	
	etc	etc	

III. Key water quality parameters and their sources

A. Turbidity

Turbidity is a measure of the extent to which water loses its transparency as a result of the presence of suspended particles in it [44]. It is the most widely used parameter for monitoring the quality of treated water and evaluating the effectiveness of treatment process; it is used in almost all WTWs because of its low cost and easy application [45]. The suspended particles' adsorptive properties make turbidity a significant parameter to monitor because they harbour bacteria, viruses, parasites and other toxic organic compounds. [46] reports that turbidity is a suitable performance indicator for online monitoring of membrane treatment facilities' performance since it is easy to detect in a case of physical membrane damage, indicating that not only is turbidity a nuisance, but also helps in system efficiency monitoring.

Agricultural activity increases soil erosion, resulting in turbidity changes in rivers [47]. During rainy seasons, the loose top soil is transported into the main rivers through tributaries. [47] found that water turbidity is low in less turbulent waters. This is supported by studies by [48] [49] [50] which mentioned that seasons characterised by wave actions, coastal currents, and mixing-stratification of water column results in re-suspension of sediments, due to its high water turbidity. The re-suspension phenomenon of particles is explained using Stoke's Law of equilibrium, which gives the relationship between particle size and fluid turbulence as shown below [51];

$$Re_f = w_s d/\mu \quad (1)$$

where:

w_s – the fall velocity

Re_f – Reynolds number

d – particle diameter

μ – kinematic viscosity of water

Based on Equation 1, when all parameters remain constant, it requires a larger particle to settle for high velocities, thus, resulting in high Re_f values. This is consistent with settling velocities for different soil particle sizes shown in Table III.

TABLE III
Settling Velocity of Particles as a Function of Particle Size [52]

Particle size (μm)	Settling velocity $*10^{-3}$(m/h)
1000	600000
100	2000
10	300
1	3
0.1	0.01
0.01	0.0002

From Table III, settling velocity is observed to decrease with particle size. Therefore, this suggests that the type of soil on which agricultural activities are carried also determines the extent of turbidity in a downstream body of water. For a soil whose composition is predominantly clay, the water is likely to be more turbid because it consists mainly of fine particles which get re-suspended easily than sandy soils whose particles would settle in lower turbulent conditions. If the downstream water will be used for fish pond culture or in aquaculture system, the desirable range of turbidity is 30-80 cm for optimal fish growth [53].

B. pH

The pH of water is a measure of the acid-base equilibrium and in most natural waters, is controlled by the carbon dioxide –bicarbonate-carbonate equilibrium system [54]. Most dams are basic (alkaline) when they are newly constructed, and become acidic with time due to the build-up of carbon dioxide (CO_2) as organic material decompose. An increased CO_2 concentration lowers pH due to the formation of carbonic acid [55], whereas its decrease will cause pH to rise [54]. Temperature will affect this equilibrium [54]. pH has corrosive effects on water conveyance structures. It also has effects on human health such as eye irritation and exacerbation of skin disorders at pH levels greater than 11 [54]. Below pH 4, redness and irritation of eyes have also been reported [54]. The above dynamics on pH therefore spell out the importance of its quantification before and after water purification.

If the downstream water will be used for cultivating plants, its pH level should range from 5.5 to 7.5. If the pH of water is not within the acceptable range, plants experience nutrient deficiencies [56] [57]. For fish pond culture, the pH level of downstream water

to be used should range from 6.0 to 9.0 to ensure fish growth [58] [59].

C. Temperature

Water temperature is a function of both natural and artificial activities. It is an important parameter because it affects the rate of bacterial activity in water, oxygen solubility, as well as the rate of gas exchange between the water body and the environment [60]. Temperature affects the efficiency of some treatment processes as it determines the chemical dissolution and reaction rates [60]. Treatment of water in winter requires more chemicals for efficient coagulation and flocculation than in summer [60]. This means that with respect to coagulants and flocculants, it is cheaper to purify warm water. On the other hand, warm water has also been found to increase chlorine demand because of increased reactivity and increased levels of algae and other organic matter in water [60]. Even though this parameter is not commonly used for water quality evaluation, it is very important when optimization assessments are to be made on a water purification system. Therefore, an optimum temperature ought to be determined to balance the coagulant/flocculant costs with the chlorine-related costs. If the downstream water will be used in aquaculture set-up, the acceptable values of water temperature for optimal fish growth is 16^{o}C to 33^{o}C [61] [57].

D. Nitrates

Agriculture, industrial activities, and urban development have increased nitrogen discharge in the natural water bodies over the years. Water contamination by nitrates is thus one of the most widespread threats that needs to be dealt with [62] [63]. A study by [40] which trace the fate of anthropogenic nitrogen estimates that about 150Tg ($150*10^{12}$ g) of anthropogenic nitrogen is produced annually, and about 23% of it is lost to river flow. Increased nutrient fluxes cause eutrophication, hypoxia and acidification of water bodies [64]. In their attempt to track different nitrate sources, [65] [66] recommended establishment of policies aimed at reducing the introduction of pollutants in the environment. In many countries such policies exist, but their implementation is ineffective.

Like many other pollutants, sources of nitrates in water are both natural and anthropogenic. In surface waters, they originate from natural nitrification of soil organic matter, with additional concentrations from such anthropogenic activities as wastewater discharges [64]. The breakdown of organic matter first forms ammonia, then nitrites, and finally nitrates, suggesting that a laboratory test of ammonia gives an indication of the nitrate levels in water. In groundwaters, nitrate sources are mainly nitrification of soil organic matter, and to a lesser extent, manure and septic systems [64]. Agricultural activities, such as application of nitrogen-containing fertilisers, have also been found to increase nitrate levels in water sources [5] [67]. For aquaculture activities, the acceptable range of downstream water to be used is from 0.1 to 4.5 mg/L to ensure fish growth and survival [53].

E. Chemical Pollutants-Organics

Decaying leaves, trees and weeds are the principal natural sources of organic matter in water. Anthropogenic sources include industrial compounds such as pesticides [68] [60]. The presence of organic matter causes colour, taste and odour problems in water [60]. It can also contribute to the formation of halogenated compounds when water is disinfected using chlorine [60]. The presence of organic matter in water attracts microbes. As they metabolize the organic material, they consume oxygen and eventually deplete the available oxygen [69] [60]. Other sources of organic contaminants are summarized in Table IV.

TABLE IV
Summary of Some Sources of Organic Water Pollutants [60]

Contaminant	**Sources**
Benzene	Industrial chemicals, paints, plastics, pesticides
Toluene	Industrial solvent
Vinyl Chlorine	PVC pipe
Xylene	Gasoline production, paint ink, detergent
Endrin	Insecticides
Lindane	Insecticides
Pentachlorophenol	Wood preservative
Total trihalomethanes (TTHMs)	Chloroform, drinking water chlorination by-product.

From Table IV, both industrial and agricultural activities are found to directly or indirectly contribute to the addition of organic pollutants in watersheds. For example, the furniture manufacturing process is an industrial activity which uses wood as a raw material. Wood is a product of agricultural activity, which in addition to being a source of organic matter in water, is a source of such other pollutants as nitrates.

Based on Table 4, the most common source of organic contaminants is industrial activity. Properly implemented regulatory policies could reduce downstream pollution of water bodies. An immediate method of managing the point source pollutants is pre-treatment of effluent before discharge. However, distributed sources are difficult to measure and manage because they are spread over a large area.

F. Chemical Pollutants- Inorganics

The inorganic load of water is affected by effluent discharges and geologic conditions and formations [60]. Natural water also dissolves rocks and minerals, which also increase the inorganics load in water [60]. Anthropogenic activities include pesticides, industrial waste, paint, etc. [60] which find their way into water bodies through various transportation media. Table V shows some common sources of the inorganic contaminants. It also confirms that industrial activity is also the leading source of inorganic pollutant sources. The downstream effects of pollutants can be reduced by appropriate management methods which include pre-treatment of effluent before discharge or any other suitable method determined by various operations. In Botswana, a notable advancement with respect to industrial waste discharge is the Trade Effluent Agreement entered into by industrial operators and the principal wastewater authority, which is the Water Utilities Corporation (WUC). In this agreement, WUC and affected industries set the limits of inorganic pollutants to be discharged into wastewater system. The discharging entities keep records of the effluent quality, and ensure that the agreed limits are not exceeded. This arrangement is important because it reduces the pollutant load downstream, thereby improving secondary effluent treatment efficiency.

TABLE V
Summary of Sources of Some Common Inorganic Contaminants [60]

Contaminant	Sources
Nitrate	Sewage, fertilisers, soil and mineral deposits
Fluoride	Geological deposits, drinking water additive, aluminium industries
Copper	Corrosion of household plumbing, natural deposits, wood preservatives
Lead	Corrosion of lead service lines and fixtures
Arsenic	Industrial waste, Geological, pesticide residues, smelter operations
Mercury	Industrial manufacturing, natural deposits, fungicides

G. Biological Pollutants-Bacteria

The process of testing individual pathogens takes time, and the associated costs are high [60]. Accepted practice is to test for a single species of indicator organism Escherichia coli (E.coli), whose presence in water indicates sewage contamination [70] [60].

E. coli are more prevalent in waters whose turbidity is high. This is because they attach themselves to the sediment particles which happen to be the main constituent of water turbidity. Because E-coli are used to living in the warm environment of human intestines, their counts are higher in warmer waters. On the other hand, sufficient ultraviolet rays of sunlight may kill them, thereby lowering their numbers from expected counts [71].

IV. Methods

Different water sources were identified, and the water quality parameters measured at each of the prior treatment were noted. In Botswana, the source of data was Water Utilities Corporation (WUC), which is the sole water authority tasked with management and operation of potable water sources. For other countries, data was obtained through review of related literature. This data was then used to determine the common water quality parameters, and the most significant ones for discussion.

V. RESULTS

Table VI summarizes the different raw water parameters measured in the respective dams and treatment facilities. The data were obtained from WUC and other related literatures. A tick mark indicates that the water quality parameter is determined before purification at that particular facility.

[46] identified key bulk water quality parameters as those including pH, turbidity, chemical oxygen demand (COD), dissolved organic carbon, and biomass concentrations. These parameters must be determined in raw water samples before treatment. The individual parameters are discussed in detail in Section 4.

VI. DISCUSSIONS

Water quality parameters have been found to be a result of anthropogenic activities, and to a lesser extent, naturally occurring. The prevalent anthropogenic activities are land use-related, while natural dynamics include washing off of minerals from rocks. At high concentrations, the water quality parameters become undesirable, and are therefore referred to as pollutants.

Industrial activities have a large contribution towards the addition of pollutants in water. These activities are therefore significant land use parameters affecting downstream reservoir water quality.

With respect to agriculture, many studies focus on sediment concentrations (suspended solids) and nutrients in water bodies from agricultural activities. Sediments are higher in areas of greater agricultural intensity. Their yield can be up to ten times greater in agriculture intensive locations than in catchments of mixed use for a similar storm [72].

Urbanization results in deterioration of downstream water quality [73]. Therefore, when rapid urbanization is anticipated in a locality, effective and efficient waste management facilities must be implemented. The percentage population in urban centres connected to

TABLE VI
WATER QUALITY PARAMETERS MEASURED IN DIFFERENT FACILITIES

Parameter	Facility							
	Shashe Dam*	Lotsane Dam*	Gaborone Dam*	Palapye Water Works*	Lake Mead	Hoover Dam	Randfontein Municipality**	Johannesburg Metro**
pH	✓	✓	✓	✓	✓	✓	✓	✓
Turbidity	✓	✓	✓	✓			✓	✓
Conductivity	✓	✓	✓	✓	✓	✓	✓	✓
TDS	✓	✓	✓	✓	✓	✓	✓	✓
COD	✓	✓	✓	✓				
Chlorides	✓	✓	✓	✓	✓	✓	✓	✓
Total Coliform	✓	✓	✓	✓				✓
E-coli	✓	✓	✓	✓			✓	✓
Faecal streptococci	✓	✓	✓	✓				
Nitrates	✓	✓	✓	✓	✓	✓	✓	✓
Calcium	✓	✓	✓	✓	✓	✓	✓	✓
Magnesium	✓	✓	✓	✓	✓	✓	✓	✓
Potassium	✓	✓	✓	✓	✓	✓	✓	✓
Sulphate	✓	✓	✓	✓	✓	✓	✓	✓
Silica	✓	✓	✓	✓	✓	✓		
Phosphate	✓	✓	✓	✓	✓	✓		
Mercury	✓	✓	✓	✓				

*Water Utilities Corporation

**Water resource information centre for the Vaal barrage & Vaal Dam catchment forums.

flush toilets for Botswana stood at 47.9% and 64.8% in 2001 and 2011 respectively [74]. This could have been a welcome development if treatment facilities were equally effective in treating the waste to acceptable limits. The low efficiency of such facilities makes them sources of pollutants. In this study, it was found that even though most pollutants are of significant importance given their impact on human health, turbidity stands out as the most significant parameter to monitor since it harbours viruses and bacteria, and on the other hand, it is useful for performance assessment of membrane treatment processes because it can be detected quicker than other pollutants. Other pollutants observed to be of great importance in no particular order are pH, temperature, E-coli, DO, and Nitrates. Comparing the effects of land use activities involves extensive studies on their corresponding downstream pollutants, which is beyond the scope of this paper.

To minimize pollution from agricultural land activities, soil less farming method such as hydroponics and aquaponics are recommended. In aquaponics system, water recycling and waste management are utilized to cultivate plants in hydroponic beds and raise fish in aquaculture tanks [61] [59]. The usage of minimal water exchange, organic fertilizer from fish waste and natural biofilter from plant roots reduce the operating cost of the aquaponics system, making it a cost-effective system [61] [59]. It could also minimize the pollution caused by soil farming activities. In addition to this, the harvested fish and vegetable crops from an aquaponic system are organic, healthy and safe for human consumption [61] [59] [75].

VII. Conclusion

Upstream land use parameters have a contribution to the water quality of downstream water sources. Population density, area and intensity of land use have a positive correlation with downstream pollutant loading. Distance from a pollutant source to the receiving environment has also been found to affect the pollutant concentration; some decompose during transportation, while new compounds are formed as pollutants interact with the environment. Vegetation cover reduces downstream turbidity. Raw materials and industrial technologies also determine the downstream pollution of water bodies. Adoption of best environmental practices and pre-treatment technologies before effluent discharge are proven methods of managing downstream pollution. The next study shall focus on the use of machine learning techniques to optimize land use allocation. A case study on water quality management for sustainable agriculture may be done as a future directive.

References

[1] J. Allan, "Landscapes and riverscapes: The influence of land use and stream ecosystems," *Annual Review of Ecology, Evolution, and Systematics,* vol. 35, pp. 257-284, 2004.

[2] H. Cheng and Y. Hu, "Water pollution during China's industrial transition," *Environmental Development,* vol. 8, pp. 57-73, 2013.

[3] X. Miao, Y. Tang, C. Wong and H. Zang, "The latent causall chain of industrial water pollution in China," vol. 196, pp. 473-477, 2016.

[4] T. Kistemann, A. Rechenburg, E. Rind and C. Schreiber, "The impact of land use on microbial surface water pollution," *Environmental Health,* vol. 218, no. 2, pp. 181-187, 2015.

[5] O. Buck, D. Niyogi and C. Townsend, "Scale-dependence of land use effects on water quality of streams in agricultural catchments," *Environmental Pollution,* vol. 130, pp. 287-299, 2004.

[6] S. Gu, H. Han, S. Li, W. Liu and Q. Zhang, "Water quality in relation to land use and land cover in the upper Han River Basin, China," *Catena,* vol. 75, pp. 216-222, 2008.

[7] L. Lin, Q. Liu, G. Qian, K. Yang and J. Zhao, "Influences of land use on water quality in a reticular river network area: A case study in Shanhai, China," *Landscape and Urban Planning,* vol. 137, pp. 20-29, 2015.

[8] B. M. Meneses, R. Reis, R. Savaira and M. Vale, "Land use and land cover changes in Zezere watershed (Portugal)-Water quality implications," *Science of the Total Environment,* pp. 527-528, 439-447, 2015.

[9] L. Moschini, A. Oliveira, A. Souza and M. Tanaka, "Influence of watershed land use and riparian characteristics on biological indicators of stream water quality in south eastern Brazil," *Agriculture, Ecosystems and Environment,* vol. 219, pp. 333-339, 2016.

[10] D. Ahearm, M. Anderson, R. Dahlgren, J. Johnson, R. Sheibley and K. Tate, "Land use and land cover influence on water quality in the last freeflowing river draining the western Sierra Nevada, California," *Journal of Hydrology,* vol. 313, pp. 234-247, 2005.

[11] X. Flotasts, A. Gil, B. Rebolledo and J. Sanchez, "Assessment of groundwater vulnerability to nitrates from agricultural sources using GIS-compatible logic multicriteria model," *Journal of Environmental Management,* vol. 171, pp. 70-80, 2016.

[12] European Commission, "Directive of the Council of December 12, 1991 concerning the protection of waters against pollution caused by nitrates from agricultural sources," *European Commission, Brussels,* pp. 1-8, 1991.

[13] C. Rougoor, A. Tiktak and H. Van Grinsven, "Evaluation of the Dutch implementation of nitrates directive, the water framework directive and the national emissions ceilings directive," *NJAS-Wageningen Jouranal of Life Sciences,* 2016.

[14] J. Eledi and E. Kuusaana, "Customary land allocation, urbanization and land use planning in Ghana: Implications for food systems in the Wa Municipality," *Land Use Polic,* vol. 48, pp. 454-466, 2015.

[15] Statistics Botswana, "Population and housing census 2011 analytical report," *Statistics Botswana,* 2011.

[16] X. Q. Zhang, "The trends, promises and challenges of urbanization in the world," *Habitat International,* vol. 54, no. 3, pp. 241-252.

[17] D. Nir, "Man, a geomorphological agent: An introduction to anthropic geomorphology," *D Reidel Publishing Company,* 1983.

[18] S. Belayutham, V. Gonzalez and T. Yiu, "The dynamics of proximal and distal factors in construction site water pollution," *Journal of Cleaner Production,* vol. 113, pp. 54-65, 2016.

[19] A. Burton and R. Pitt, Storm water effects handbook: a toolbox for watershed managers, scientists and engineers, USA: Lewis Publishers, 2002.

[20] X. Li and P. Liu, "Embedding sustainable development strategies in agent-based models for use as a planning too," *International Journal of Geographical Information Science,* vol. 22, pp. 21-45, 2008.

[21] Y. Liu, Y. Pan, Z. Yu and P. Zhang, "Land use pattern optimization based on CLUE-S and SWAT models for agricultural non-point source pollution control," *Mathematical and Computer Modelling,* vol. 58, pp. 588-595, 2013.

[22] B. Ai, X. Li, X. Liu and J. Ou, "Combining system dynamics and hybrid particle swarm optimization for land use allocation," *Ecological Modeling,* vol. 257, pp. 11-24, 2013.

[23] X. Li, L. X. P. and Z. Tan, "Zoning farmland protection under spatial constraints by integrating remote sensing, GIS and artifitial immune systems," *International Journal of Geographical Information Science,* vol. 25, pp. 1829-1848, 2011.

[24] M. Fu, W. Fu, J. Tao, J. Zhang and Z. Zhang, "A tradeoff approach of optimal land allocation between socioeconomic development and ecological stability," *Ecological Modeling,* vol. 272, pp. 175-187, 2014.

[25] G. Mendoza, "A mathematical model for generating land use allocation alternatives for agroforestry systems," *Agroforestry Systems,* vol. 5, no. 4, pp. 443-453, 1987.

[26] T. Bannet and T. Svoray, "Urban land use allocation in a Mediterranean ecotone: habitat heterogeneity model incorporated in a GIS using a multi criteria mechanism," *Landscape and Urban Planning,* vol. 72, pp. 337-351, 2005.

[27] A. Vold, "Optimal land use and transport planning for the Greater Oslo area," *Transportation Research Part A,* vol. 39, pp. 548-565, 2005.

[28] A. Basile, A. Cassano and N. Rastogi, "18-Membrane technologies for water treatment and reuse in the food and beverage industrie," *Advances in Membrane Technologies for Water Treatment,* pp. 551-580, 2015.

[29] P. Anmesto, L. Barreiro, A. Delgado, M. Estevez, J. Munoz, E. A. Rodriguez, P. Rodriguez and M. Sanjurjo, "Lithological and land-use based assessment of heavy metal pollution in soils surrounding a cement plant in SW Europ," *Science of the Total Environment,* vol. 562, pp. 179-190, 2016.

[30] S. Bosowski, O. Botalova, D. L., S. Illgut and J. Schwarzbauer, "Identification of characteristic organic contaminants in wastewater from modern paper production sites and subsequent tracing in a river," *Journal of Hazardous Materials,* vol. 300, pp. 254-262, 2015.

[31] G. Siciliano and L. Smith, "A comprehensive review of constraints to improved management of fertilizers in China and mitigation of diffuse water pollution from agriculture," *Agriculture, Ecosystems & Environment,* vol. 209, pp. 15-25, 2015.

[32] D. Norse, "Non-point pollution from crop production: global, regional and national issues," *Pedosphere,* vol. 15, pp. 499-508, 2005.

[33] A. Collins and Y. Zhang, "Exceedance of modern 'background' fine-grained sediment delivery to rivers due to current agricultural land use and uptake of water pollution mitigation options across England and Wales," *Environmental Science & Policy,* vol. 61, pp. 61-73, 2016.

[34] D. Pimentel, "Soil erosion and the threat to food security and the environment," *Ecosystem Health,* vol. 6, no. 4, pp. 221-226, 2000.

[35] C. Anser, C. Barford, G. Bonan, F. Carpenter, M. Chapin, G. Coe, G. Daily, R. DeFries, J. Foley, H. Gibbs, J. Helkowski, T. Holloway, E. Howard, C. Kucharik, J. Monfreda. C.' Patz, I. Prentice, N. Ramankutty and P. Snyder, "Global consequences of land use," *Science,* vol. 22, pp. 570-574, 2005.

[36] A. Ghulam, S. Hartling and Y. Jordan, "Traits of surface water pollution under climate and land use changes: A remote sensing and hydrological modeling approach," *Earth-Science Reviews,* vol. 128, pp. 181-195, 2014.

[37] J. Kros, J. Lesscehn, Z. Miatkowski, O. Oenema, S. Pietrzak, M. Pinto, G. Velthof and J. Webb, "The impact of Nitrates Directive on nitrogen emissions from agriculture in the EU-27 during 2000-2008," *Science of the Total Environment,* pp. 468-469, 1225-1223, 2014.

[38] 3M, "How freshwater becomes polluted," [Online]. Available: http://www.3m.co.uk/intl/uk/3Mworldlywise/geography-river-pollution-3.htm. [Accessed 8 June 2015].

[39] R. Rickson, "Can control of soil erosion mitigate water pollution by sediments?," *Science of the Total Environmen,* pp. 468-469, 1187-1197, 2014.

[40] W. Schlesingher, "On the fate of anthropogenic nitrogen," *Environmental Sciences,* vol. 106, pp. 203-208, 2009.

[41] G. Billen, E. Boyer, N. Breemen, Dam, M. D. N. Eve, C. Goodale, R. Howarth, N. Jaworski, K. Lajtha, B. Mayer, K. Nadelhoffer, K. Paustian and S. Seitzinger, "Where did all the Nitrogen go? Fate of nitrogen inputs to large watersheds in the northeastern U.S.A.," *Biochemistry,* vol. 57/58, pp. 267-293, 2002.

[42] J. Alizadeh and R. Kavianpour, "Development of wavelet-ANN models to predict water quality parameters in Hilo Bay, Pacific Ocean," *Marine Pollution Bulletin,* vol. 98, pp. 171-178, 2015.

[43] Botswana Bureau of Standards, "Drinking water specification," *Botswana Bureau of Standards,* 2009.

[44] H. Cao, Y. Cao, H. Gui, J. Liu, L. Lu, H. Wang, Y. Yang and H. You, "The design of rapid turbidity measurement system based on single photon detection techniques," *Optics & Laser technology,* vol. 73, pp. 44-49, 2015.

[45] T. Chen, J. Nan and M. Yao, "Effect of particle size distribution on turbidity under various water quality levels during flocculation processes," *Desalination,* vol. 354, pp. 116-124, 2014.

[46] A. Branch, G. Carvajal, H. Coleman, J. Drewes, S. Khan, P. Le-Clech, R. Stuetz and T. Trinh, "Hazardous events in membrane bioreactors- Part 1: Impacts on key operational and bulk water quality parameters.," 2015.

[47] S. Cambell, R. Marchant, D. Reading, J. Ridd and P. Ridd, "A drifter for measuring water turbidity in rivers and coastal oceans," *Marine Pollution Bulletin,* vol. 91, pp. 102-106, 2015.

[48] G. Allen, P. Bassoullet, C. De Grandpre and Y. Du Penhoat, "Effects of tides on mixing and suspended sediment transport in macrotidal estuaries," *Sediment Geol.,* vol. 26, pp. 69-90, 1980.

[49] N. Bi, A. Wang, H. Wang, H. Xiao and X. Zeng, "Seasonal distribution of suspended sediment in the Bohai Sea, China," *Continental Shelf Research,* vol. 90, pp. 17-32, 2014.

[50] H. Chiang, C. Lee and Y. Lee, "Adrupt state change of river water quality (turbidity): Effect of extreme rainfalls and typhoons," *Science of the Total Environment,* pp. 557-558, 91-101, 2016.

[51] T. Aras and S. Tigrek, Reservoir Sediment Management, London, UK: Taylor & Francis Group, 2012.

[52] N. Gray, Water Technology, Oxford, U: Elsevier Ltd, 2010.

[53] A. Bhatnagar and P. Devi, "Water Quality Guidelines for the Management of Pond Fish Culture," *International Journal of Environmental Sciences,* vol. 3, no. 6, pp. 1980-2009, 2013.

[54] World Health Organization, "pH in drinking water," World Health Organization, Switzerland, 2003.

[55] Central Statistics Office Botswana, "Botswana Water Statistics," Gaborone, Botswana, 2009.

[56] Somerville, C; et al., "Small-scale Aquaponic food production: Integrated fish and plant farming," FAO technical technical paper no. 589, FAO, Rome, 2014.

[57] A. M. Nagayo, E. Vega, C. Mendoza, R. S. Al Izki and R. Jamisola, "An Automated Solar-Powered Aquaponics System towards Agricultural Sustainability in the Sultanate of Oman," *2017 IEEE International Conference on Smart Grid and Smart Cities, Singapore, July 23-26, 2017,* p. [submitted for publication], 2017.

[58] J. Buttner, R. Soderberg and D. E. Terlizzi, "An Introduction to Water Chemistry in Freshwater Aquaculture," *NRAC Fact Sheet No. 170-1993,* pp. 1-4, 1993.

[59] A. Nagayo, R. Al Yahmadi and E. Gonzalez, "Work in Progress: A Smart Solar-Powered Aquaponics Greenhouse System to Promote Sustainable Agriculture to Engineering Students," *The 47th Frontier in Educ. Conf., Indianapolis, Indiana, USA, October 18-21, 2017,* p. [submitted for publication], 2017.

[60] J. E. Drinan and F. Spellman, "Water and wastewater treatment," Taylor & Francis Group, New York, USA, 2013.

[61] A. Nagayo and R. Jamisola, "Cloud-based Wireless Monitoring System and Control of a Smart SolarPowered Aquaponics Greenhouse to promote Sustainable Agriculture and Fishery in an Arid Region," *BIUST Research and Innovation Forum 2017, Palapye, Botswana,* pp. 144-151, 2017.

[62] A. Andres, J. Gilliam, J. Karr and W. Showers, "Tracing nitrate transport and environmental impact from intensive swine farming using delta nitrogen-15," *Journal of Environmental Quality,* vol. 30, pp. 1163-1175, 2001.

[63] T. Addiscott and N. Benjamin, "Nitrate and human health. Soil Use Management, 20," pp. 98-104, 2004.

[64] L. Harker, I. Hutcheon and B. Mayer, "Use of major ion and stable isotope geochemistry to delineate natural and anthropogenic sources of nitrate and sulfate in the Kettle River Basin, British Columbia, Canada," *Comptes Rendus Geoscience,* 2015.

[65] L. Cong-Qiang, Y. Fu-Jun, H. Jian, L. Si-Liang and Z. Zhi-Qi, "Using dual isotopes to evaluate sources and transformation of nitrogen in the Liao River, northeast China," *Applied Geochemistry,* vol. 36, pp. 1-9, 2013.

[66] J. Hu, S. Li and F. Yue, "The distribution of nitrate sources in Liao Rivers, China, based on isotopic fractionation and Bayesian mixing model," *Procedia Earth and Planetary Scienc,* vol. 13, pp. 16-20, 2015.

[67] P. Athanasopoulos, "Using stable isotopes to develop a regional hydrogeological model and characterise nitrate sources in groundwater (MSc Thesis)," *Department of Geological Sciences, University of Saskatchewan,Saskatoon, Saskatchewan,* 2009.

[68] A. Botero-Coy, M. Bustos-Lopez, R. Diaz, C. Fuentes, F. Hernandez, M. Inabez, G. Penuela and T. Portoles, "Use of time-of-flight mass spectrometry for large screening of large organic pollutants in surface waters and soils from rice production area in Colombia," *Science of the Total Environment,* vol. 439, pp. 249-259, 2012.

[69] J. Lin, S. Liu, Y. Wu, J. Zhang and Z. Zhu, "Hypoxia off the Changing (Yangtze River) Estuary: Oxygen depletion and organic matter decomposition," *Marine Chemistry,* vol. 125, pp. 108-116, 2011.

[70] Minnesota Pollution Control Agency, "Bacteria: Sources, types, impact on water quality- A general overview," 2008.

[71] U. S. d. o. Agriculture, "Chapter 2: Bacteria and water quality," 2008.

[72] J. E. D. Allan and J. Fay, "The influence of catchment land use on stream integrity across multiple spatial scales," *Freshwater Biology,* vol. 37, pp. 149-161, 1997.

[73] X. Wang, "Integrating water quality management and land use planning in a watershed context," *Journal of Environmental Management,* vol. 61, pp. 25-36, 2001.

[74] Statistics Botswana, "Botswana environment statistics: Human settlements report 2013," Statistics Botswana, 2014.

[75] S. Diver and L. Rinehart, Aquaphonics – Integration of Hydrophonics with Aquaculture. NCAT., 2010.

Foraging Behaviors – Pheromone, Task Allocation, and Trophallaxis -A Relative Comparison for Robotic Swarm Foraging

Ralph Nicole R.Barcos, Angelo R. Dela Cruz, Edison A. Roxas, Argel A. Bandala, Laurence Gan Lim, Elmer P. Dadios and Ryan Rhay P. Vicerra

***Abstract* — A group of algorithm enhancing collective behavior is inspired by the animals working together as a group such as ants, bees, and etc. In connection, swarm is defined as a set of two or more independent homogenous or heterogeneous agents acting upon a common environment in a coherent fashion which generates emergent behavior. The development of artificial swarms or robotic swarms has attracted a lot of researchers in the last two decades including pheromone, trophallaxis and task allocation algorithms. However, among these swarm based algorithms, the most efficient in terms of group performance, efficiency and interference in collecting the dusts or objects in an environment with variable terrains has not been identified. With this, the researchers see the need to developed swarm simulation platform that would compare the swarm-behavior-based algorithms for an ideal use of robots in different environments in dust collection.**

***Index Terms* — Swarm intelligence, swarm foraging, swarm simulation platform development**

I. Introduction

Design and implementation of collective behavior of agents in accomplishing tasks are gaining popularity nowadays. Social animals and insects are the key inspiration of creating distributed behavior amongst independent agents. In connection, swarm is defined as a set of two or more independent homogeneous or heterogeneous agents acting in a common environment in a coherent fashion, which generates emergent behavior. The creation of artificial swarms or robotic swarms has attracted many researchers in the last two decades. Many studies have been undertaken using practical approaches to swarm construction such as investigating the navigation of the swarm, task allocation and elementary construction.

Examination of the behaviors of ants has led to the recently developed field of Swarm Intelligence. Ants can perform diverse collective tasks such as foraging, nest building, sorting, and cooperative transport. In this proposed study, three different behavior of ant system will be studied with certain given measures: speed, accuracy, efficiency, and collision avoidance. The goal is to obtain the best or most effective ant-based swarm behavior in foraging, specifically in dust collection, within a given platform environment.

A number of researchers have proposed many swarm robotics algorithm and the emerging trend in the field of interest are the study of ant-based algorithms like the pheromone, trophallaxis and task allocation. However, among these swarm based algorithms, the most efficient, in terms of speed, efficiency, and collision avoidance has not yet been determined. Thus, there is a need to develop a swarm simulation platform to compare the swarm behavior based algorithms for an ideal use of swarm robots in different environments for dust collection.

Ralph Nicole R. Barcos, Angelo R. Dela Cruz and Edison A. Roxas are affiliated with Faculty of Engineering University of Santo Tomas, Espana Blvd, Manila, 1008 Philippines

Ryan Rhay P. Vicerra, Argel A. Bandala, Laurence Gan Lim and Elmer P. Dadios are affiliated with De La Salle University, 2401 Taft Ave, Malate, Manila, 1004 Metro Manila (e-mail: ryan.vicerra@dlsu.edu.ph; argel.bandala@dlsu.edu.ph; laurence.ganlim@dlsu.edu.ph; elmer.dadios@dlsu.edu.ph)

II. Swarm Behaviors

This section will discuss the different swarm behavior algorithms as presented by select models. The first part presents the three ant-based swarm behaviors and their basic description; we also state the algorithm that will represent them in the study. The second part will present the strengths of each behavior as opposed to the others; need for the comparison of the behaviors.

A. Trophallaxis (mouth-to-mouth feeding)

Trophallaxis is a basic behavior observed in majority of social animals and insects [5]. Its main purpose is to provide nutrition to offspring in nursing stage. However, it is also observed in several colony-based insects, that trophallaxis occurs among adults to better distribute food. In [6, 7] it was shown that trophallaxis plays an important role in the regulation of collective foraging decisions in honeybees. Aside from its function to transfer nutrients, trophallaxis is also observed as a tool in exchanging information about available food sources in honeybees. A trophallaxis-based algorithm is a self-organized task exchange in a swarm of autonomous, movable, and reconfigurable agents. In our study, the trophallaxis-based algorithm will be the BEECLUST Algorithm [5].

B. Task Allocation

Task allocation and learning is normally quite important to a swarm of robots. Task decomposition and allocation can greatly improve efficiency for especially complex tasks. In [8], they compared the costs and benefits of different types of task allocation approaches in noisy world. Learning is also useful since the parameters of the control mechanism are hard to tune. With the help of self-adaptive learning and optimizing methods, the swarm shows better adaptability in the different environments [4]. Task allocation assigns the robot members among different tasks in an adaptive and flexible way [7]. Task allocation will be represented by the Task Partitioning Model in [10].

C. Pheromone

Ant colonies in the nature are famous for their navigation and migration behaviors with the help of pheromones. The researchers of the swarm robotics society employed such scheme into swarm robotics by simulating the pheromones using part of the robots in the swarm which serve as the beacons [4]. Usage of pheromone for swarm robotics vary with its purpose such as in [11] where it is unique to a location on a map which was used to create a path from garbage sites to dump sites or in [12] where it was a signal the robot always carried to be able to inform robots of its current position and heading when they are close enough to each other. It may also be a numerical value in shared memory such as in [9] that acts as a request to other robots for assistance in a task. In our study, Pheromone-based behavior will be represented by the model in [12].

III. Unique Characteristics

Pheromone-based swarm robots select different tasks of the same type with different probabilities according to the pheromone amounts to assign themselves in the performing of these tasks [9]. They can use simple attraction or repulsion behaviors and they also do not require distinct step of map generation [12]. Though communication is indirect, they move with respect to pheromones “left” by other bots and “drop” their own for other robots [4]. Thus Pheromone-based swarms provide a robust, scalable approach for achieving the swarm level behaviors using a large number of small-scale robots in tasks such as reconnaissance and path-finding [13][15]. Trophallaxis-based swarm robots do not require such information nor do they need to know the position of other robots meaning that there is no need for a collection of the information of bots [5], like in Pheromone-based swarms [9], since communication happens at the instance when two robots meet [5]. Trophallaxis-based robots can also exchange tasks between robots of different capabilities to reduce the energy consumption of reconfiguration when and if they meet [10]. Trophallaxis-based swarm robots also do not require additional hardware for onboard processing or memory [5]. Task-allocated swarms on the other hand boast high adaptability in different environments and greatly improve efficiency for especially complex tasks [4]. Taskallocated swarm bots are also specialized and can switch between specializations if the remaining tasks require more participants [9].

IV. SIMULATION PARAMETERS

Based on parameters used in [10], the measurement of group performance, individual efficiency, and interference:

Group Performance is the total number of prey objects collected within the time period while Individual Efficiency is the number of prey objects collected by each individual robot [10].

Interference is measured as the time spent performing actions not strictly related to the task, but rather those actions that are lost due to negative interactions with the environment (e.g., obstacle avoidance maneuvers) [10]

V. BEHAVIOR ALGORITHM

A. Trophallaxis

Figure 1 shows the logical representation of the flow of events in a BEECLUST algorithm. First, to achieve random movement, each bot is assigned a direction and moves in a straight line in that direction until it encounters an obstacle, boundary or other bot. Bot collisions are detected by determining whether bots are within a certain distance of each other. Then, the bot determines whether it has collided with an obstacle or another bot. Once a bot is stopped (as a result of collision with another bot), then it measures the value of the function at that location. Lastly, cluster finding is done when the search is terminated. In general, the bots begin to collide/stop/wait at the beginning of the search. Thus, the bots tend to cluster soon after the search begins so the search can be stopped at any time to observe the location(s) of the clusters.

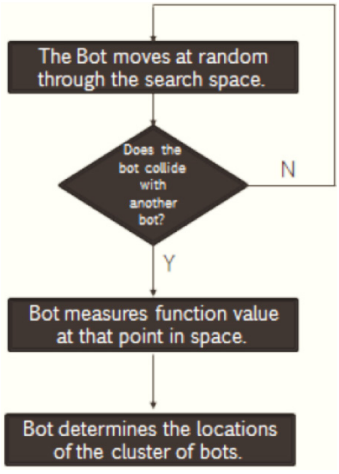

Fig. 1. Simplified state diagram of trophallaxis behavior based on BEECLUST algorithm

B. Task Allocation

Figure 2 shows the state diagram for the Task Allocation Algorithm [10]. Gray states belong to the harvest task, while the white states to the store task. The obstacle avoidance state has been omitted for clarity, as it is applicable in all states of the robot. t_w is the time spent in the exchange zone and θ is the threshold.

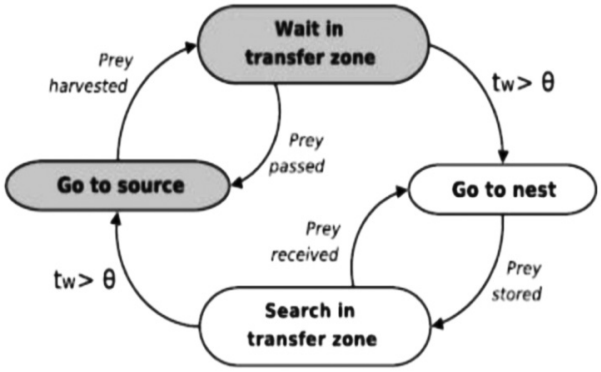

Fig. 2. Simplified state diagram of the controller of the robots

The first step of the algorithm is spatially partitioning the environment. The global foraging task is automatically partitioned into two subtasks particularly; harvesting prey objects from a harvesting area (source) and then transporting them to a home area (nest).

These subtasks have a sequential inter-dependency in the sense that they have to perform one after the other in order to complete the global task once: delivering a prey object to the home area [12].

A robot in the first subtask has to wait for a specific time before passing an object to the robot in the second subtask. A long waiting time could mean insufficient robots in subtask. The robots have the capability to switch a subtask. The waiting time could be used by the robot to decide whether it will switch a subtask or not.

C. Pheromone

Pheromones are locally transmitted without specifying a recipient. This obviates the need for unique identities that are impractical in a large group. Figure 3 shows the Pheromone's diffusion gradients that provide important navigational cues and it can also encode useful information about barriers in the environment that block pheromone propagation. But Pheromones decay over time, which reduces obsolete

or irrelevant information and obstacles are sensed by the robot when pheromone messages bounce off them. The robot will remember the direction of the received virtual pheromone and will serve as guideposts for the following robots.

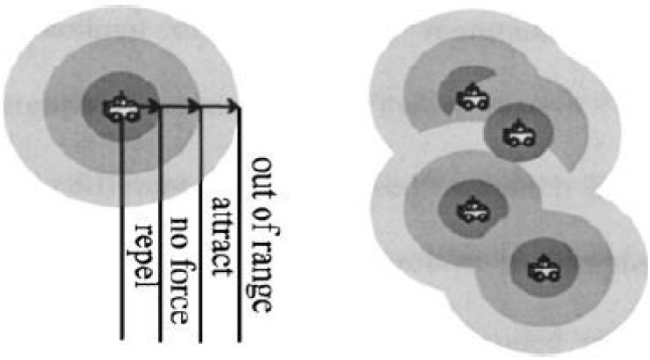

Fig. 3. Diagram of Pheromone field strength

VI. SIMULATION ENVIRONMENT

The testing environment has an area of 90 cm x 90cm, including the walls at the edge of the environment, divided into 3 cm x 3 cm sections called "patches". The environment will be leveled throughout. The test will also include static obstacles which will be expressed as a percent of the total area of the environment. In this study, the percentages will be: (a) 0% or no obstacles, (b) 25%, (c) 50% and (d) 75%. The environment will be generated so that all dust particles (not enclosed by obstacles) can be collected and that there are no single-block obstacles. The same generated environment will be used for testing all bots and algorithms so that all results can be compared. Each combination will be simulated 10 times with an upper limit of 40 if results are inconclusive. There will be a total of 50 dust particles in static tests and may be formed in clumps called "dust sites" or individual pieces simply called "dust". In dynamic tests, the first 25 dust particles will be placed on the field and the last 25 dust particles will be dropped randomly across the field.

VII. DIMENSIONS AND SPECIFICATION OF SWARM ROBOTS

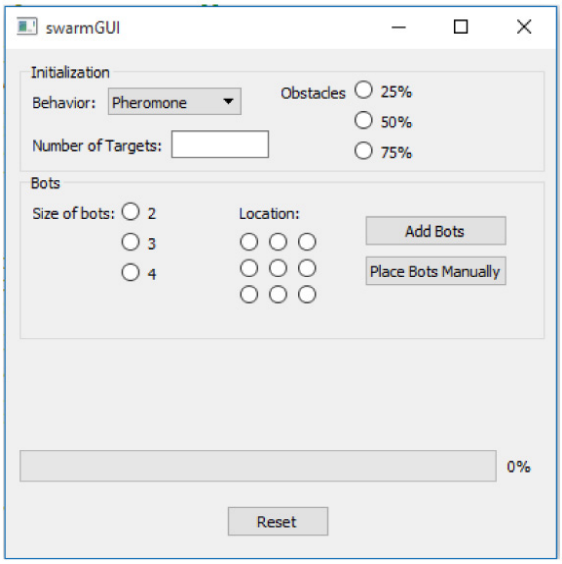

Fig. 4. Swarm robot and environment GUI

The robots in general will be able to move, rotate in place, detect the dust particle when they are near or over it, and carry the dust. Other specifications such as LEDs will be incorporated depending on the algorithm they will be using to perform the test.

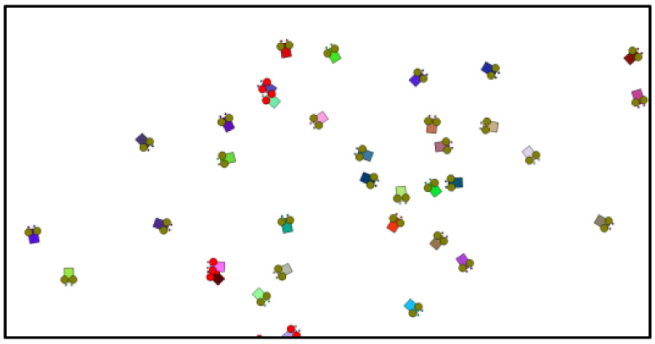

Fig. 5. Swarm robots in random movement (55 bots)

The size of the robots will be less than one patch, exactly the width of one patch and larger than one patch to allow for robot exploration. The diameter of the robots will be: (a) 2 cm, (b) 3 cm and (c) 4 cm. This study will use (a) 50 robots, (b) 100 robots, (c) 150 robots, (d) 200 robots of each size. The goal of the robots is to collect the dust scattered across the environment and bring it back to the nest located at the center. The dust will have no dimensions and no

weight. The robots will be programmed to follow the algorithms presented in Chapter 2 to search for, collect and, return the dust.

The main algorithm used for the program of the graphical user interface and the environment is as follows:

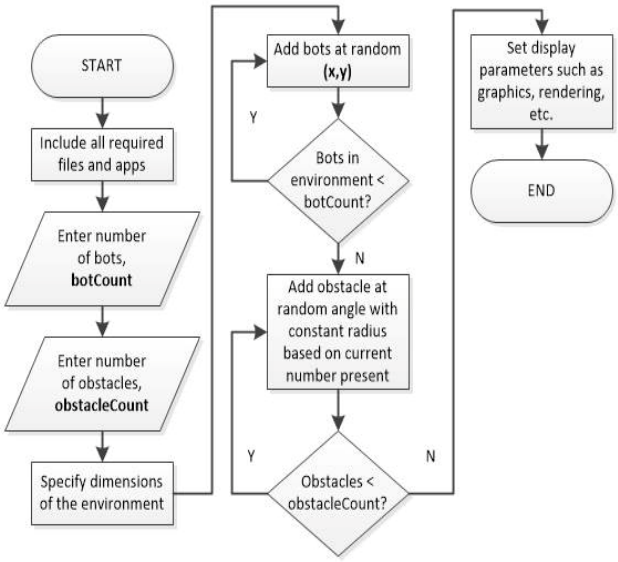

Fig. 6. Main algorithm of the simulation platform

VIII. SIMULATION RESULTS

In the simulation environment with 50 bots, it is observed that more or less 40 bots on average intersect at periods of random movements.

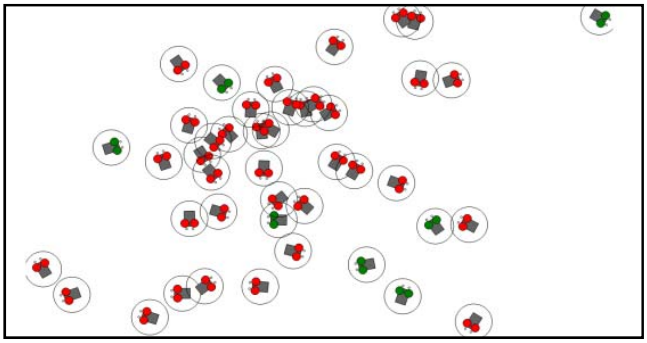

Fig. 7. Random movements of 50 Bots

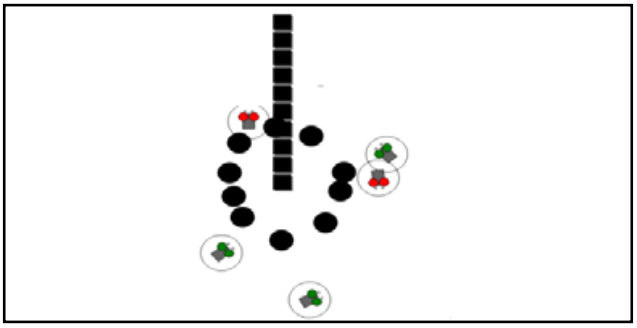

Fig. 8 Initial position of Dynamic Obstacles

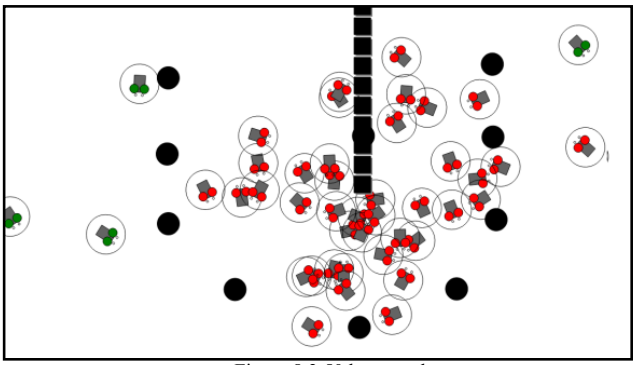

Figure 9. 50 bots used

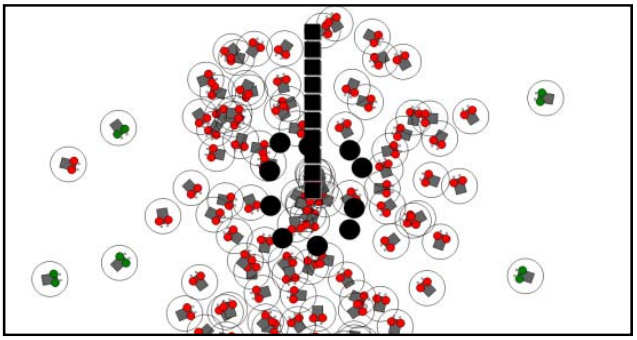

Figure 10. 100 bots used

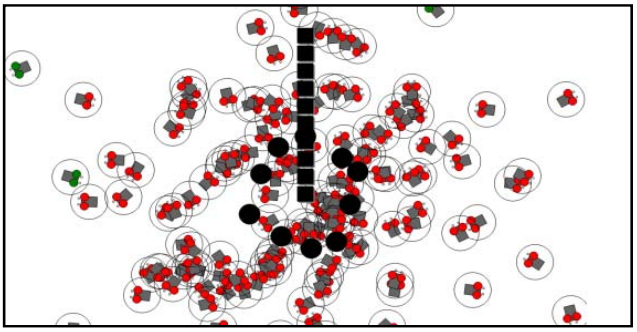

Figure 11. 150 bots used

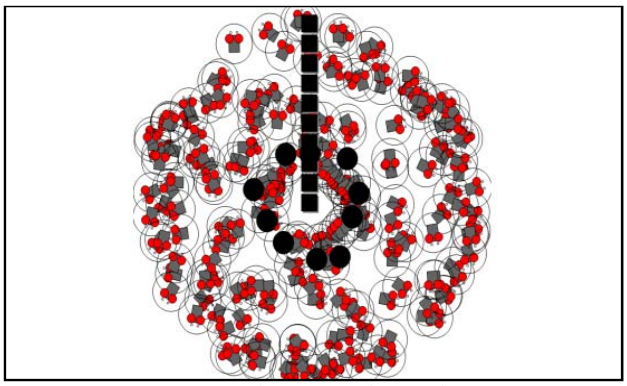

Figure 12. 200 bots used

Dynamic obstacles were added to the environment. These obstacles are movable depending on where the simulator/ user desires to put the obstacles in the environment area for testing purposes. 50 bots were first tested to walk-through the environment with the dynamic obstacles placed in the desired points by the user. It is observed that the bots avoid the obstacles (marked by black squares and circles) and somehow, tried to escape the area they are located in the environment. The bots still experience collisions with an average 40 bots per period. It was then followed up by using 100 bots, 150 bots and lastly, 200 bots.

IX. CONCLUSIONS

In the initial simulation of the swarm robots in an indefinite area, the source code is modifiable in terms of the number of bots to be added or robots present in the environment, the area of the environment is not yet determined since limitations is yet to be implemented in the area. The robots in the environment have collision detectors. In the simulation, it was able to send a signal (red blinking ears) that represents collision. The initial reaction of the robots is to avoid going to the path where the other bot it bumped into is heading. The robots are moving randomly and are initially in a circular formation. The GUI developed is to modify the size of each bot (as specified in the robots' specification) number of robots present in the environment, size of the environment, and the percentage of obstacles based in the platform. Initially, 50 bots were put in the environment with random movements and it shows normal movement without lag. As the number of bots is increased, it was observed that among the ranges 50-200 the most number of bots with normal movement and without lag is at 55-60 bots. Using a hundred bots in the environment, it experienced a lot of collisions in the obstacles and with bots. In spite of that, it still managed to explore the environment with a few bots not experiencing collisions.

With 150 and 200 bots in the environment, the bots experienced most of the collisions with all of the bots experiencing collisions at the initial position assigned to the bots. The simulation with 150 bots, however, gave a better response and less delay compared to the simulation with 200 bots.

REFERENCES

[1] E. Bonabeau, G. Theraulaz, "Swarm smarts", *Scientific American, Inc.* , pp. 73–79, March 2000.

[2] W.A.F.W. Othman, B.P. Amavasai, S.P. McKibbin, F. Caparrelli, "An Analysis of Collective Movement Models for Robotic Swarms", *The International Conference on "Computer as a Tool"*, pp. 2373-2380, 2007.

[3] F. Gholami, M. J. Mahjoob, "An Investigation of Parameters in Ant Colony Optimization for a Path Optimization Algorithm", *International Conference on Mechatronics and Automation*, August 2007.

[4] Y. Tan, Z. Zheng, "Research Advance in Swarm Robotics", *Defence Technology vol. 9*, pp. 18 - 39, 2013.

[5] J. Hereford, "Analysis of a New Swarm Search Algorithm Based on Trophallaxis", *IEEE*, 2010.

[6] S. Camazine, "The Regulation of Pollen Foraging by Honey Bees: How Foragers Assess the Colony's Need for Pollen", *Behavioral Ecology and Sociobiology, vol. 32*, pp. 265 - 273, 1993.

[7] S. Camazine et al., "Protein Trophallaxis and the Regulation of Pollen Foraging by Honeybees (Apismellifera L.)", *Apidologie, vol. 29*, pp. 113-126, 1998.

[8] N. Kalra, A. Martinoli, "Comparative study of market-based and threshold-based task allocation", *Distributed Autonomous Robotic Systems vol. 7*, pp. 91 – 101, 2006.

[9] D. Zhang, "Adaptive task assignment for multiple mobile robots via swarm intelligence approach", *Robotics and Autonomous Systems 55*, 2007

[10] G. Pini, "Interference reduction through task partitioning in a robotic swarm", *IRIDIA Technical Report Series,* April 2009.

[11] D. O. Sales, M. A. Dias, F. S. Osorio, "Grid Ant Colony Optimization Applied to a Multi-robotic Garbage Collection System", *Robotics: SBR-LARS Robotics Symposium and Robocontrol,* pp. 187 – 192, October 2014.

[12] D. Payton, M, Daily, R. Estowski, M. Howard, C. Lee, "Pheromone Robotics", *Autonomous Robots 11*, pp. 319 – 324, 2001.

[13] D. Payton, R. Estkowski, H. Mike. "Compound behaviors in pheromone robotics", *Robot Autonomous Systems*, 2003.

[14] R. Moritz, "Trophallaxis-Inspired Self-Organized Task Exchange in Heterogeneous Swarms", *IEEE Conference,* 2011.

[15] A. Bandala, R. Vicerra and E. Dadios, "Swarming Algorithm for Unmanned Aerial Vehicle (UAV) Quadrotors in Swarm Behavior for Aggregation, Foraging, Formation and Tracking," Journal of Advanced Computational Intelligence and Intelligent Informatics, vol. 8, no. 9, 2014.

Lift Enhancement of the LRN 1015 Airfoil using a Gurney Flap: A Computational Fluid Dynamics Investigation

Lemuel F. Banal and Aristotle T. Ubando

Abstract— **A Gurney flap is a small tab installed at the trailing edge of a wing to enhance the lift of an airfoil. The LRN 1015 airfoil has a high lift-to-drag ratio but is not considered to be a high-lift airfoil. If its lift is improved, additional benefits such as reduced take-off and landing roll, reduced stalling velocity, and increased payload capacity, among others, can be gained. In this light, the effects of the integration of the flap into the airfoil were investigated using a computational fluid dynamics approach. Part of this study is the validation of the computational fluid dynamics model used through investigation of the unflapped airfoil using ANSYS CFX with a Shear Stress Transport *k*-ω turbulence model, and comparison of the results with wind tunnel data. The same computational model was used to investigate the effects on the airfoil performance of the flap with heights of 1.58%, 2%, 3% and 4% of the chord. Results revealed that 46% increase in the maximum lift coefficient was achieved by a flap height of 3% of the chord, at a Mach number of 0.2 and a Reynolds number of 500,000. In addition, the drag and the pitching moment were also increased, but no degradation in the lift-to-drag ratio was observed for low angles of attack typically used for cruise.**

Index Terms — **Computational Fluid Dynamics, LRN 1015 airfoil, Gurney flap, SST turbulence model, ANSYS**

I. Introduction

The airfoil chosen for this study is the NASA-developed LRN 1015 due to its high lift-to-drag ratio which is an indication of good aerodynamic efficiency and associated to high aircraft performance. The profile is shown in Fig. 1 based on the coordinates given in [1]. The LRN stands for Low Reynolds Number and the first two digits in the number designation gives the design lift coefficient in tenths (i.e. 1.0), while the last two digits indicates the approximate maximum thickness-to-chord ratio in hundredths (i.e. 0.152). This airfoil is designed for a Mach number of 0.55 and a Reynolds number of 500,000 [1].

Fig. 1. The NASA LRN 1015 airfoil profile.

Hicks and Cliff [1] conducted an experimental study on the LRN 1015 using the 2-by-2-ft. variable speed, continuous flow, ventilated wall, variable pressure transonic wind tunnel at Ames Research Center. The results are used in the validation study conducted in this paper.

The stellar performance specifications of the High Altitude Long Endurance (HALE) UAV, RQ-4 Global Hawk can be attributed in part to the use of the LRN 1015 for its wing [2, 3]. However, a high L/D does not necessarily imply a high maximum lift coefficient, $C_{L,max}$. In fact, the LRN 1015 only has a moderate $C_{L,max}$ and is not considered to be a high-lift airfoil. If the LRN 1015 had a higher lift at a range of operational angles of attack, additional performance capabilities such as shorter take-off and landing, reduced stalling velocity, increased payload capacity, to name a few, can be achieved. Hence, the question arises whether the lift characteristics of the LRN 1015 can be improved in such a way that the degradation of its L/D is minimized. In this paper, the addition of a Gurney flap (GF) as a device for lift enhancement with minimal attendant adverse effects is considered.

L.F. Banal is a M.S. Candidate of Mechanical Engineering at the De La Salle University, Philippines and a faculty at the Department of Aeronautical Engineering and Aircraft Maintenance Technology, FEATI University.

A.T. Ubando is an Associate Professor and Research Fellow at the Mechanical Engineering of De La Salle University, Philippines

A GF is a strip or a small tab attached to the trailing edge of a wing on the pressure side as shown in Fig. 2. It can be made of rubber [4], spruce [5], aluminum sheet bent to shape [5] or thin brass shim stock bent and cut to shape. The name is a homage to Dan Gurney, a car racing icon who was the first to use it in a spoiler to increase downforce and thus wheel traction. Gurney himself recounts of its discovery in [6]. The device has also been called the wickerbill and is patented in 1935 as the Zaparka flap [7].

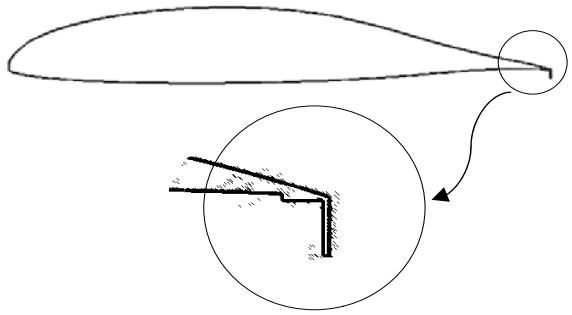

Fig. 2. The Gurney flap.

There exists considerable work on the potential of the GF in improving the aerodynamics of airfoils. Wang, et. al. [8] presents a review of existing studies and discusses the effects of height, location, mounting angle and configuration (e.g. serrated: sawtooth, rectangular etc.) of a GF. In general, GF integration results to an increase in lift and drag with an attendant increase in pitching moment. The geometric parameters of the GF are shown in Fig. 3 [8]. For optimal performance of airfoils with GF, the height, h of the GF should be below the boundary layer thickness, the best location, s is at the trailing edge, and best mounting angle, ϕ is 90°.

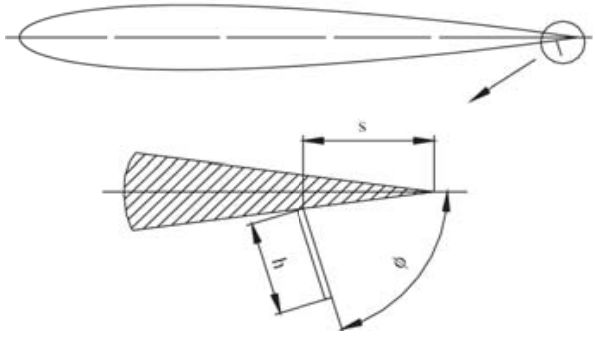

Fig. 3. The Gurney flap parameters [8].

Wang, et. al. [8] also gives the mechanism for lift enhancement which is consistent with that given by Jeffrey et. al. [5]. The GF changes the Kutta condition by moving the stagnation point downstream, aft of a pair of counter rotating vortices that sheds into a Kármán vortex street. This results in increased circulation, reduced adverse pressure gradient, delayed separation, reduced boundary layer thickness, more suction near the trailing edge and reduced pressure. Upstream of the GF velocity is reduced and pressure is increased. The increased pressure differential results in more lift. The vortex structure can also be considered to be an extension of the airfoil which increases chord and camber, thus increasing lift.

Other studies on the Gurney flap include that by Li, Wang, and Zhang [9], Meyer, et. al. [10], Giguere, et. al. [11] Daniel and Traub [12], Traub [13], Liu and Montefort [14], Traub and Akerson [15], and Traub and Chandrashekar [16]. Different airfoils are considered by different researchers. Existing studies on certain airfoils are shown in Table I.

TABLE I.
STUDIES ON GURNEY FLAP INTEGRATED TO SPECIFIC AIRFOILS

Airfoil	**References**
NACA 4412	Storms & Jang [17] and Jang, et. al. [18, 19]
LA203A & Gottingen 797	Giguere, et. al. [20]
NACA 0011	Myrose, et. al. [21, 22, 23]
NACA 0012 & Eppler E423	Jeffrey, et. al. [5, 24]
NACA 0012	Jain, et. al. [25]
Clark Y-14	Kleir-aldeen & Hamid [26]
NACA 23012	Cavanaugh, et. al. [27]
S1223	Tejnil [28]
S903, S408, S415, HTR 1555 & XV-15	Cole et. al. [29]
SFYT15thick	He, et. al. [30]
NACA 0000 (flat plate), 0006, 0012 & 0018	Meena & Taira [31]
NACA 0015	Shah, et. al. [32]
DU97-W-300	Yan, et. al. [33]
NACA 2412 & NACA 4421	Amini, et. al. [34]

The main objective of this paper is to determine the GF height (normalized by the chord) that provides satisfactory lift enhancement with

acceptable degradation in drag, pitching moment and lift-to-drag ratio. The semi-empirical formula for optimal height by Brown and Filippone [35] is used as a starting point:

$$h_{opt} = 37.155\left(\frac{c^{0.8}}{V_{\infty}^{0.2}}\right) \quad (1)$$

where c is the chord length and V_{∞} is the freestream velocity. Heights of 2%, 3% and 4% of the chord are also investigated.

II. METHODS

This study is conducted in the framework of computational fluid dynamics using the commercial application *CFX*® within *ANSYS Workbench*®. A parametric set up is employed such that output parameters update upon change of input parameters with minimal user-program interaction.

A. Virtual Wind Tunnel Settings

Mach number, M and Reynolds number Re cannot be input directly into *CFX*. To determine the velocity, pressure and temperature for a target M and Re, equations (2)-(5) are used:

$$T = \left[\left(\frac{\mathrm{Re}}{M}\right)\left(\frac{K_2}{K_1}\right)\right]^{\frac{-2}{2n+1}} \quad (2)$$

$$V = \frac{M}{K_2}\left[\left(\frac{\mathrm{Re}}{M}\right)\left(\frac{K_2}{K_1}\right)\right]^{\frac{-1}{2n+1}} \quad (3)$$

where,

$$K_1 = \frac{cpT_0^{\,n}}{\mu_0 R} \quad (4)$$

$$K_2 = \sqrt{\frac{1}{\gamma R}} \quad (5)$$

c is the airfoil chord length; γ is the specific heats ratio (1.4 for air); R is the specific gas constant (287.08 *J/kg-K for air*), μ_0 and T_0 are reference viscosity and temperature, respectively (i.e. value at sea level: $1.79\text{x}10^{-5}$ *kg/m-s and* 288.16 *K*); n is the viscosity power law exponent (0.7 or 2/3), and p, T and V are the freestream pressure, temperature and velocity, respectively that are input into *CFX*. Equations (2) to (5) are based on the viscosity power law [36] rather than Sutherland's Law which gives a more complicated coupling of viscosity and temperature.

Table II presents the freestream conditions used in this study.

TABLE II.
FREESTREAM CONDITIONS

Freestream parameter	**Value**
Reynolds number	500,000
Mach number	0.20
Pressure	12,159 Pa
Temperature	316.2579 K
Velocity	71.3043 m/s

B. Computational Domain

The computational domain is shown in Fig. 4. This topology is common for airfoil analysis but a simple rectangular and a parabolic domain have also already been used. The far field is placed 10 chord lengths upstream and 20 downstream. This is within the limits prescribed by Athadkar and Desai [37]. More conservative dimensions are prescribed by Murcia and Pinilla [38], Ma and Liu [39], Eleni et. al. [40] and others. The results would show that the selected domain size is satisfactory.

Two strategies in varying the angle of attack (AOA) are tested. One actually changes the incidence of the airfoil with an incoming horizontal flow and the other changes the direction of the incoming flow with the airfoil fixed in its position. In the former, the AOA is implemented through a rotation of the geometry, and the associated angle is promoted into a parameter. In the latter, the velocity is resolved into horizontal and vertical components according to the AOA, and the associated angle is promoted to a parameter.

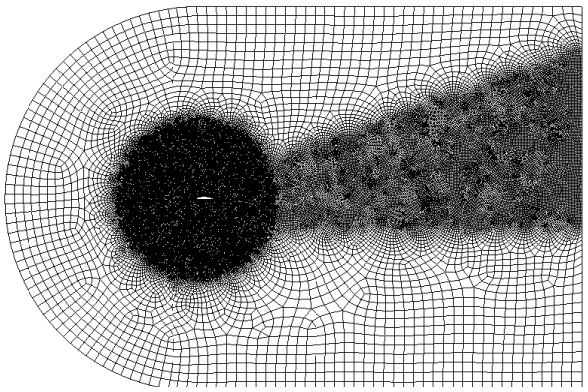

Fig. 4. The computational domain with mesh.

The nature of each strategy requires different boundary conditions for the domain. To minimize the effects of domain boundaries on the flow, an entrainment opening boundary condition with zero gradient turbulence is applied to the upper and lower walls for the changing velocity strategy. A free-slip wall condition is used for the fixed velocity strategy. Both cases use an inlet with medium turbulence, a zero relative static pressure outlet, and two symmetry faces to simulate two-dimensional flow.

The changing velocity strategy brings about complications and asymmetries but it ensures that the mesh is independent of the AOA. The disadvantage of the fixed velocity strategy is that the mesh changes with the rotation of the airfoil and at a certain AOA the inflation may fail to form.

C. Meshing Strategy

A swept unstructured mesh with inflation, edge sizing and body of influence sizing around the airfoil is employed. A structured grid is generally faster to solve but an unstructured grid offers more flexibility which means more resolution can be placed only where it is needed, thus may actually result in a faster overall solution time. The sweep method ensures a single element is sandwiched between the symmetry faces which promotes span wise uniformity or two-dimensionality. Inflation layers are added to resolve the gradients within the boundary layer especially in the wall normal direction.

For proper near-wall resolution, the y^+ approach is employed. The y^+ is a dimensionless parameter similar to Reynolds number used to measure distance from a wall to the center of a mesh element in a wall. It is defined as,

$$y^+ = \frac{\rho V_\tau y}{\mu} \tag{6}$$

where y is the wall distance, ρ is density, μ is viscosity, and V_τ is called the friction velocity,

$$V_\tau = \sqrt{\frac{\tau_w}{\rho}} \tag{7}$$

where τ_w is the wall shear stress,

$$\tau_w = \tfrac{1}{2}\rho V^2 C_f \tag{8}$$

where V is the freestream velocity and C_f is the skin friction coefficient.

Skin friction coefficient can be correlated to Reynolds number and considerable semi-empirical equations have already been developed in the past to describe this correlation. Equation (9) developed by Date and Turnock [41] is among the more recent ones.

$$\frac{1}{\sqrt{C_f}} = 4.06 \log_{10}(\mathrm{Re} \bullet C_f) - 0.725 \tag{9}$$

Equation (9) can be solved iteratively through the Newton-Raphson method with the first estimate derived from Schlichting's correlation,

$$C_f = \left[2 \log_{10} \mathrm{Re} - 0.65\right]^{-2.3} \tag{10}$$

Equations (6) to (9) are combined to compute the required wall distance or first inflation layer height for a given target y^+. The required y^+ for accurate near-wall modeling is less than 1.0 [42, 43].

To ensure the flow that trails behind the airfoil is resolved, local body of influence sizing is applied to refine the mesh in the corresponding part of the domain. For the changing velocity strategy, this refinement also has to capture the changing general direction of the wake. This is manifested in the asymmetry of the mesh as shown in Fig. 4.

Vertex sizing is added around the GF for better resolution of the counter rotating vortices downstream of the flap.

D. Turbulence Model

The *k*-ω Shear Stress Transport (SST) model by Menter [44] is chosen for closure of the Reynolds

Averaged Navier-Stokes (RANS) equations. SST is an eddy viscosity model which is recommended for simulations with significant boundary layer effects. It is able to predict the location and extent of flow separation caused by the presence of an adverse pressure gradient. Bardina et. al. [45, 46] conducted validation studies that demonstrate the capabilities of this model. Eleni et. al. [40] has also shown that SST was the most appropriate model for the simulation of the flow over the NACA 0012 airfoil. Murcia and Pinilla [38] and He, et. al. [30] also used this model in their work.

III. Results and Discussion

A validation study was able to determine the model that reproduces the experimental results. A mesh with a relevance of 10, a body sizing with an element size of $0.04m$, an edge sizing of 300 divisions, and an inflation with a first layer thickness of $0.00002m$ that grows 20% up to 20 layers provided results closest to that of Hicks and Cliff [1].

Fig. 5 presents the computational results for the lift coefficient superimposed on the experimental results. There is good agreement between the results especially at moderate AOAs, in the linear part of the lift curve. Some degree of divergence can be observed at the ends, at relatively high negative AOAs and near the stalling region. At any rate, $C_{L,max}$ has been captured to a reasonable degree of accuracy.

Several mesh strategies were tested to duplicate the experimental results. The results for the near-stall regime were found to be very sensitive to mesh properties. A certain mesh would be able to accurately capture the experimental results at a certain AOA near the stall regime but it would no longer work for a different AOA. The results for the AOAs in the linear portion of the lift curve, on the other hand, were insensitive to mesh changes.

The difficulty in capturing the experimental results at high AOAs can be attributed to the very complex nature of flow separation which is highly viscous and turbulent. Other investigations have also encountered this problem. As mentioned in [47], in the near-stall regime the lift coefficient can be over-predicted as in [48], [49] and [50], or under-predicted as in [51], [52] and [53]. Another cause can be attributed to the turbulence model. A modification to the k-ω SST model is prescribed in [47] to improve its accuracy in the stall region.

Fig. 6 presents the drag polar. The drag coefficient is slightly over-predicted. This can be attributed to the turbulence model incorporating more turbulence into the boundary layer than there should be. Certain adjustments to SST parameters, may be able to remedy this.

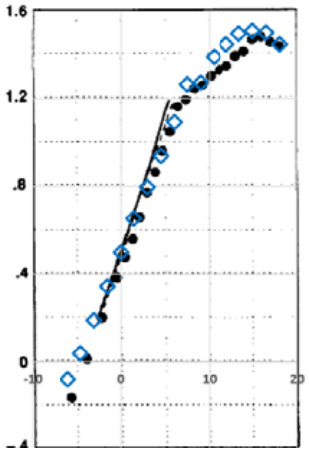

Fig. 5. Lift coefficient versus angle of attack.

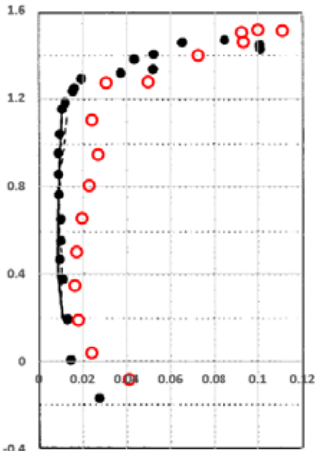

Fig. 6. Lift coefficient versus drag coefficient.

Fig. 7 presents the pitching moment coefficient about the quarter-chord point which is slightly more negative than the experimental results. It is seen that the pitching moment is insensitive to AOA which implies the quarter-chord point is close to the aerodynamic center as predicted by thin airfoil theory.

The same computational model was used to investigate the effects of integrating a GF into the baseline airfoil. To improve the resolution around the

GF, the model was modified to include a vertex sizing centered at the tip of the GF with just enough radius to capture the counter-rotating vortices. Good agreement in the results for the two cases were found, especially within the range corresponding to the linear portion of the lift curve. The results that follow are based on the modified model.

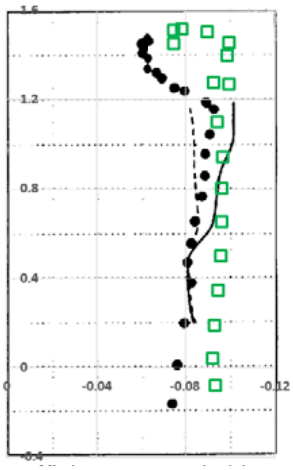

Fig. 7. Lift coefficient versus pitching moment.

Fig. 8 presents the variation of lift coefficient with GF height. Consistent with the results of former investigations, the GF is able to improve the lift of the airfoil. The lift curve slope and the AOA for C_{Lmax} are slightly changed, and the zero-lift AOA is shifted to the left. However, it is difficult to ascertain the accuracy of the results in the near-stall range of AOAs and at negative AOAs because significant variation in the results was found, being sensitive to mesh changes and also depending on the simulation run (i.e. doing a re-run changes the results). Moreover, the choice of a parametric study of GF heights (by promoting the height of the GF to a parameter) or otherwise also seem to affect the results in the said range.

A GF with a height of 3% of the chord appears to be a good choice, being able to provide satisfactory lift enhancement to the airfoil, increasing the maximum lift coefficient by about 46%. At moderate AOAs the drag penalty is comparable with that of the shorter GFs that gives less lift as shown in Fig. 8 and 9. This penalty is more severe for a GF with a height of 4% of the chord although this GF can generate more lift. Also, the moment about the quarter-chord point is most negative for this GF as shown in Fig. 11. The pitch-down tendency can be counteracted by a bigger horizontal tail but the weight penalty can cancel the lift enhancement causing an overall reduction in performance.

The maximum L/D appears to shift to the left with the integration of a GF as shown in Fig. 10. Higher values of L/D are achieved at low AOAs desirable for cruise. The spikes are natural because they happen within a region where the drag is decreasing and the lift is increasing, however their magnitude may be off.

Fig. 12 shows that the simulation was able to capture the counter-rotating vortices downstream of the GF. The high pressure upstream of the GF was also manifest. Fig. 13 plots the non-dimensional pressure over the non-dimensional length of the airfoil at zero AOA, showing there is increased positive pressure on the lower surface and there is more suction on the upper surface for the airfoil with a GF. This explains the lift enhancement.

Fig. 14 shows that for the flapped airfoil at zero AOA, the target $y+$ of less than 1.0 was captured by the simulation. This is the same for the other cases at other AOAs: throughout most of the airfoil surface, a $y+$ of less than 1.0 was achieved, except in a very small region near the leading and trailing edge.

Interestingly, a computational model with a first layer thickness that corresponds to a $y+$ greater than 1.0 was also able to output values very close to the experimental results. The wall function capability of the solver may have kicked in automatically as there was not enough near-wall mesh resolution.

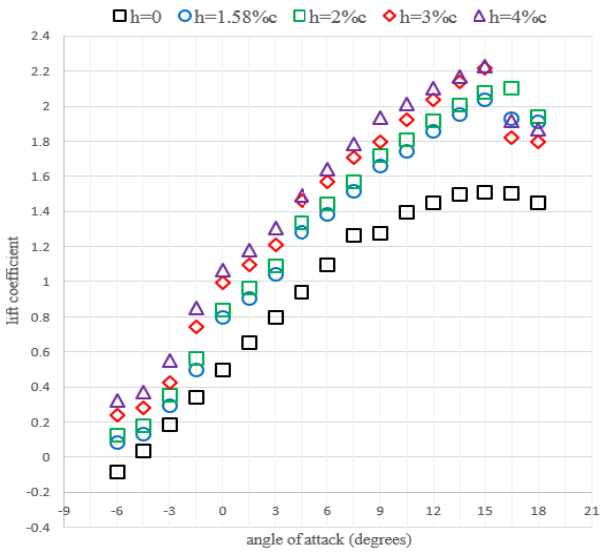

Fig. 8. Lift coefficient versus angle of attack.

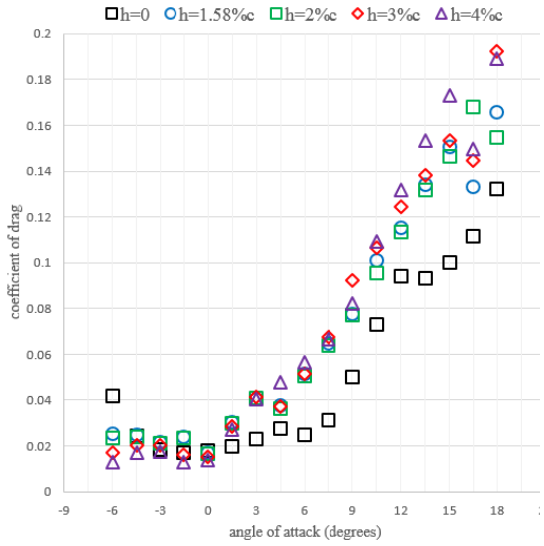

Fig. 9. Drag coefficient versus angle of attack.

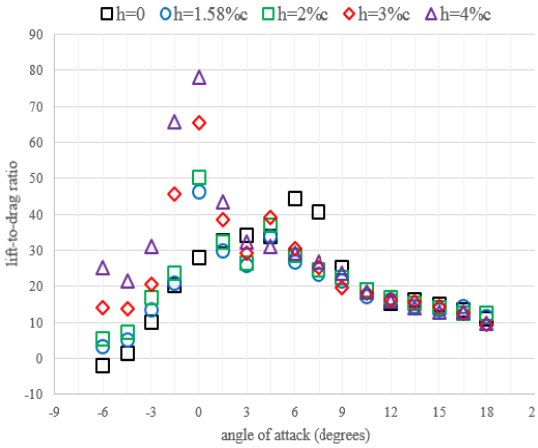

Fig. 10. Lift-to-drag ratio versus angle of attack.

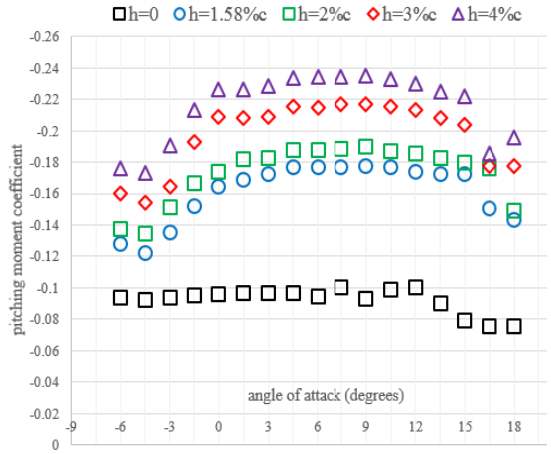

Fig. 11. Pitching moment coefficient versus angle of attack.

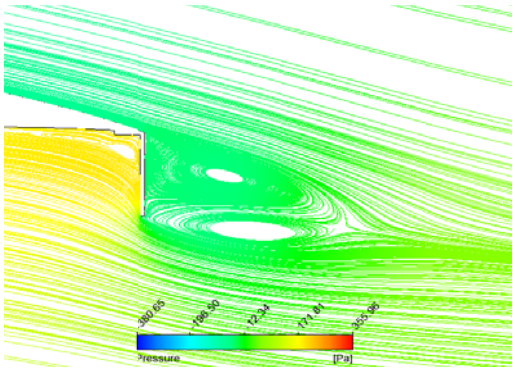

Fig. 12. Counter-rotating vortices downstream of the GF.

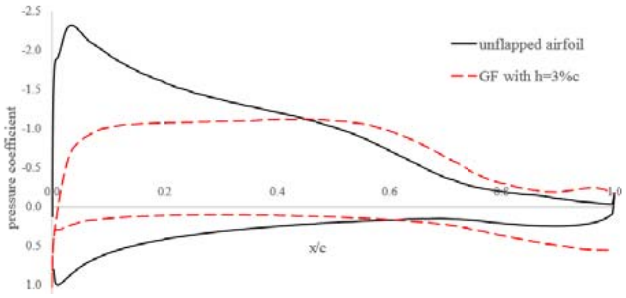

Fig. 13. The pressure distribution.

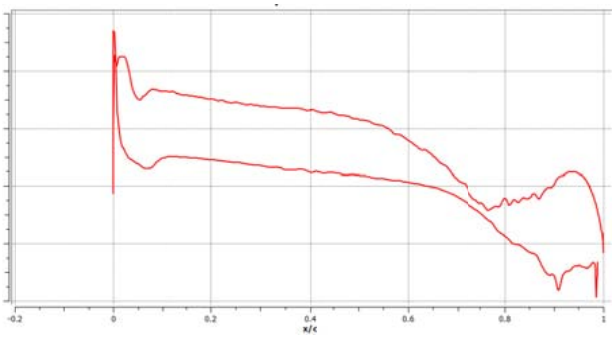

Fig. 14. The $y+$ distribution.

IV. CONCLUSION AND FUTURE WORK

The Gurney flap is able to improve the lift of the LRN 1015 airfoil at a Mach number of 0.2 and a Reynolds number of 500,000. For a flap with a height of 3% of the chord, the maximum lift coefficient can be increased by about 46%. The drag and pitching moment are also increased but the lift-to-drag ratio is not degraded at low angles of attack desirable for cruise.

It may be possible to reduce the drag by employing a mounting angle other than 90 degrees or by strategically incorporating serrations into the flap.

The computational model used lacks accuracy in the near-stall region and at relatively high negative angles of attack. Mesh improvement and adjustment of the Shear Stress Transport model parameters may be able to generate more accurate results.

The effects of varying Mach number and Reynolds number must also be investigated to capture a desired range of flight conditions. A preliminary study has already been conducted to this end and it was found out that it is more difficult to duplicate the wind tunnel results for Mach numbers beyond the incompressible flow regime ($M > 0.3$). A new computational model which resolves the energy equation and takes into account energy transfers (i.e. uses thermal energy for heat transfer option) will have to be used.

REFERENCES

[1] R. M. Hicks and S. E. Cliff, "An Evaluation of Three Two-Dimensional Computational Fluid Dynamics Codes Including Low Reynolds Numbers and Transonic Mach Numbers," National Aeronautics and Space Administration, Moffett Field, California, 1991.

[2] C. Lafountain, K. Cohen and S. Abdallah, "Camber Controlled Airfoil Design for Morphing UAV," in *47th AIAA Aerospace Sciences Meeting Including The New Horizons Forum and Aerospace Exposition*, Orlando, Florida, 2009.

[3] D. Lednicer, "Airfoils of US and Canada," [Online]. Available: www.aerofiles.com/airfoils.html. [Accessed 2 Aug. 2016].

[4] D. H. Neuhart and O. C. Pendergraft, Jr., "A Water Tunnel Study of Gurney Flaps," National Aeronautics and Space Administration, 1988.

[5] D. Jeffrey, X. Zhang and D. W. Hurst, "Aerodynamics of Gurney Flaps on a Single-Element High-Lift Wing," *Journal of Aircraft,* vol. 2, no. 37, pp. 295-301, Mar.-Apr. 2000.

[6] D. Gurney, Interviewee, *Dave Despain Bonus Footage - Dan Gurney, The Gurney flap.* [Interview]. 19 Aug. 2014.

[7] F. E. Zaparka, "Aircraft and control thereof". US Patent RE19412E, 1 Jan. 1935.

[8] J. J. Wang, Y. C. Li and K.-S. Choi, "Gurney flap—Lift enhancement, mechanisms and applications," *Progress in Aerospace Science,* vol. 44, pp. 22-47, 2008.

[9] Y. C. Li, J. J. Wang and P. F. Zhang, "Influences of Mounting Angles and Locations on the Effects of Gurney Flaps," *Journal of Aircraft,* vol. 40, no. 3, pp. 494-498, 2003.

[10] R. Meyer, W. Hage, D. W. Bechert, M. Schatz and F. Thiele, "Drag Reduction on Gurney Flaps by Three-Dimensional Modifications," *Journal of Aircraft,* vol. 43, no. 1, pp. 132-140, 2006.

[11] P. Giguere, G. Dumas and J. Lemay, "Gurney Flap Scaling for Optimum Lift-to-Drag Ratio," *AIAA Journal,* vol. 35, no. 12, pp. 1888-1890, 1997.

[12] L. Daniel and L. W. Traub, "Effect of Aspect Ratio on Gurney-Flap Performance," *Journal of Aircraft,* vol. 50, no. 4, pp. 1217-1225, 2013.

[13] L. W. Traub, "Prediction of Gurney-Flap Lift Enhancement for Airfoils and Wings," *AIAA Journal,* vol. 52, no. 9, Sept. 2014.

[14] T. Liu and J. Montefort, "Thin-Airfoil Theoretical Interpretation for Gurney Flap Lift Enhancement," *Journal of Aircraft,* vol. 44, no. 2, pp. 667-671, 2007.

[15] L. W. Traub and A. Akerson, "Airfoil Lift Augmentation at Low," *Journal of Aircraft,* vol. 47, no. 6, pp. 2103-2114, 2010.

[16] L. W. Traub and S. M. Chandrashekar, "Experimental study on the effects of wing sweep on Gurney flap performance," *Aerospace Science and Technology,* vol. 55, pp. 57-63, 2016.

[17] B. L. Storms and C. S. Jang, "Lift enhancement of an airfoil using a Gurney flap and vortex generators," *Journal of Aircraft,* vol. 31, no. 3, pp. 542-547, 1994.

[18] C. S. Jang, J. C. Ross and R. M. Cummings, "Numerical investigation of an airfoil with a Gurney flap," *Journal of Aircraft Design,* vol. 1, pp. 75-88, 1998.

[19] C. S. Jang, J. C. Ross and R. M. Cummings, "Computational evaluation of an airfoil with a Gurney flap".

[20] P. Giguere, J. M. Lemay and G. Dumas, "Gurney flap effects and scaling for low-speed airfoils," in *13th Applied Aerodynamics Conference*, San Diego, California, 1995.

[21] R. Myrose, I. Heron and M. Papadakis, "Effects of Gurney flaps on a NACA 0011 airfoil".

[22] R. Myrose, I. Heron and M. Papadakis, "Gurney flap experiments on airfoils, wings, and reflection plane model," *Journal of Aircraft,* vol. 35, no. 2, pp. 206-211, 1998.

[23] R. Myrose, I. Heron and M. Papadakis, "The post-stall effect of Gurney flaps on a NACA0011 airfoil".

[24] D. R. Jeffrey, "An investigation into the aerodynamics of Gurney flaps," 1998.

[25] S. Jain, N. Sitaram and S. Krishnaswamy, "Computational Investigations on the Effects of Gurney Flap on Airfoil Aerodynamics," *International Scholarly Research Notices,* 2015.

[26] M. Kheir-aldeen and A. Hamid, "Experimental Study to the Effect of Gurney Flap on the Clark Y-14 Airfoil Wing Model," *International Journal of Innovation and Scientific Research,* vol. 9, no. 1, pp. 120-132, Sep. 2014.

[27] M. A. Cavanaugh, P. Robertson and W. H. Mason, "Wind Tunnel Test of Gurney Flaps and T-Strips on an NACA 23012 Wing," *Aerospace and ocean engineering,* 2008.

[28] E. Tejnil, "Computational investigation of the low speed S1223 airfoil with and without a gurney flap," 1996.

[29] J. A. Cole, A. Vieira, O. Coder, J. Premi and M. D. Maughmer, "Experimental Investigation into the Effect of Gurney Flaps on Various Airfoils," *Journal of Aircraft,* vol. 50, no. 4, pp. 1287-1294, 2013.

[30] X. He, J. Wang, M. Yang, D. Ma, C. Yan and P. Liu, "Numerical simulation of Gurney flap on SFYT15thick airfoil," *Theoretical & Applied Mechanics Letters,* vol. 6, pp. 286-292, 2016.

[31] M. G. Meena and K. Taira, "Low Reynolds number wake modification using a Gurney flap," in *55th AIAA Aerospace Sciences Meeting*, Grapevine, Texas, 2017.

[32] J. Shah, A. Sciacchitano and S. Pröbsting, "Investigation of aeroacoustics and flow dynamics of a NACA 0015 airfoil with a Gurney flap using TR-PIV," in *18th International Symposium on the Application of Laser and Imaging Techniques to Fluid Mechanics*, Lisbon, Portugal, 2016.

[33] P. Yan, S. Han, Y. Liu, L. Gao and L. Li, "Effects of Gurney Flap and Trailing-Edge Wedge on a Blunt Trailing-Edge Aerofoil," in *International Conference on Renewable Power Generation*, Beijing, China, 2015.

[34] Y. Amini, H. Emdad and M. Farid, "Adjoint shape optimization of airfoils with attached Gurney flap," *Aerospace Science and Technology,* vol. 41, pp. 216-228, 2015.

[35] L. Brown and A. Filippone, "Aerofoil at low speeds with Gurney flaps," *THE AERONAUTICAL JOURNAL,* vol. 107, no. 1075, pp. 539-546, 2003.

[36] F. M. White, Fluid Mechanics, 7th ed., McGraw-Hill, 2008, p. 30.

[37] M. Athadkar and S. Desai, "Importance of the Extent of Far-Field Boundaries and of the Grid Topology in the CFD Simulation of External Flows," in *9th IRF International Conference*, 2014.

[38] J. P. Murcia and Á. Pinilla, "CFD Analysis of Blunt Trailing Edge Airfoils Obtained with Several Modification Methods," *Revisita de Ingeniera,* no. 33, pp. 14-24, June 2011.

[39] R. Ma and P. Liu, "Numerical Simulation of Low-Reynolds-Number and High-Lift Airfoil S1223," in *Proceedings of the World Congress on Engineering*, London, 2009.

[40] D. C. Eleni, T. I. Athanasios and M. P. Dionissios, "Evaluation of the turbulence models for the simulation of the flow over a National Advisory Committee for Aeronautics (NACA) 0012 airfoil," *Journal of Mechanical Engineering Research,* vol. 4, no. 3, pp. 100-111, March 2012.

[41] J. C. Date and S. R. Turnock, "A Study into the Techniques Needed to Accurately Predict Skin Friction Using RANS Solvers with Validation Against Froudes's Historical Flat Plate Experimental Data," 2009.

[42] G. Kalitzin, G. Medic, G. Iaccarino and P. Durbin, "Near-wall behavior of RANS turbulence models and implications for wall functions," *Journal of Computational Physics,* vol. 204, pp. 265-291, 2005.

[43] S. Jain, N. Sitaram and S. Krishnaswamy, "Effect of Reynolds Number on Aerodynamics of Airfoil with Gurney Flap," *International Journal of Rotating Machinery,* Aug. 2015.

[44] F. R. Menter, "Two-equation eddy-viscosity turbulence models for engineering applications," *AIAA Journal,* vol. 32, no. 8, pp. 1598-1605, 1994.

[45] J. E. Bardina, P. G. Huang and T. J. Coakley, "Turbulence Modeling Validation".

[46] J. E. Bardina, P. G. Huang and T. J. Coakley, "Turbulence Modeling Validation Testing and Development," 1997.

[47] T. Chitsomboon and C. Thamthae, "Adjustment of k-ω SST turbulence model for an improved prediction of stalls on wind turbine blades," in *World Renewable Energy Congress*, Linköping, Sweden, 2011.

[48] P. Catalano and M. Amato, "An evaluation of RANS turbulence modeling for aerodynamics," *Aerospace Science and Technology,* vol. 7, pp. 493-509, 2003.

[49] D. J. Mavriplis, "Three-dimensional high-lift analysis using a parallel unstructured multigrid solver," 1998.

[50] C. L. Rumsey and T. B. Gatski, "Recent turbulence model advances applied to multi element airfoil computations," *Journal of Aircraft,* vol. 38, no. 5, pp. 904-910, 2001.

[51] W. P. Wolfe and S. S. Ochs, "CFD Calculations of S809 Aerodynamic Characteristics," in *Proceeding 35th AIAA Aerospace Sciences Meeting and Exhibit*, 1997.

[52] F. Bertagnolio, N. N. Sørensen and J. Johansen, "Status for the Two-Dimensional Navier-Stokes Solver EllipSys2D," 2006.

[53] R. Chow and C. P. van Dam, "Computational Investigations of Deploying Load Control Microtabs on a Wind Turbine Airfoil," 2007.

Development of a microalgal automated cultivation system on *Tetradesmus obliquus*

Andres Philip Mayol, Aristotle T. Ubando, Emelina Mandia,
Dion Michael M. Mendoza, Edwin Sybingco, Alvin B. Culaba and Elmer Dadios

***Abstract*—An automation system for various applications has been proven to be effective in attaining productivity and efficiency. Moreover, it can be used in monitoring biological culture growth parameters. Microalgae have been a potential source of food, cosmetics, pharmaceutical, and fuel. However, monitoring the growth parameters of microalgae such as the pH level, salinity, dissolved oxygen, and its color density over time has not yet been achieved in previous studies. This paper presents an automated monitoring system for a closed microalgae photobioreactor. Contemporary continuous monitoring of bioprocesses can be challenging, considering parameters crucial to the growth of microalgae, such as pH and dissolved oxygen. Dissolved oxygen, pH, and salinity sensors are installed on the system and are programmed using LabVIEW to take measurements at regular intervals. The set-up includes a vision system to monitor the changes in the color of the solution, corresponding to the population growth of the microalgae cells. Optical density readings are also done to characterize the growth of the microalgae organisms to serve as a benchmark for the experiment results. The system is employed and tested on *Tetradesmus obliquus* (Turpin) M.J.Wynne species, also known as [syn. *Scenedesmus obliquus* (Turpin) Kützing]. Results show that the optical density readings increased at a value of 0.025 in day 1 to the value of 0.27 in day 27 and ended at 0.24 in day 29. This correlates with the increasing values of the RGB values. Hence, the development of a vision system can be used in monitoring algal growth with respect to its change of color.**

***Keywords*: Photobioreactor, Tetradesmus obliquus, microalgae, LabVIEW**

Andres Philip Mayol, Aristotle T. Ubando, and Alvin B. Culaba are affiliated with Mechanical Engineering Department; Center for Engineering and sustainable Development Research, De La Salle University, 2401 Taft Avenue, 0922 Manila, Philippine (e-mail: andres_mayol@dlsu.edu.ph; aristotle.ubando@dlsu.edu.ph; alvin.culaba@dlsu.edu.ph)

Emelina Mandia is affiliated with Biology Department, De La Salle University, 2401 Taft Avenue, 0922 Manila, Philippines (e-mail: emelinda.mandia@dlsu.edu.ph)

Dion Michael M. Mendoza and Edwin Sybingco are affiliated with Electronics and Communications Engineering Department, De La Salle University, 2401 Taft Avenue, 0922 Manila, Philippines (e-mail: dion_mendoza@dlsu.edu.ph; edwin.sybingco@dlsu.edu.ph)

Elmer Dadios is affiliated with Center for Engineering and sustainable Development Research; Manufacturing Engineering and Management Department, De La Salle University, 2401 Taft Avenue, 0922 Manila, Philippines (e-mail: elmer.dadios@dlsu.edu.ph)

I. Introduction

World population is tremendously increasing with the current estimated value of seven billion [1]. This event increased the demand for commodities such as food, water, and energy. However, these commodities do not meet the current population demand. Achieving sustainability of these commodities are the focus of stakeholders. One of the popular solutions proposed is to utilize microorganisms that produce high valued products, and one of these microorganisms is microalgae.

The use of microalgae for food, wastewater treatment, and energy has become a widespread research worldwide. Microalgae are a vast group of autotrophic, heterotrophic or mixotrophic organisms which have an extraordinary potential for cultivation as energy crops. They can be cultivated under difficult agri-climatic conditions and can produce a wide range of commercially interesting byproducts such as fat, oil, sugar and functional bioactive compounds [2]. As a group, they are of interest in the development of food sustainability and future renewable energy scenarios. In terms of land area required for cultivation, microalgae are also estimated to have much higher biomass productivity than other energy crops [3]. Aside from biodiesel, microalgae are potentially attractive

to a wide range of applications such as nutrition and waste water treatment.

Though many microalgae species are easy to reproduce and are relatively resilient to environmental factors, parameters such as pH and dissolved oxygen plays an important role in the growth of the organisms [4]. Extreme levels of pH and dissolved oxygen may result in a declined growth of most microalgae strains. To minimize this effect, commercial cultivation of microalgae on closed environments are mostly done on photobioreactors (PBRs). However, continuous monitoring of the culture conditions is still of utmost importance. The cultivation monitoring of microalgae can be tedious, time-consuming, and is prone to human errors. There are studies that used automation system to improve cultivation performance. Nucleic biosensors were already being used in monitoring phytoplankton in the ocean. [5] Lens-free shadow imaging systems (LSIS) have been used to monitor the floc size analysis using an image sensor. [6] In this study, a web camera will be used to capture images of the photobioreactor set-up. Studies have shown that the use of web camera is viable in finding parameters such as the height of the water level as well as in relating the growth of the organisms with image features such as RGB and grayscale values is feasible. [7] Quantification of microalgae biomass using digital image processing also yielded positive results [8] Automation system was used in the preparation of the algal culture medium, illumination, and control of carbon dioxide (CO_2) condition in optimizing microalgae production conditions [9].

However, there is still research gap in the continuous monitoring of the growth of the algal species in terms of algae density with respect to time and its growth parameters such as the pH level, salinity, and dissolved oxygen. Hence, this paper discusses the implementation of a vision system in which the color of the microalgae is monitored with respect to its growth. The objective of this paper is to create a system that monitors the pH, dissolved oxygen, and the color of the algae instantaneously online while observing the algal growth via optical density analysis. The temperature was monitored manually using a thermometer that was dipped inside the reactor. The data gathered in this study can be used to predict the growth of *Tetradesmus obliquus* in a real time setting. Moreover, we can compare this to a study where we inject CO_2 to the algal species while monitoring it real time.

II. AUTOMATED SYSTEM

The methodology of the automation system is of the following: 1) Microalgae Culture, this discusses the nature of the microalgal species used in this study and where it was gathered. Moreover, in this subsection, the overall conditions of the reactor are also discussed., 2) Data monitoring system, this subsection discusses the schematic procedure of the automated system which is used to gather data in real time situation. Table 1 shows the materials and equipment that was used in the system.

TABLE I
Equipment and Specifications Used in the Study

Equipment	**Specification / Model**
Reactor	Measurement (0.61 m long x 0.30 m width x 0.40 m depth)
pH Sensor	Vernier PH-BTA pH Sensor
Dissolved Oxygen Sensor	Vernier DO-BTA dissolved oxygen probe
Salinity sensor	Vernier SAL-BTA salinity probe
Data Acquisition System	LabQuest Data Aquisition
Data Acquisition Software	LabView National Instruments
Light Meter	EXTECH Instruments Easyview ™ 30 Light meter
Optical Density	GENESYS 10 UV spectrophotometer
Culture Media	TMRL

A. Microalgae Culture

The experiment made use of *Tetradesmus obliquus*, a planktonic green alga isolated from Carmona River, Binan, Laguna within the vicinity of the De La Salle University-Science and Technology Complex. The mother cultures were grown for a month in TMRL medium at ambient temperature of 22°C and light intensity of 40µmol $m^{-2}s^{-1}$ continuously provided by cool-white LED fluorescent tubes. *T. obliquus* cultivation was carried out in a photobioreactor (PBR) containing 16L of TMRL culture medium and 10% inoculum. The PBR (0.61 m long x 0.30 m width x 0.40 m depth) was constructed of fiber-glass material fitted with sensors. Mixing of the microalgae and culture medium within the PBR was accomplished using an air compressor that introduced air through spargers. The set-up was observed for 29 days.

B. Data Monitoring Set-up

The automation system consisted of the following: 1) The Tank for microalgae culture, 2) Data Acquisition, 3) Computer LabView Software, 4) sensors (pH, Dissolved Oxygen,Salinity), and 5) image and video collection for image processing. Fig. 1 shows the schematic diagram of the overall experimental setup and Fig. 2 shows the actual experimental set up of the data monitoring system of the algal cultivation system.

Introducing artificial light source to the microalgal species for photosynthesis, a cool-white 16 W fluorescent lamp was used that provides light at an intensity of 2500 lux that was measured using EXTECH Instruments Easyview ™ 30 Light meter and had cycles 15 h light / 9 h dark. The fluorescent lamp was positioned at the front side view of the reactor which has a surface area of 0.244 m^2. The location of the reactor was covered to keep the effect of other light sources to a minimum.

Measuring the value of the dissolved oxygen, salinity, and pH value of the culture system over time sensors were used and are integrated in the data acquisition system. This ensures that the growth environment of the culture is stable with respect to the culture's growth conditions. The tip of the dissolve oxygen, salinity and pH sensors were dipped 10 mm from the surface of the water. Calibration of the sensors was first conducted before their actual use to ensure the accuracy of the data acquired from the developed automated system. Labquest Mini served as the interface to gather data from the sensor, and transfer them to the computer. The sensors measured the three parameters in real-time and were programmed to get measurements at one-hour interval. The measurements were then saved as database in excel format. The dissolved oxygen sensor used can measure dissolved oxygen level from 0 to 15 mg/L and has a tolerance of 02 mg/L. The pH sensor can measure pH values from 0 pH to 14 pH units, which is the maximum range of values for pH. The salinity sensor can measure up to 50 ppt (50,000 ppm) and has an accuracy of

Relating algal growth (change of color) to its value when obtaining its optical density, a camera was used as pictures was taken this was processed using LabView software integrating it to the data acquisition system. Recording the color change of the culture strain over time, a camera was used to get the color value of the image which is RGB. The Camera was located five inches away from the reactor, facing the right-side view of the reactor which has a surface area of 0.1239 m^2. The camera was programmed to capture images and videos every hour for the duration of the experiment. The videos were recorded for five seconds at every interval of the video acquisition process. The images and videos were then stored on in specific folders in the computer. The images were saved in Joint Photographic Experts group (JPEG) format at a resolution of 800 pixels by 448 pixels, while the videos were saved in AVI (Audio Video Interleaved) format.

Monitoring the growth of the microalgal species, daily optical density readings at 750 nm wavelength were obtained using GENESYS 10 UV spectrophotometer. A daily optical density was taken for 29 days. There were three points in the reactor where the strain is collected. The optical density value of the three points where then averaged and graphed using Microsoft excel software. Lastly, temperature readings are then recorded manually using a thermometer that is dipped into the reactor.

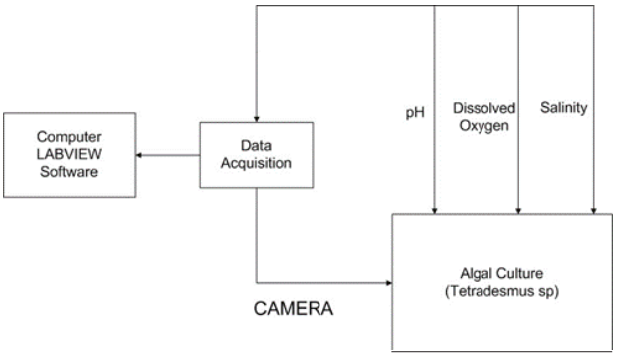

Fig. 1. Schematic diagram of the experimental set-up.

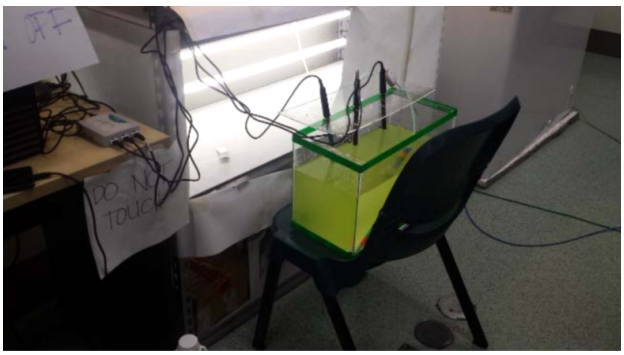

Fig. 2. The actual set-up of the experiment.

III. RESULTS AND DISCUSSIONS

The implementation of an automation system in monitoring a microalgal photobioreactor system was conducted. Dissolved oxygen, pH, and the factors affect the algal growth. Moreover, video and images was captured for images processing using LabView.

The growth of the microalgal species was monitored for 29 days via optical density. Moreover, the algal samples that were taken in the photobioreactor had three replicates; Fig.3 shows the growth curve of the microalgal species. The curve indicates that there is a gradual growth of the species. We can see that from the value of 0.025 in day 1 it increased to the value of 0.27 in day 27 and ended at 0.24 in day 29.

Based on the data acquired, it is observable that the values on day 0 for pH of the culture is higher than the latter days. However, from day 1 onwards, the values of pH normalize. For the rest of the duration of the experiment, the value of pH fluctuates to a maximum of 9.5% from the median which is 8.0135.

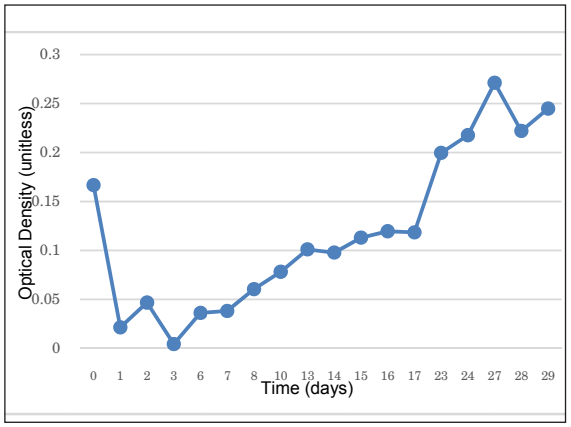

Fig. 3. Optical density growth curve of *Tetradesmus obliquus*.

The highest pH level was acquired on day 23 at a value of 8.7785, while the lowest level of pH was acquired on day 1, which is 7.5175. The highest temperature recorded is 25.4 degree Celsius, taken at day 10, whereas the lowest temperature is recorded on day 29, at a level of 22.5 degree Celsius. The median temperature for the duration of the experiment is 24.5 degree Celsius. The median of the dissolved oxygen values, on the other hand, is 0.6785 mg/L, whereas 0.7190 mg/L and 0.6380 mg/L are the highest and lowest recorded values respectively, taken at day 29 and day 7.

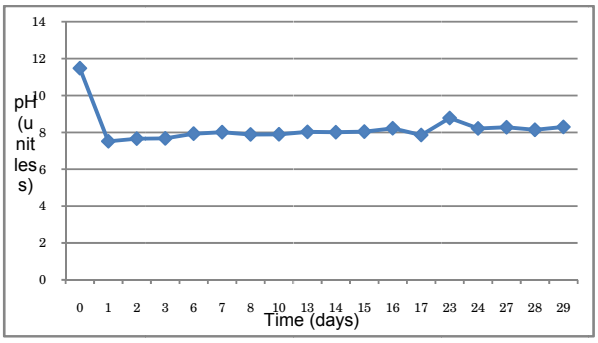

Fig. 4. The resulting pH level versus time.

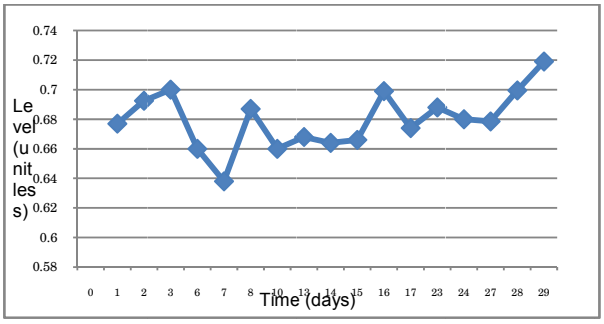

Fig. 5. The resulting dissolved oxygen versus time.

The images captured were processed through an algorithm executed using LabView. The algorithm allows the researchers to select a region of interest on the series of pictures taken by the web camera, extracting the RGB features of the image. The images captured in the daylight cycle; *i.e.,* when the light source is on, are used as the samples for the program. Images in which the culture is not well-mixed is also removed to prevent erroneous results.

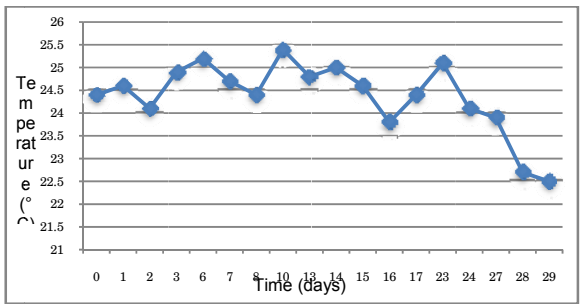

Fig. 6. The temperature versus time (in days).

Based on the data gathered, the RGB levels of the culture changes as the microalgae thickens. The green component of the images has a level that is noticeably higher than the red and blue values. As time passes,

the RGB values vary, but in all of the images that are used as samples, the green component is always higher than the red and blue components, which is akin to the green tint of the culture. A more appropriate observation is that as the days pass, the red and blue component of the images taken diminishes at a faster rate than the green component. However, the growth of the microalgae are not well-represented by the changes in the RGB values due to the variation of the image features used as samples. Changes in camera position, as well as with the tank orientation, can result to discrepancies in image features; *i.e.,* different image brightness, different image perspectives. A more appropriate parameter to consider in this matter would be the difference between the red and blue levels with respect to the green levels.

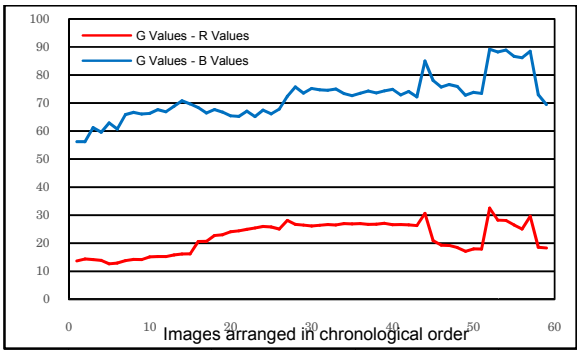

Fig. 7. The RGB values and their differences.

As shown in Fig. 7, it can be observed that the difference between the red and blue level with respect to the green level of the images is increasing as the time passes. It affirms the decreasing values of red and blue components of the culture in comparison with the green color component.

By visual inspection of the videos taken by the system, the bubbles caused by the aeration of the air pump can be observed. It was also observed that as the solution becomes darker, the bubbles become less visible. From day 8 onwards, the bubbles are no longer visible on the web camera when the culture is well-mixed.

IV. CONCLUSION

An automated monitoring system for closed bioreactors has a huge potential when it comes to the commercial production of microalgae. The use of vision system on the set-up can be a potential substitute to optical density readings. The changes in the pigment of the culture constitute to the population of the organisms. However, based on the optical density readings, a very high growth rate of the *Tetradesmus obliquus* is not observed and can be further be explored in future studies.

The videos that are recorded by the system can be used for analysis of the bubbles. Algorithms for tracking such as mean-shift and Kalman filter can be implemented to the system to analyze the behavior of the bubbles as the culture grows. However, the visible observation of the pattern of the bubbles gets harder as the solution darkens. Without supplemental image processing algorithms, analysis of the bubbles may not be viable.

After analysis of the captured images, it can also be concluded that the green pigment of the culture is caused not by the increase of the green component of the algae, but rather by the diminishing red and blue levels, resulting to a greener culture pigment. Although the green component of the images also varies, the rate at which it increases or decreases is different with the changes in the red and blue components. As the culture darkens, the RGB level decreases, however, the red and blue levels decrease at a faster rate. The general decrease of the RGB level results to a darker culture, while the faster rate of decrease in the blue and red level with respect to the green level results to the green pigment of the culture.

For future work, several points can be improved. The number of aerators can be increased to ensure that the solution is well agitated and the organisms will not settle at the bottom of the tank. Changing the design of the tank may also be feasible, to allow better circulation of the microalgae in the culture. Further isolation of the system can also be done to eliminate the effect of other light sources completely. Securing the web camera to prevent any changes on its orientation can be done to avoid changes in image perspective. Isolation of the system from light sources and securing the web camera position will preserve the homogeneity of the images captured by the web camera and may account to better parallel analysis of the images. This means that direct analysis of the RGB levels of the captured images alone may become sufficient. Further processing of the images can also be done. Extraction of the brightness levels can supplement the RGB levels for better analysis of the sample images.

ACKNOWLEDGEMENTS

This research was funded by the University Research Coordinating Office (URCO) Interdisciplinary Research Project with the project number 03IR3TAY14-3TAY15 of De La Salle University. Acknowledgement also goes to the USAID STRIDE CARWIN funding with the fund number 0213997-G-2016-012-00 for research engagement with the Philippine algae industry.

REFERENCES

[1] Dadax, "World Population Clock," [Online]. Available: www.worldometers.info/world/population. [Accessed 25 November 2016].

[2] K. Chew, J. Yap, P. Show, N. Suan, J. Juan, T. Ling, D.-J. Lee and J.-S. Chang, "Microalgae biorefinery: High value products perspectives," *Bioresource Technology,* vol. 229, pp. 53-62, 2017.

[3] J. Pittman, A. Dean and O. Osundeko, "The potential of sustainable algal biofuel production using wastewater resources," *Bioresource Technology,* vol. 102, no. 1, pp. 17-25, 2011.

[4] Y. Liang, N. Sarkany and Y. Cui, "Biomass and lipid productivities of Chlorella vulgaris under autotrophic, heterotrophic and mixotrohic growth conditions," *Biotechnology,* vol. 31, no. 7, pp. 1043-1049, 2009.

[5] Katja Metfies, Sonja Diercks, Friedhelm Schröder, Wilhelm Petersen, Thomas Hanken, "Automated Nucleic Biosensors – A Key to High Resolution Monitoring of Marine Phytoplankton," *IEEE,* 2009.

[6] Dongmin Seo, Mohendra Roy, Jaewoo Kim, Kiyoung Ann, Yongha Hwang, Yeon Hwa Kwak, Sangwoo Oh, Moonjin Lee, Jae Woo Lee, Sungkyu Seo , "High-throughput and real-time microalgae monitoring," *IEEE,* 2015.

[7] YoungHoon Na, Sin Kim, Jietae Lee, Ho-sung Yoon, "Web Cam for Easy-Monitoring of the Growth of Organisms," in *International Conference on Control, Automation and Systems*, Kimdaejung Convention Center Gwangju, Korea, 2013.

[8] H.-J. L. J.-Y. L.-M. O. MohammadH. Sarrafzadeh, "Microalgae biomass quantification by digital image processing and RGB color analysis," *Journal of Applied Phycology,* vol. 27, no. 1, pp. 205-209, 2014.

[9] A. Radzun, J. Wolf, G. Jakob, E. Zhang, E. Stephens, I. Ross and B. Handkamer, "Automated nutrient screening system enables high-throughput optimization of microalgae production conditions," *Biotechnology for Fuels,* vol. 8, no. 1, p. 65, 2015.

Portable Water Purification System using Electrodialysis Reversal

Ira C. Valenzuela and Ronnie O. Serfa Juan

***Abstract* - The quality of drinking water is one of the factors that people consider before drinking it. Water is usually exposed to various organic and inorganic substances that are possibly harmful to one's health. The main objective of this study is to develop a water purification system using electrodialysis reversal that can be carried in remote or rural areas and can be powered either by AC supply or solar energy. This system provides an easy way to treat brackish water by using electrodes and current to mitigate the impurities, including the bacteria present in the contaminated water. It is mainly composed of the power supply, photovoltaic cell, battery, treatment and test tanks, electrodes, carbon and resin filters, LCD display, numeric keypad and microcontroller. Three (3) microbiological tests are performed to determine the quality of water produced namely: fecal coliform, total coliform test and heterotrophic plate count test. Through a series of experiments with the support of an accredited Department of Health (DOH) water testing laboratory, it is proven that an hour of treatment is enough to produce five (5) gallons of potable water.**

***Index Terms*: electrodialysis reversal, mobile water purifier, solar power, potable water**

I. Introduction

The surface of earth is comprised of about 70.9% of water [1]. Odorless, tasteless, and clear liquid are the characteristics of a pure water that is essential for mankind. Water also conttributes to good health because it is needed for the digestion and absorption of food. It also helps for proper toning of muscles, for supplying oxygen and nutrients to the cell, and for serving as a natural air conditioning system which is why the health personnel recommends drinking eight glasses of water daily.

Ira C. Valenzuela and Ronnie O. Serfa Juan are affiliated with Electronics Engineering Department, Technological University of the Philippines, Manila (e-mail: ira_valenzuela@tup.edu.ph)

Drinking water is classified as potable water which is fit for consumption by human. Usually, water is naturally potable if it comes from unspoiled sources. But if one is not sure if the water is safe for drinking, laboratory tests should be done to see if there are contaminants present in the water.

There are people who drink water from inadequate sources due to desperation. Contaminated sources of drinking water which contains high level of pathogens and heavy metals are the main cause of illnesses and high risk of death. Water might contain unacceptable level of toxins since it is known for being a universal solvent. Drinking unsafe water is one of the world's major problems.

Several studies regarding water purification have been conducted to develop new water treatment techniques and methods that can provide clean drinking water to people living in remote areas such as Proportional-Integral-Derivative (PID) Control, Microwave Plasma UV Lamp, vacuum filtration, electric discharge and packed bed reactor. PID Control helps in regulating the pH of water, the clarity and the presence of micro-organisms in water [2]. Microwave Plasma UV Lamp emits light which destructs most waterborne bacteria and viruses. Conventional lamps are limited to a maximum output power of 30W per meter while MPUVL can deliver any amount of power per unit length and tube can any be of any shape, length, or diameter [3]. Two-dimensional graphene oxide (GO) membrane with their ultrafast permanence, outstanding mechanical properties, and high chemical stability is used for water purification process and fabricated by vacuum filtration [4]. Use of electric discharge and packed bed reactor is focused on removing *Escherichia coli* (E. coli) [5][6].

The main objective of this study is to develop a portable and solar-powered water purifier system using electrodialysis reversal. Specifically, it aims (1) to design a control system for an effective water purifier system; (2) to develop a water purifier system that can produce potable water; and, (3) to measure the

parameters required for the water output to be potable through an accredited DOH water testing laboratory.

Today, there is a global effort to keep the environment free of pollution. An adequate supply of pure water is absolutely essential to human existence. Therefore, maintaining and providing clean, purified and disinfected water is a top priority. This study presents the electrodialysis reversal as a process for water purification.

II. RESEARCH BACKGROUND

In the electro dialysis reversal process, an electrical current is transmitted directly between electrodes through the electrolytic channel: water. Electrical charge has been used to isolate minerals from other elements that are present in the water [7]. The resulting ions are transferred through the membranes from a less concentrated to a more concentrated solution. Varying the amount of electric charge causes the removal of the dissolved solids in the water. Using electro dialysis reversal, it can remove or separate sediments present in water. Periodically, the direction of ion flow is reversed by reversing the polarity applied electric current. The success of the study depends on having good and reliable electrodes. In this study, aluminum was used as electrode. Aluminum is non-corrosive, cheaper in price compared to others like graphite or nickel coated galvanized iron, and it has abundant supply in the market. The project has a timer to control how much time is needed for the water to undergo on the process of electrodialysis.

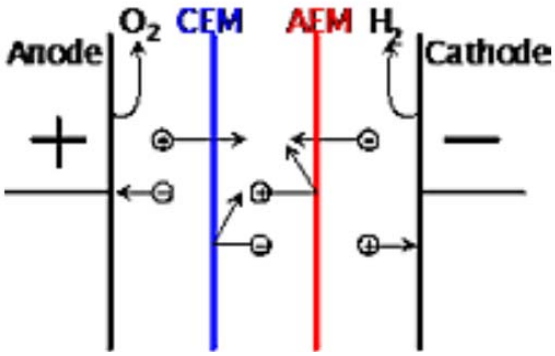

Fig. 1. Electrodialysis Reversal (EDR) process diagram [7]

In order for the electrodialysis reversal process to take place, non-corrosive rods are preferably used, such as aluminum and graphite. Aluminum is ideal to use due to low cost and are readily available in the market, Graphite rods are considerably expensive and hard to find in the market since graphite rods are scarce and consumers prefer Aluminum. Two electrodes will be used for the anode and cathode. These electrodes will be placed into the liquid. These electrodes are connected in a DC source such as a battery or a direct current generator. As the current flows through the electrolytic cell, chemical changes take place at the surface of the electrodes. At the cathode, the electrolyzed liquid combines with electrons supplied by the battery. This process is called reduction. At the anode, the liquid gives electrons to the anode. This process is called oxidation.

Electrodialysis reversal has been used in determining the effects of ion current rectification on energy harvesting [8]. Based on this study, the power efficiency from the electrolyte gradient has improved. For mixing waters with different salinity, reverse electrodialysis has been used [9]. It is noted that power generation is possible even in high concentration. Reduction of the discharge problem of polymer-flooding that produced water through electrodialysis reversal has been reported in the study of [10]. In a review conducted by [11], electrodialysis reversal has been considered economic when used in purifying water compared to reverse osmosis and electrodialysis. Also, clean microenergy generation has been possible with the use of electrodialysis reversal [12].

The study covers the development of a portable, solar and electric powered water purifier using electrodialysis reversal. It is designed in producing safe and reliable potable water for every individual. It also has a time circuitry system to control the process depending upon the source of the water. The system is to be restricted by some conditions, namely the system cannot use water from excessive dirt places like drainage, flood and septic systems. It is only intended to purify water coming from deep well and tap water. However, the system of the project does not recognize the pH of the water.

III. RESEARCH DESIGN

Figure 2 shows the block diagram on water purification system. Brackish water or deep-well water will be placed in the container. Then it will undergo electro-dialysis reversal to dissolve the unwanted solids in the water. The output produce a safe drinking water.

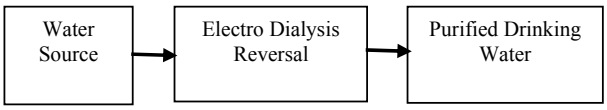

Fig. 2. Water Purification System using EDR

The block diagram of the system is shown in Figure 3. The system is solar-powered so that it can be moved in different places even if there is no available on-grid power supply. The microcontroller will control the overall function of the system to provide clean water.

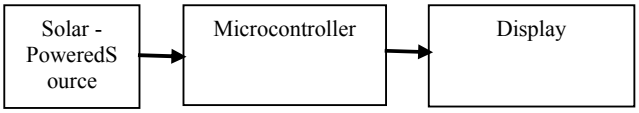

Fig. 3. Block Diagram of the System

A. Hardware Development

The circuit designing is one of the crucial steps in the development of the project because this is about interfacing the electronic components particularly, the six major devices which are PIC16F877A Microcontroller, Pumps, Electrodes, 16x2 LCD, battery and solar panel. After the circuit design is finalized, Trax Maker is used to fabricate the printed circuit board. The schematic diagram and the PCB layout for the PIC16F877A Microcontroller and Relay section are shown in Figure 4 and Figure 5 respectively.

The aesthetics of the entire project is the least priority however, there is still a need for a new or innovated product to be out in the market for commercial purposes. Aesthetics is about making the project look good and presentable. Also, portability is a factor needed to be justified in this device since it is intended to be easily carried and brought anywhere. The image of the actual prototype is shown in Figure 6.

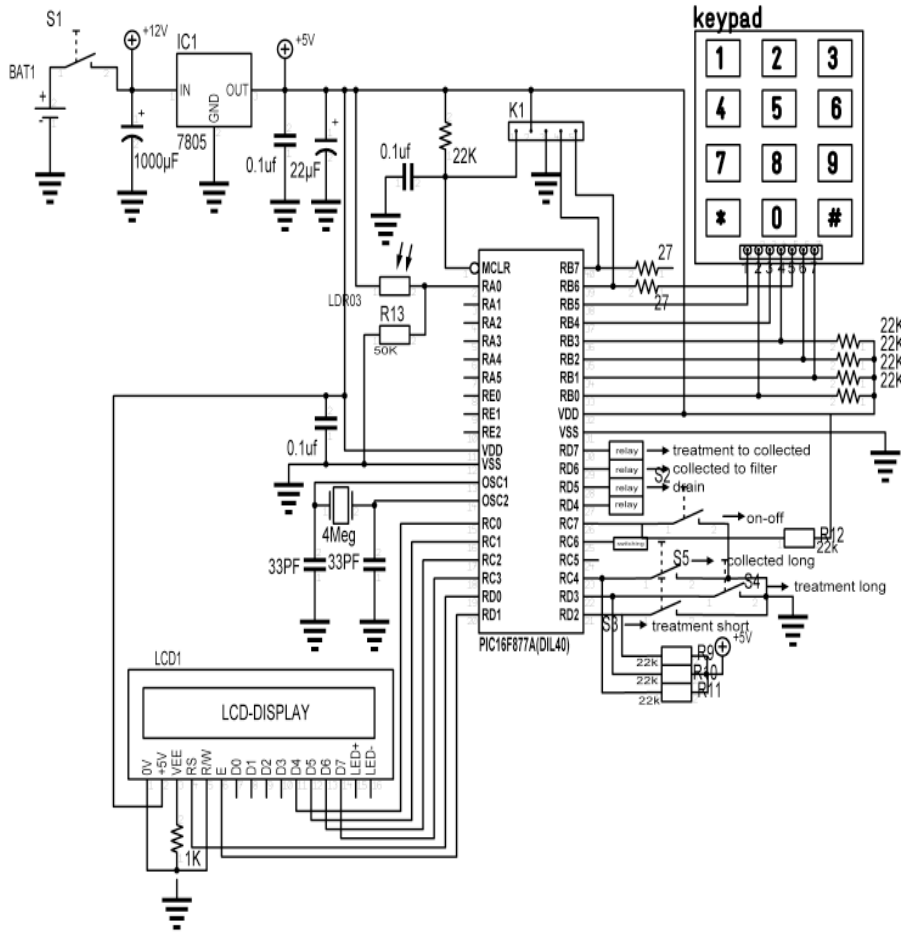

Fig. 4. MicrocoC2ntroller Circuit Design

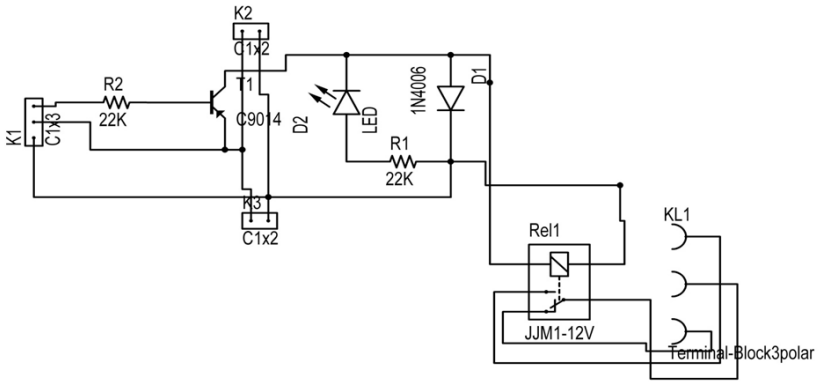

Fig. 5. Relay Schematic Diagram

Fig. 6. Actual Prototype

B. Software Development

PIC16F877A Microcontroller is used as the brain of the whole project. Assembly Language is used to control and regulate all the functions and behaviors of the electronic system of the project. Pic kit is the software used in encoding and burning the project's program codes.

Figure 7 shows the process flowchart. The first step to operate the project is to fill the container with five gallons first. Then a time option will appear in the LCD to set the time depending on the type of water (15mins, 30mins, 60mins, and custom time). It can also be interrupted by pressing the interrupt button and proceed to the next step with an option (Transfer water, treat again and Drain). If the transfer water is selected, the first pump will transfer the purified water to the other container. When the second container is filled with the purified water, then it is ready to dispense and will flow in the filter for filtration process. If treat again is selected, the operation will start from the start again. And if Drain is selected, the second pump will transfer the water to the disposal container.

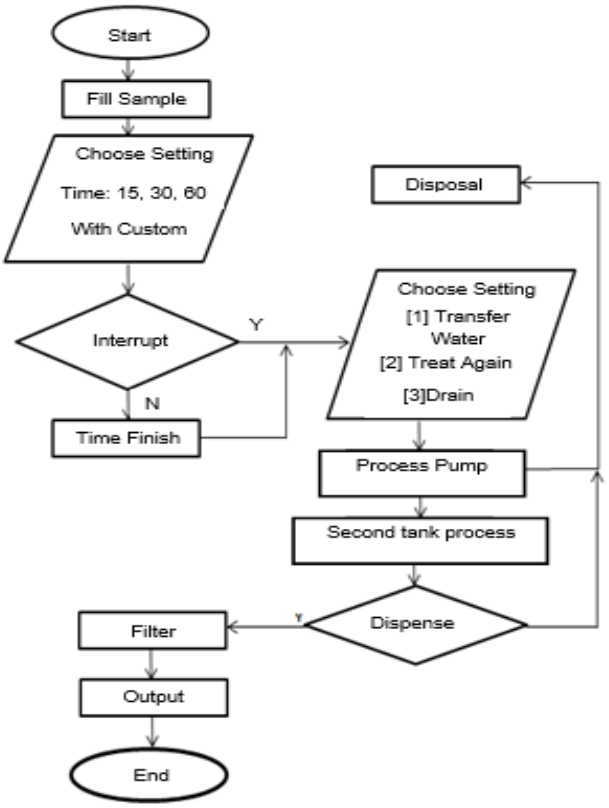

Fig. 7. Program Flowchart

C. Experiment Setup

The brackish water is obtained from the deep-well source. It was put in the container and the floater indicates if the water placed is about 5 gallons. Three

different water samples are treated under the changing polarity for 15 minutes, 30 minutes and 60 minutes. Then, it passed through carbon and resin filters for water softening. The produced water is brought in the Department of Health for laboratory testing. The tests performed are total coliform test, fecal coliform test and heterotrophic plate count. These was compared to the Philippine National Standard on Drinking Water standards.

Also, charging time and discharging time for battery are measured and compared with ac source.

IV. Results and Discussion

In order to compare and evaluate the performance of the project, several experiments have been made. Shown below are the results of all the experiments: All microbiological test results, over all system microbiological test results, and voltage measurement of battery using solar panel and alternating current.

Tables 1 and 2 are the qualitative results of the water testing laboratory that tested the untreated water and the processed water of the prototype. It comprises of the three analysis that are prescribed by the Philippine National Standard for Drinking Water (PNSDW) to determine the potability of the water.

The first test is the Total Coliform test. This test determines the presence of coliform bacteria such as E.coli, as well as other types of harmful bacteria that are naturally found in soil.

Secondly, the Fecal Coliform test. This test indicates the potential presence of pathogens as well as human wastes and animal wastes that has been dissolved on the water.

Lastly is the HPC test or the Heterotrophic Plate Count test. It determines the ability of the water to culture colony formation of the bacteria. From the data that has been gathered upon performing experiments, it can be concluded that the longer the time the water is treated by using the prototype, it eradicates harmful elements that are present on the water and the prototype is efficient and has the capability to produce processed water that can meet the standards of the Philippine National Standard for Drinking Water.

TABLE 1
All Microbiological Tests

		Results (MPN/100mL)					
Analysis	PNSDW Limit (MPN/100mL)	Raw Water	Filter	OS @ 15 mins.	OS @ 30 mins.	OS1 @ 60 mins.	OS2 @ 60 mins. (EDR)
Total Coliform	less than 1.1	>8.0	2.6	4.6	<1.1	<1.1	<1.1
Fecal Coliform	less than 1.1	>8.0	2.6	4.6	<1.1	<1.1	<1.1
HPC	less than 500 CFU/ mL	> 6 0 0 0 CFU/ ml	>3000 CFU/ ml	> 6 0 0 0 CFU/ ml	> 3 0 0 0 CFU/ ml	4 CFU/ml	20 CFU/ml

TABLE 2
Over All System Microbiological Test Results

Time (mins.)	Total Coliform	Fecal Coliform	HPC
15	4.6	4.6	>6000 CFU/ml
30	<1.1	<1.1	>3000 CFU/ml
60	<1.1	<1.1	4 CFU/ml

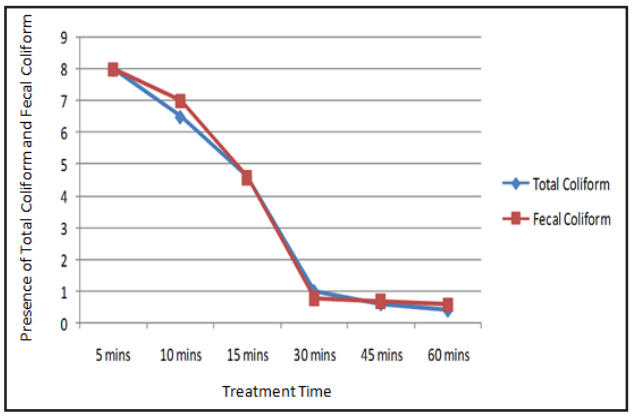

Fig. 8. Total Coliform and Fecal Coliform Comparison versus time

Figure 8 illustrates that the treatment time is indirectly proportional to Total Coliform and Fecal Coliform. It shows that the longer the electrodialysis reversal treatment process is applied to the raw water, the bacteria present on the water can be further removed.

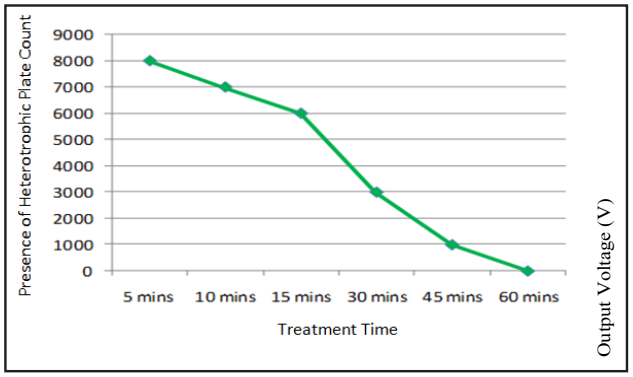

Fig. 9. Heterotrophic Plate Count versus time

Figure 9 shows that the longer the electrodialysis reversal treatment process is applied to the raw water, the accumulation of the colony or the Heterotropic Plate Count of the bacteria present on the water can be further removed. Heterotropic Plate Count is the ability of the water to culture colony formation of the bacteria.

TABLE 3
VOLTAGE MEASUREMENT OF BATTERY USING SOLAR PANEL AND ALTERNATING CURRENT

Medium Of Charging	Measured Voltage		Charging Duration
	Before	After	
Solar Panel	4.2	12	12hours
	3.4	12	12 hours 14mins.
AC	4.2	12.3	8hours 30 mins.
	3.4	12.1	7 hours 50mins.

Table 3 are the parameters acquired by performing experiments on how long the average charging time of the battery using the solar panel source versus the Alternating Current (AC) source. From the results acquired, it shows that the battery can be charged faster than by using the Alternating Current (AC) source.

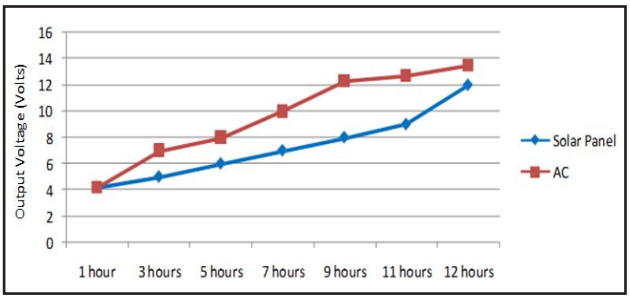

Fig. 10. Trial No. 1 - Solar Panel and AC Charging Comparison

Figure 10 is the first trial of the comparison of the charging time of the battery. It illustrates the graphical representation of the charging time of the battery by using the Alternating Current (AC) source and the Solar Panel. The graph depicts that when it comes to charging time, the Alternating Current (AC) source is much faster than the Solar Panel. By charging the battery using the Alternating Current (AC) source, the maximum output voltage of the battery can be obtained much faster compared to solar panel.

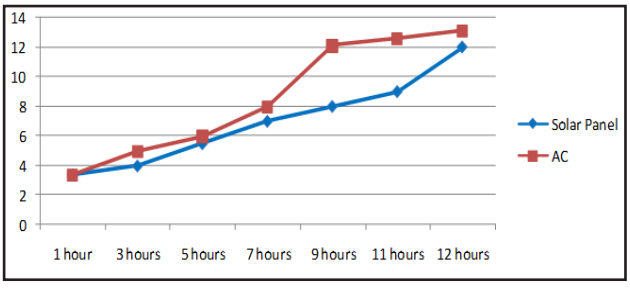

Fig. 11 Trial No. 2 – Solar Panel and AC Charging Comparison

Figure 11 is the second trial of the comparison of the charging time of the battery. Same results have also been acquired as compared to the 1st trial. It still shows that the battery can be charged much faster by using the Alternating Current (AC) source as compared to the Solar Panel.

V. CONCLUSION

Based on the results of the study, the following conclusions were derived. A portable, solar and electric powered water purifier system using Electrodialysis Reversal was developed and proved experimentally that the whole system works well with the help of a water testing laboratory that is accredited by the Department of Health. The project has successfully met the parameters required by the Department of Health and the Philippines National Standard for Drinking Water. The reliability and efficiency of the project has also been successfully verified with the help of these parameters. The PIC16F877A microcontroller was effectively interfaced to the relays, numeric keypad and to the whole circuitry. The microcontroller was proven effective given that the whole system worked well and no problems were encountered. The control system was also proven to be effective in view of the fact that the water purifying process worked well and produced water that can be consumed by humans.

ACKNOWLEDGMENT

The authors would like to thank all the scientists that extended their help in the completion of this study.

REFERENCES

[1] Retrieved from http://flowingdata.com/2010/04/01/discuss-drinkable-water-in-the-world [Online]

[2] N. Mehendale, O. Sharma, S. Shah and S. Vishwakarma, "Metropolitan water tank pollution monitoring and purification using PID control", *2016 International Conference on Communication and Signal Processing (ICCSP)*, 2016.

[3] A. Al-Shamma'a, I. Pandithas and J. Lucas, "Low pressure microwave plasma UV lamp for water purification and ozone production", *PPPS-2001 Pulsed Power Plasma Science 2001. 28th IEEE International Conference on Plasma Science and 13th IEEE International Pulsed Power Conference. Digest of Papers (Cat. No.01CH37251)*.

[4] Jin Hyeok Jang, Ju Yeon Woo, Jaeyeol Lee and Chang-Soo Han, "Ultrathin graphene oxide membranes for water purification", *2015 IEEE 15th International Conference on Nanotechnology (IEEE-NANO)*, 2015.

[5] V. Goryachev, P. Rutberg, A. Ufimtsev and V. Korobochko, "Electric discharge method of water purification from microbe and chemical contamination", *MELECON '98. 9th Mediterranean Electrotechnical Conference. Proceedings (Cat. No.98CH36056)*.

[6] Y. Takeda, H. Kurita, Y. Taino, K. Takashima, H. Yasuda and A. Mizuno, "Water purification using a packed bed reactor", *2015 IEEE Industry Applications Society Annual Meeting*, 2015.

[7] Retrieved from http://www.professorh2o.com/Electrodialysis-Reversal-EDR--1667 [1]

[8] Wang, C., Choi, E., Yang, G.T., and Park, J. "Effect of Ion Current Rectification on Energy Harvesting by Reverse Electrodialysis," in 29th International Conference on Micro Electro Mechanical Systems (MEMS), Shanghai, 2016.

[9] Chang, H.K., Choi, E., Lee, J.H. and Park, J. "Paper Based Reverse Electrodialysis Power Generator," in 18th International Conference on Solid-State Sensors, Actuators and Microsystems (TRANSDUCERS), Anchorage, 2015.

[10] Goulin, J., Yang, L., Tan, Z., and Chunjie, H., " Reclamation of the Polymer-Flooding Produced Water," in 2nd International Conference on Bioinformatics and Biomedical Engineering, Shanghai, 2008.

[11] Tabors, R., Nagendrapsad, S., and Brant, J., "The Manufacture of Potable Water: case analyses of Electric System Alternatives," in 45th Hawaii International Conference on System Sciences, Maui, 2012.

[12] Choi, E., Kwon, K., Kim, D., and Park, J., " Ion Transportation Control in Nanofluidics through Geometrically Controlled Nanoparticle Assembly," in 14th International Conference on Control, Automation and Systems, Gyeonggi-do, 2014.

Self-Adaptive WLAN Access Point for Optimizing Network Performance Using Multi-Objective Genetic Algorithm (MOGA)

Joel C. Delos Angeles and Elmer P. Dadios

***Abstract* — Current deployment of WLAN access points (AP) require manual configuration of wireless parameters. Wireless parameters are commonly set haphazardly without being aware of the basic wireless conditions. This paper proposes a self-adaptive AP based on genetic algorithms (GA). The AP adapts to interference and link quality of client stations. Interference is mitigated and client link quality is improved or optimized. A chromosome consists of genes of parameters such as frequency channel, channel width, maximum data rate, maximum transmit power, and guard interval. Often competing objectives such as mitigating interference, maximizing the data rate, and minimizing the error rates necessitate that the GA be multi-objective. The MOGA comes up with the fittest candidates by running them through a fitness function which scores the genes based on the survey scan of other interferer AP and the wireless performance statistics of client devices. The GA's chosen configuration is applied and its effect is continuously assessed. Finally, the result of the self-adaptive WLAN AP genetic algorithm is compared against the Linux hostapd Automatic Channel Selection scheme.**

***Index Terms*— access point, AP, IEEE 802.11n, WiFi, automatic configuration, interference, self-adaptive, genetic algorithm, GA, multi-objective, MOGA**

I. Introduction

WIRELESS devices have become so ubiquitous that there are now almost as many mobile phones as there are people in the world. Most people also own at least two mobile phones from different mobile operators for voice, short messaging service, and Internet use. Moreover, demand for Internet speed and reasonable cost of access resulted in mobile phones having multiple radio access technologies – such as mobile 2G/3G/4G and WiFi. The choice of which radio access technology to use when connecting to the Internet is driven by quality, cost, and availability resulting to what is called Heterogenous Networks (HetNets). In HetNets, access to the Internet does not converge to a single wireless access technology but instead takes advantage of the different wireless technologies available to the user. Users can even share their Internet access with other mobile phone users within their vicinity using hotspot tethering. In hotspot tethering, multiple devices connect, using WiFi or Bluetooth, to a primary device which accesses the Internet access via 3G or 4G. Direct wireless connection to a high-power base station tower is replaced with ad-hoc user-to-user connectivity and the primary device is said to act as a WiFi base station. Eventually, this trend could result to a new cellular paradigm shift where there will be more base stations than cellular phones [1].

Frequency Channel	Channel Setting	Max Data Rate	Max Transmit Power Reduction	Guard Interval
1 to 11 (or 13 in some AP)	HT20 or HT40+ or HT40-	MCS0 to 7 (or with 8 to 14 for HT 40 MHz)	in dB (to be subtracted from max tx power of AP)	400 or 800 nsec

Fig 1. Chromosome representation and example showing the wireless parameters available for manipulation by the GA. Note that transmit power reduction (in dB) is used for the gene instead of absolute unit of maximum power (in dBm) which varies from AP to AP

As the number of hotspots increase, new ways of managing spectrum use and interference are called for. Traditional methods of interference management like frequency reuse or base station coordination do not directly translate to HetNets [1]. Current hotspot

Joel C. Delos Angeles is affiliated with Electronics and Communications Engineering, De La Salle University - Dasmarinas, Dasmarinas City, Cavite, Philippines (e-mail: joel_delosangeles@dlsu.edu.ph)

Elmer P. Dadios is affilaited with Manufacturing Engineering and Management, De La Salle University - Manila, Manila, Philippines (e-mail: elmer.dadios@dlsu.edu.ph)

access point (AP) deployments are uncoordinated, particularly the choice of WiFi frequency channel in commercial establishments, residences, or personal tethered hotspots. One can easily find that 2.4 GHz channel frequencies overlap by performing a spectrum scan using a laptop with software like inSSIDER from metageek.com. Of course, non-overlapping 20 MHz frequency channels can be used for 3 nearby access points – channels 1, 6, 11 standing for 2.412, 2.437, and 2.462 GHz respectively. This is an ideal and desired scenario but the deployment becomes more complex as the number of access points in the area grows, as in HetNets. Furthermore, the WiFi IEEE 802.11n standard implements 40 MHz channels to double the data rate making operating in overlapping channels more likely.

From an AP's perspective, any interferer operating or leaking into its own *frequency channel* of operation is a co-channel interferer. Co-channel interference is not the only type of interference that can affect an AP. An interferer present in an adjacent channel is an adjacent channel interferer. Adjacent Channel Interference (ACI) causes problems that are related to the carrier sensing mechanism in IEEE 802.11 and are especially severe in multi-radio systems, where the radios are very closely spaced [2]. The number of available orthogonal (or non-interfering) channels in 2.4 GHz IEEE 802.11n depends on the spatial spacing between the radios, the *channel width* (HT20 vs. HT40), and traffic pattern. In a multi-radio system scenario, the separation between the three non-overlapping WiFi channels is almost nullified. The situation becomes worse since no two frequency channels can be considered orthogonal. ACI can be addressed by placing enough spatial separation between the access points. If there are constraints to the space limitations, the only option to overcome ACI problems is through *transmit power* control [2]. For this study, *frequency channel*, *channel width*, and *transmit power* are some of the AP wireless parameters included in the chromosome for evaluation by the genetic algorithm (GA). Figure 1 show all the parameters used in this paper and includes *maximum data rate* and *guard interval (GI)*. Maximum data rate puts a limit on the maximum modulation coding scheme (MCS) for the downlink (AP to STA). Guard interval by default is 800 nanoseconds although this can be adjusted to 400 nsec during better network conditions to increase network throughput but at the risk of higher transmission errors. In this research, only 802.11n radios are used but in no way does this constraint limit the validity of the findings to 802.11n only. The same theoretical wireless concepts and experimental results should apply to 802.11a/b/g or even to mobile technologies like 3G and 4G.

The chromosome's genes represent the adjustable wireless parameters in a given radio, and by genetically manipulating the chromosomes, the GA can find a set of parameters which optimize the radio to meet certain objectives. Some of these objectives can be utilized to improve performance and Quality of Service (QoS), to enhance spectrum usage in the midst of interferers, or to further advance wireless ubiquity [3].

A genetic algorithm that takes into consideration multiple and often-competing objectives for optimization and decision making is a multi-objective GA (MOGA). A paper written by Rondeau et al. [3], as they developed the GA-based adaptive component of a cognitive radio in Virginia Tech (VT) Center for Wireless Telecommunications (CWT), gave a thoughtful consideration on the application of a multi-objective genetic algorithm (MOGA) to a wireless system. Rondeau et al. cited the limitation of a particular GA selection and evaluation method in which evaluations along different dimensions are combined into a single metric. In the case of wireless communications, the dimensions can be bit error rate (BER), bandwidth, power consumption or network latency, to name a few. According to this paper, the single-metric method breaks down in cases where the values of the dimensions can vary greatly in magnitude (as in BER of 10^{-6} versus data rate of 10^{6}) and normalizing each dimension requires a great deal of domain knowledge. Nonetheless, one contribution of the present study is to propose a single metric, which will be called *PRR-MCS*, to evaluate and score each of the genes in a chromosome (Figure 1). *PRR-MCS* is the packet reception rate in percent (%) multiplied by the MCS data rate in megabits per second (Mbps). Each gene is given a score whose unit is in terms of PRR-MCS. As the wireless parameters or genes reflect the dimensions of the MOGA, normalization across the different dimensions is simplified since all of the gene scores have a common unit of measure. Basic operations such as summing, averaging, or weighted sum/average of the gene scores can then be used to operate an AP toward a desired objective such as optimizing network performance in the presence of radio interference.

Genetic algorithms have common processes such as

the definition and representation of data into genes and chromosomes, the operations of crossover and mutation, the selection of chromosome for the succeeding generations, and the existence of a fitness function to determine chromosome fitness. A main contribution of the present study is to design and implement into a software code a genetic algorithm with a fitness function which utilizes two key inputs: (a) a survey scan of interferer access points operating in the area and (b) associated client station (STA) statistics such as signal level, packet retransmit and failure rates, and MCS data rates for uplink and downlink. The genetic algorithm used is multi-objective and takes into consideration certain dimensions such as frequency channel of operation, bandwidth, maximum data rate, and maximum transmit power. Finally, to the knowledge of the authors, the metric proposed to score each of the chromosome genes is a novelty. PRR-MCS is a common unit to evaluate each of the wireless parameters or genes which the self-adaptive AP takes in as recommended configurations.

In this paper, Section 2 cites related researches to the current subject. Section 3 covers the background of the problem and the objectives of this paper as well as its scope. Section 4 describes the MOGA as a method to converge to a solution to the problem. The fitness function is discussed in detail in Section 5, specifically how each of the chromosome genes is scored and how PRR-MCS for each is computed. Section 6 discusses the experimental result and also gives a comparison of the proposed self-adaptive GA and the Automatic Channel Selection (ACS) feature of `hostapd`. Finally, Section 7 concludes the present paper and identifies future work and enhancements.

II. RELATED WORK

The need to automate the deployment and configuration of radio access points or base stations to achieve certain objectives is extensively studied [2],[4],[5]. The studies can be classified in general as (1) whether the optimization applies to a whole network planning and deployment, or 2) whether the configuration applies locally to a single radio or access point. As will be shown in the following discussion, while there are numerous literatures related to the former subject, the latter subject seems to lack significant attention. The present paper falls under the latter category as it proposes self-adaptation of a single AP to interfered states and optimizing network performance using the wireless statistics of associated client stations.

For network-wide application of wireless parameter configurations, Zubow, et al. [2] recommend sufficient spatial spacing to obtain more orthogonal channels out of the 2.4 GHz WiFi band. Moreover, control of transmit power becomes vital in space-limited, multi-radio systems. Garcia-Saavedra, et al. [4] presents a novel Self-Optimizing, Legacy-Compatible Opportunistic Relaying (SOLOR) framework, which optimizes the network topology and relay schedules while considering different node performance and power consumption trade-off preferences. Recommendations in optimizing the configuration of wireless parameters have been investigated, often targeting automatic adaptation to specific trade-off preferences. A load-balancing algorithm for reducing Radio Frequency (RF) Electromagnetic Fields (EMF) exposure while maintaining a level of QoS performance has also been proposed by Sidi, et al. [5]. They developed a stochastic approximation based self-optimizing algorithm that dynamically adapts the network to reduce the exposure index (EI) in a heterogeneous network with macro- and small cells.

Some works on radio network planning and deployment used genetic algorithms to optimize the radio configurations. Such works investigated the usability of genetic algorithms for optimizing wireless mesh networks. Pries, et al focused on the routing and channel assignment in large-scale wireless mesh networks to achieve a max-min fair throughput allocation [6]. It should be noted that the terms mesh and relay have something in common with user-to-user type connectivity such as hotspot tethering. A few other papers focused channel assignment problems and planning [7] - [11]. The paper by Chia, et al. [7] introduces an adaptive genetic algorithm (GA)-based channel assignment strategy for resource management and to reduce the effect of EMC interferences. Fu, et al. [8] developed a new heuristic algorithm which includes GA to tackle the same channel assignment problem to assign a minimum number of channels under certain constraints to requested calls in a cellular radio system. Ding et al. [9] used a weighted conflict graph to model interference between wireless links more accurately. They also presented a novel genetic algorithm to demonstrate that the network performance can be dramatically improved by properly utilizing

partially overlapping channels. The genetic algorithm was also found to outperform the greedy algorithm in mitigating the interference within the network leading to higher network throughput. The paper by Jalili, et al. [10] compared Taboo Search and GA in planning and optimization of 3rd Generation (3G) Universal Mobile Telecommunication System (UMTS) networks. Finally, Cacciani, et al. [11] attempted to solve the problem of identifying sites where to place the resources (or access points) for the optimal coverage of a given area using genetic algorithms.

Genetic algorithms continue to find more applications in mobile wireless networks. The paper by Paikaray [12] presents a design of an adaptive multi-attribute, vertical handoff decision algorithm for 4th Generation mobile networks based on fuzzy logic and genetic algorithms. The minimization of the number of handoffs in heterogenous 4G networks has been shown to be achievable in the paper by Chandralekha and Behera [13] through optimization of network parameter values. They proposed a multi criteria vertical handoff decision algorithm which will select the best available network with optimized parameter values (such as cost of network should be at a minimum). The decision problem was formulated as multiple objective optimization problems and simulated using genetic algorithm.

In comparison to studies of network-wide optimization of wireless parameters, papers which aim to develop GA-based programs for a single access point are limited. One such study uses GA for cognitive radios [3]. This paper by Rondeau et al. is part of an initiative by Virginia Tech (VT) Center for Wireless Telecommunications (CWT) to develop a cognitive radio engine and presents its adaptive component which uses GA and is cited quite extensively in the present study.

A few more references were used for the present paper as they provide key concepts and data for the computations used in the program code. Zhang, et al. [14] emphasized a limitation of WiFi IEEE 802.11 protocols in handling frame losses which are not due to link quality but is rather due to interference. In their study, rate adaptation is guided by signal-to-noise ratio (SNR) for handling of interference. It should be noted that rate adaptation is just one of the components of the self-adaptive access point. As shown in the chromosome genes, frequency channel selection and transmit power optimization are also features of the self-adaptive AP. Like the present study and the paper by J. Zhang et al., another paper which attempted to restore confidence to theoretical prediction of wireless link quality is that of D. Halperin et al. [15]. They introduced the concept of effective SNR to make packet delivery predictions. As for the guard interval parameter, the literature is limited and the effect of changing the GI from the default value is not well-studied. Measurements conducted by the University of Hampshire Interoperability Laboratory [17] estimated the effect of GI on packet error rates. Experimental result of software program coded in C++ for the self-adaptive AP is compared to that of the Automatic Channel Selection (ACS) feature of Linux-based access points.

`Hostapd` is a user-space daemon commonly used in Linux-based access points. One of its options is Automatic Channel Selection (ACS) so that a WiFi device can automatically figure out which channel to operate on depending on the level of interference. ACS utilizes the same information provided by `iw wlan0 survey dump`. ACS introduces a metric called *interference factor* which is computed from the formula: (busy time – tx time) / (active time – tx time). The rationale for this formula is given in [16]. The formula is intuitive in that it gives the percentage of time in which a channel is busy. This ratio is also used in the current study. However, the ratio is not treated as a final metric, rather the ratio is used to give a correction factor to the interference noise floor generated from survey scan of interferer access points. The correction factor was found reasonable as in the case where an AP does not generate any data traffic and just transmits beacon signals. The average transmit power is approximated as the signal power during beacon transmissions multiplied by the channel busy time divided by the channel active time. The correction of the interference noise floor using the busy time / active time ratio is discussed in detail in the previous sections.

The ACS first takes the average of 5 readings of the busy time/active time ratio. This average becomes the interference factor for a channel. It does this for all the channels on which an AP can operate on (channels 1 up to 11 or up to 13). When the 11 readings are computed, ACS computes the total interference for each channel. It does this by summing up the interference factor for 5 neighboring channels since 5 channels always overlap with a specific channel of choice. If HT40+ or HT40-

is used, ACS will add up the interference factors of 9 neighboring channels. The 5 or 9 neighboring channels apply for the centermost channels and not the ones on the edges. For the edge channels 1 and 11, for instance, only 3 channels will be summed up while for channels 2 and 10, 4 channels will be summed up. A similar scheme will apply to 40 MHz configurations.

With the current computation of ACS of simply summing up the interference factors, it is obvious that a 40 MHz channel will never be chosen by the algorithm since it will always have a higher sum of interference factors than that of 20 MHz channel. Thus, the self-adaptive AP algorithm will be compared with a modified ACS algorithm in which the total interference is taken as the average, not the sum, of interference factors of 5 (for 20 MHz) or 9 (for 40 MHz) neighboring channels. Also, instead of taking 5 readings for each channel, only 2 readings will be performed which are spaced 5 seconds apart and the busy time/active time ratio becomes the ratio of the difference of two busy times to the difference between two successive active time readings.

Unlike the self-adaptive AP GA algorithm, ACS does not take into account how much a channel is affecting the channel of operation. It is expected that the effect of one channel is less as its distance from the channel of choice increases. Thus, the authors do not see enough justification to simply average the interference factors. A weighted average could be more fit in quantifying the interference to a channel. It can also be observed that the interference in ACS is quantified as ratio of busy and active times. The self-adaptive AP expresses interference in the proper unit – dBm or mWatts. Thus, although ACS can tell what percentage of time a channel is busy, it says nothing about how strong is the power of interferer signal making the channel busy. The self-adaptive AP starts with the strength of the interferer access points to generate an interference noise floor for the whole 2.4 GHz band. After that, this interference noise is corrected because the signal strengths measured are not present in the air for the whole time. The busy time/active time ratios for several channels are gathered for the whole band, these ratios are expressed in dB, and they are subtracted from the initial interference noise floor. A major advantage of the self-adaptive AP algorithm is the use of correct units in expressing interference. Nevertheless, the ACS has the properties of simplicity of computation and ease of implementation. Now that the ACS has been introduced and compared with the self-adaptive AP algorithm, this paper will proceed with the quantitative comparison between the results of both algorithms.

III. Background and Scope of the Study

Rondeau et al. gave 3 parts of a cognitive radio which made it cognitive: the ability to sense the RF spectrum even at a minimum sensing, geographical surroundings, and the user's needs; the capacity to learn, ideally in both supervised and unsupervised modes; and finally, the capability to adapt within any layer of the radio communication system [3]. This definition is useful in scoping the current paper.

The primary objectives of a self-adaptive Wireless LAN (WLAN) AP are: 1) to operate optimally in a wireless medium in which interferers are present and 2) to do so while improving its wireless performance to deliver sufficient QoS to its connected clients. As in some of the citations in the related works, it may also be desirable to have a secondary objective where human exposure to EMF is reduced after attaining the primary objectives. Thus, in the context of the definition of cognitive radios by Rondeau, et al., the self-adaptive AP can do the following: sense the RF spectrum to detect interferers and to gather wireless statistics of associated client stations performance. It can also learn which configurations are most fit using a genetic algorithm based on the knowledge of other interfering access points and the wireless performance of the client devices.

The scope of the present study is self-adaptation *only* at the level of the wireless configuration which is accessible to users and administrators. The self-adaptive AP automates the configuration by network administrators and even improves on it by making informed decisions on which combination of values of wireless configuration parameters to use. In addition to this, the adjustments made by the self-adaptive AP to its own configurations are dynamic due to changing wireless network conditions. For instance, the turning on of a new interferer AP will result to a new configuration evaluated by the genetic algorithm. The self-adaptive AP is informed of the new recommended configuration and applies it at appropriate times to reduce instability and minimize the downtime of associated clients. The wireless performance of associated clients is also taken into consideration in

the decision to recommend new wireless configuration. Note that this adaptation mechanism is outside of the existing MAC layer mechanisms in IEEE 802.11 such as data rate adaptation. Adaptation at the 1PHY or MAC layers and protocols is outside the scope of this study. Moreover, most previous works on rate adaptation rely only on frame losses to infer channel quality, but performs poorly if frame losses are mainly caused by interference [14].

IV. The Self-Adaptive AP Program Flow

This section will discuss the overall flow of the program whose code will be installed on a Linux-based Access Point (AP) to make it self-adaptive and optimize itself for network performance under interfered scenarios. Another key topic of this section is the fitness function, which utilizes a single-metric (PRR-MCS) method and normalizes each dimension of the multi-objective genetic algorithm (MOGA). The fitness function uses the PRR-MCS to evaluate and score each of the genes in a chromosome (Figure 1).

This section also identifies the commands and programs used to gather the data needed by the fitness function. These commands or programs are installed in a Linux-based access point in order to perform data gathering functions such as channel survey scan and client station performance statistics. Whenever mentioned, these commands or programs are formatted in the `Courier font.` The device interface under test is also represented as `wlan0` to facilitate understanding of the command usage.

Before going through the details and operation of the fitness function used by the GA, it is worth mentioning what operations are inside the multi-objective GA cycle in Figure 2. The internals of the MOGA is shown in Figure 3. First, the genes of the initial chromosomes are randomly generated. The population size is 50 chromosomes whose format is shown in Figure 1. A function in the C++ code, called objective_channel(), generates the interference noise floor for the whole 2.4 GHz band from 2400 – 2483 MHz. The fitness of the chromosomes are evaluated using the output of the objective_channel() function and the chromosomes are given their corresponding

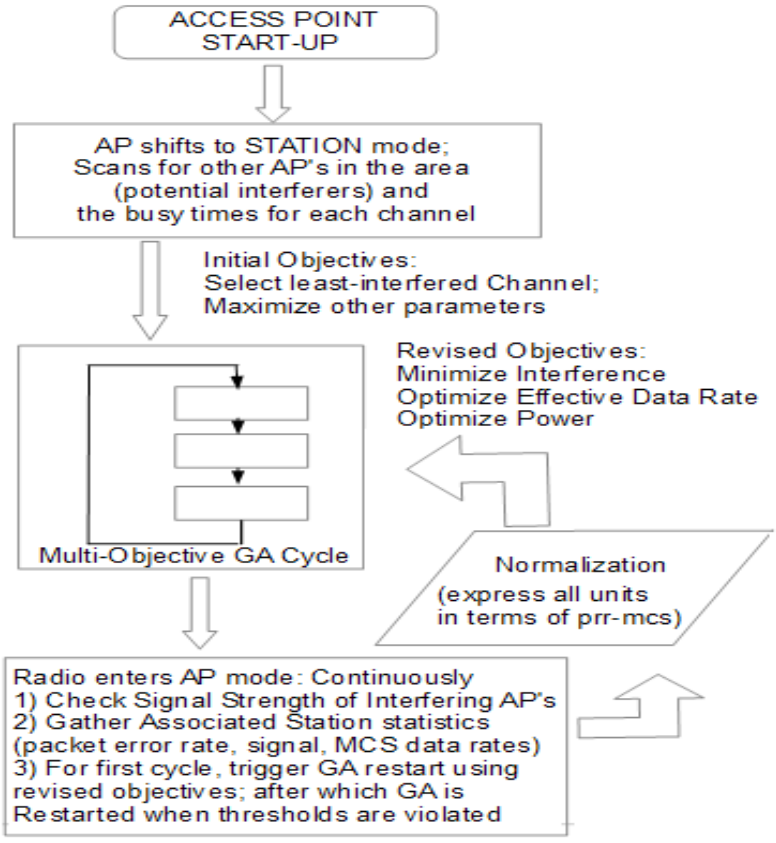

Fig. 2. Over-all flow of the program whose code is installed in an Access Point (AP) to make it self-adaptive

scores. A penalty function is also used to remove disallowed configurations resulting from incorrect combinations of channel frequency and channel setting. The chromosomes are sorted from the highest score to the lowest score for easier processing. After sorting, the standard GA operations are then applied to the initial population. The crossover() function performs single point crossover between neighboring chromosomes (parents) in the sorted array at a crossover probability of 90%. This operation produces a new generation of offspring. The mutation() function introduces random changes to the genes at a mutation probability of 20%. Fitness is again evaluated for the new generation of offspring. Then, the selection() function selects the top 50 chromosomes from the set of 100 composed of the previous generation of parents and the current generation of offspring. This cycle is repeated for 5 to 10 generations to converge to a solution. In Figure 2, this initial run of the GA cycle seeks to find a solution with the objective of identification of a least-interfered channel while maximizing the other parameters of transmit power and MCS data rate (GI is also at default of 800 nsec). In this run of the GA, the fitness function relied on the objective_channel() function which uses Linux commands to survey the interferer access points in the air. These commands are discussed in detail below. Another function, the objective_station_dump() function, which uses the wireless performance statistics of client stations associated to the AP, will be used together with objective_channel() for the succeeding runs of the GA cycle. The objectives are also revised when the fitness function is called. Interference mitigation is still part of the revised objectives. For the succeeding runs of the GA cycle, however, the revised objectives include optimization of transmit power and MCS data rate instead of just maximization of these parameters. The standard operations of genetic algorithms are also shown in Figure 3.

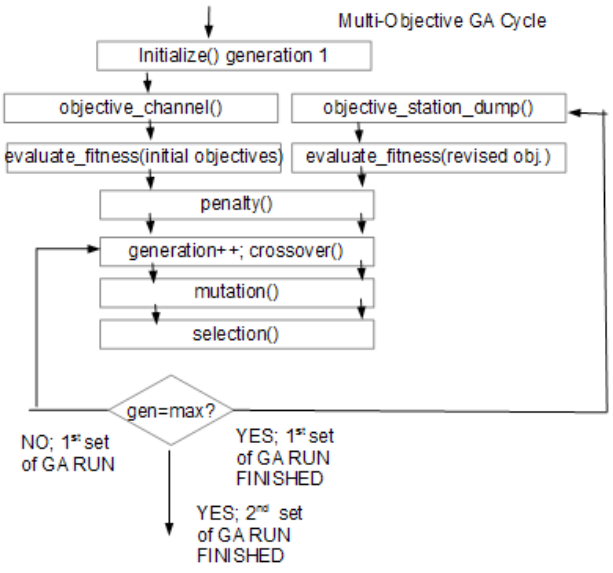

Fig. 3. The internals of the MOGA Cycle shown as a block in Figure 2

V. THE FITNESS FUNCTION

Upon start-up of the Linux-based device, it operates as a client station (STA) instead of an AP. This is necessary in order to gather a complete survey scan of the other interferer access points operating in an area. Although this feature is also possible while the device is operating as an AP using `iwinfo wlan0 scan`, a more complete set of data is gathered using `iwlist wlan0 scanning`. The latter command shows the secondary channel which an interferer AP uses and this piece of information is not in the former command. An AP uses a secondary channel when it operates in HT40+ or HT40- channel setting which means that the bandwidth used is 40 MHz instead of the usual 20 MHz. Figure 4 illustrates a sample of the data gathered by `iwlist wlan0 scanning` and what the program will construct out of these raw data.

```
Cell 01 - Address: xx:xx:xx:xx:xx:xx
...
          Mode: Master  Channel: 1
          Signal: -56 dBm  Quality: 54/70
...
Cell 02 - Address: xx:xx:xx:xx:xx:xx
...
          Frequency:2.462 GHz (Channel 11)
          Quality=53/70  Signal level=-57 dBm
...
  HT operation:
        * primary channel: 11
        * secondary channel offset: below
```

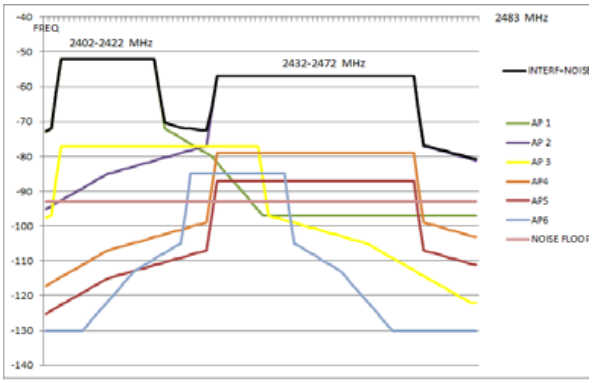

Fig 4. Sample iwlist wlan0 scanning output (truncated … and MAC addresses replaced with xx:xx:xx:xx:xx:xx) and the equivalent interference noise floor

The self-adaptive AP program makes use of the output of `iwlist wlan0 scanning` to capture the interference caused by all the other access points currently present in the air medium. Then, it constructs an interference noise floor which is the sum of the noise floor (around -93 dBm) and the contribution of each AP to its specific channel of operation. The net result if the t opmost line in the graph in Figure 4. A few more items need further explanation in the figure. If the secondary channel offset is present in the output of the program, it means that the channel used by that AP is 40 MHz instead of the usual 20 MHz. Furthermore, an above offset means that the AP occupies its primary channel and the next channel (e.g. 1+5) while a below offset means that the primary channel and channel below are used (e.g. 11+7).

The access point is also operated as a station (STA) initially to gain access to another crucial command - `iw wlan0 survey dump`. This command measures the amount of time a chosen channel is busy and the channel active time. Just before running this command, it is necessary to place the STA at the chosen for scanning through `iw wlan0 set channel <number>`. For this study, the following WiFi channels are scanned: 1 (2402-2422 MHz), 5 (2422-2442 MHz), 9 (2442-2462 MHz), and 11 (2452-2472 MHz). The readings at channels 1, 5, and 9 are used as is while the reading at channel 11 is divided by 2 to compensate the fact that the channel 9 scan already covered half of channel 11.

It will be shown later that the ratio of the busy time and the active time is a good correction factor to the interference noise floor (Figure 4) computed from the signal levels (in dBm) of all the interferer access points. If the computed interference noise floor used remains unchanged in the program, the level of interference is overestimated. The signal level received from interferer access points are only those of beacon transmissions which are typically broadcasted by an AP every 100 milliseconds and occupying the medium only for a brief 50 bytes at 1 Mbps data rate. After computing the interference noise floor, the busy time/ active time ratio for the chosen channels are expressed in dB and are subtracted from the interference noise floor for those channels resulting to reduction to more reasonable values. Figure 5 shows a sample output of `iw wlan0 survey dump` and the corrected interference noise floor. As already mentioned, channels 1, 5, 9, and 11 are measured for busy and active times. This measurement is done twice and the differences for each parameter are used to compute for the ratio. A more accurate formula which is also used by the `hostapd` Automatic Channel Selection (ACS) algorithm is (busy time - transmit time) ÷ (active time - transmit time) although this value is very near the busy time ÷ active time.

```
Survey data from wlan0
        frequency:  2412 MHz [in use]
        noise:      -95 dBm
        channel active time:  3466683 ms
        channel busy time:     386128 ms
        channel receive time:  306527 ms
        channel transmit time:  22693 ms
…
Survey data from wlan0
        frequency:  2412 MHz [in use]
        noise:      -95 dBm
        channel active time:  3467674 ms
        channel busy time:     386144 ms
        channel receive time:  306527 ms
        channel transmit time:  22703 ms
```

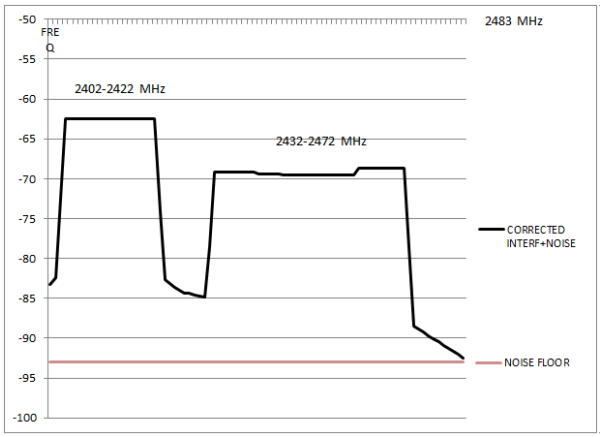

Fig. 5. Sample iw wlan0 survey output (truncated …) and the corrected interference + noise floor

In summary, the AP is started in STA mode in order to gain access to two Linux commands: `iwlist wlan0 scanning` and `iw wlan0 survey dump`. When the device enters AP mode which is its normal mode of operation, it is still useful for it to be alerted when new interferer access points are turned on. The command `iwinfo wlan0 scan here` becomes valuable. This command does not require the AP to go back to STA mode. Instead, the AP can regularly run this command in the background while serving STA clients accessing the network. The AP is effectively alerted if there are

new interferer access points in the air. The AP can then defer a more thorough survey scan using the two main commands mentioned above at scheduled times, or when there are no connected client stations. So far, the results of the survey of interferer access point are enough for the GA to select a frequency channel (1 to 11 or 13 in some AP) and the channel setting (HT20, HT40- below, or HT40+ above). For the initial objective, power and MCS data rate will be maximized and the guard interval will stay at 800 nsec. After the recommendation from the GA, the AP configures itself accordingly and clients can now associate to it.

The fitness function utilizes two key inputs: (a) a survey scan of other access points operating in the area and (b) associated client station statistics such as signal level, packet retransmit and failure rates and MCS data rates for uplink and downlink. The first input has already been discussed in detail above. In the C++ code, the first input is used by the objective_channel() function. This leads the other input to the fitness function, the associated client station statistics, used by the objective_station_dump() function. With the device now operating in AP mode, the program calls another Linux command `iw wlan0 station dump`. Figure 6 shows a sample output for a single STA associated to the AP. The data from all the associated STA are gathered and will be used to further optimize the operation of the AP. Furthermore, for more significant readings, the AP generates `ping` traffic to all associated client STA before running the station dump. A `bash` script is written for this purpose and the main *C++* code uses a system() call to occasionally run this `bash` script.

```
Station xx:xx:xx:xx:xx:xx (on wlan0)
        inactive time:  40 ms
        rx bytes:       38189
        rx packets:     351
        tx bytes:       37705
        tx packets:     521
        tx retries:     339
        tx failed:      8
        signal:         -60 dBm
        signal avg:     -61 dBm
        tx bitrate:     19.5 MBit/s MCS 2
        rx bitrate:     6.5 MBit/s MCS 0
```

Fig. 6. Sample `iw wlan0 station dump` output for a single STA associated to the AP

```
STA RX_SIGNAL RX_MCS TX_MCS TX_RETRY TX_FAIL
XX:XX:XX:73:42:68 -53.62 39.00 19.50 0.39 0.01
XX:XX:XX:3b:0a:b4 -61.46 26.00 26.00 0.68 0.04
XX:XX:XX:8d:a7:0d -65.69  6.50 52.00 0.23 0.01
XX:XX:XX:89:30:e3 -49.23 58.50  6.50 0.18 0.00
```

Fig. 7. Sample summary of `iw wlan0 station dump` as generated by a `bash` script (xx:xx:xx hides the device manufacturer)

The single-metric of PRR-MCS which will be used to score each of the genes in a chromosome is the prominent feature of the objective_station_dump() function. Each gene score will be expressed in terms of PRR-MCS which is the packet reception rate % multiplied by a corresponding MCS data rate in Mbps. In order for the C++ code not to become littered with command parsing functions, the already mentioned `bash` script also summarizes the output of `iw wlan0 station`. Figure 7 shows a sample output of the bash script.

The statistics in Figure 7 need some explanation. STA is, of course, the MAC address of the wireless client associated to the AP. RX_SIGNAL is the signal power in dBm received by the AP from the transmission of a client STA while RX_MCS is the rate if transmission from the client STA to the AP. Thus, these two readings refer to the uplink: from the STA to the AP. The following readings refer to the downlink path: AP to STA. TX_MCS is the downlink data rate to each STA, TX_RETRY is the percent of packets which were retransmitted, and TX_FAIL is the percent of packets which failed to reach the AP. One of the functions of the `bash` script is to compute these percentages from the raw output in Figure 6. In order to have a sense of the quality of the downlink, we define the transmit packet reception rate (TX_PRR) = 1 - TX_RETRY - TX_FAIL. To preview the use of the key metric PRR-MCS, one can see that the quality of the downlink can be expressed as the summation for all STA of (TX_PRR of the STA) x (MCS of the STA). This total PRR-MCS metric has the advantage of giving more weight to client stations with good link quality, that is, the stations with the poorest downlink connections (low MCS) do not contribute much to the calculation of the total PRR-MCS. This ensures that the quality of the downlink is assessed using the performance statistics of the best associated client stations, as it should be. The total downlink PRR-MCS is the key metric to score one of the genes in a chromosome – the maximum MCS data rate. A modified form of the downlink PRR-MCS will also be

used for rating the maximum transmit power and the guard interval. On the other hand, channel frequency and channel setting will be scored using an uplink PRR-MCS with one key difference. Note that the any PRR calculation for the uplink is *only* a prediction since the retransmission and failure rates are not available in the station dump. The only uplink parameters available in the station dump are RX_SIGNAL and RX_MCS. To make such prediction of the uplink packet reception rate, a graph from [15] will be used as shown in Figure 8.

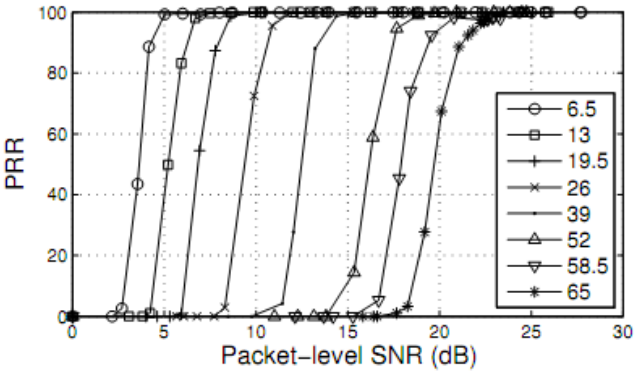

Fig. 8. A reprint of the graph in [15] relating the signal to noise ratio with the packet reception rate. This is a variant of the more well-known bit error rate (BER) versus SNR or Eb/No graphs which characterizes a digital modulation technology. The graph above applies to 802.11n MCS data rates.

One can think of packet reception rate (PRR) as a thread that ties together the indicators of link quality which are the more familiar received signal level (dBm), signal to noise ratio (dB) and interference noise floor (dBm). The graph in Figure 8 is stored as a two-dimensional array in the C++ code. Using this graph, one can either predict the downlink SNR at a client STA given the TX_MCS and the computed TX_PRR. Conversely, one can estimate the RX_PRR given the RX_MCS and the uplink SNR as seen by the AP from each STA. The uplink SNR can be estimated indirectly as the difference between the RX_SIGNAL and the average interference in the channel of operation. As discussed above, the interference information is made available to the fitness function since the output of the channel survey commands are processed into an interference noise floor.

Now, the data gathered and the tools to be used by the GA fitness function are complete and all that needs to be done is to score the genes of a chromosome (Figure 1). The formulas used by the fitness function for scoring each gene are presented in Table 1.

For channel frequency and channel setting, the score computation is straightforward. The gene score is the summation across all the associated client stations of (RX_PRR) x (RX_MCS). RX_MCS is readily available as shown in Figure 7. RX_PRR is determined in the following manner. First the uplink SNR of a client is computed as the client RX_SIGNAL minus the average interference at the particular channel. The interference noise floor is stored in an array for the whole 2400-2483 MHz band (Figure 5). The average interference for a channel frequency and setting combination is the sum of the interference for the channel band divided by the channel bandwidth. For instance, for a channel 1 HT20 setting, the average interference is the sum of the interference array (in mWatts) from 2402 to 2422 MHz divided by 20 MHz. Once SNR is derived from this computation, it becomes a simple matter to locate from the graph the expected RX_PRR given the SNR and the RX_MCS.

The maximum MCS data rate is considered as a proposition for the AP to operate at this rate at the maximum. Note that IEEE 802.11 dynamically changes the MCS data rate based in the link quality as measured by packet losses. The maximum MCS data rate gene is a proposed cap on the current MCS data rate, that is, if the proposed MCS rate is say MCS-6, then the AP cannot transmit at MCS-7 towards any STA at the downlink.

The gene score is computed as the summation for all client STA of the (PREDICTED TX_PRR) x (GENE MCS DATA RATE). The GENE MCS DATA RATE is the rate in Mbps as proposed by the gene in a chromosome, so this value is readily available for use in the computation. he PREDICTED TX_PRR is not specified and is also not available in the station dump command output. From the station dump output (Figure 7), the TX_PRR for each client can be computed using TX_PRR = 1 - TX_RETRY - TX_FAIL. Since, the TX_PRR and the TX_MCS are known, one can use the graph in Figure 8 to estimate the TX_SNR for each client STA. To get the PREDICTED TX_PRR, one again uses the same graph but this time with two new input parameters: an adjusted TX_SNR and the proposed GENE MCS DATA RATE instead of the measured TX_MCS. Take note that the MCS parameter is not the only one that changes. The MCS parameter to be considered to predict the TX_PRR is not the

TABLE 1
FITNESS SCORING FOR EACH GENE OF A CHROMOSOME

Gene	Input Parameters	Score (in unit of % Mbps)
Channel Frequency	**rx_prr** is derived from the graph and the computed snr. **snr** = rx_signal – channel interference	Σ (RX_PRR)(RX_MCS) ALL STA
Channel Setting	**rx_prr** is derived from the graph and the computed **snr**.	Σ (RX_PRR)(RX_MCS) ALL STA
Maximum MCS Data Rate	given the **tx_mcs** and the **tx_prr**., **tx_snr** is derived from the graph using an adjusted tx_snr and the proposed gene mcs, a new predicted tx_prr is obtained from the same graph for each sta	Σ (PREDICTED_TX_PRR) x (GENE_MCS) ALL STA
Maximum Transmit Power	adjusted **tx_snr = tx_snr –** db reduction of transmit power. this adjusted tx_snr is used to obtain the adjusted tx_prr at the sta tx_mcs.	Σ (ADJUSTED TX_PRR) x (TX_MCS) ALL STA
	tx_prr and tx_mcs are readily available from the station dump	For 800 nsec: Σ (TX_PRR)x(TX_MCS) ALL STA For 400 nsec: (1-1.3(1-TX_PRR)) x Σ (TX_MCS) x 1.11 ALL STA

TX_MCS of client, rather it is the MCS setting of the gene. In addition to this, the TX_SNR is also adjusted because changing the MCS data rate entails a change in the effective transmit power. IEEE 802.11n radios are required to comply with decrease in power output when the MCS data rate is increased. The AP used in this experiment has the following characteristic MCS versus transmit power: MCS0 to MCS3 28 dBm; MCS4 27 dBm; MCS5 25 dBm; MCS6 24 dBm; MCS7 23 dBm. The adjusted TX_SNR is equal to TX_SNR + (AP transmit power at the proposed gene MCS – AP transmit power at the TX_MCS). It is expected that this property of the AP of higher transmit power at lower MCS data rates together with the particular link conditions of the associated STA will lead to a trade-off in the choice of the optimum MCS data rate. That is, the highest MCS data rate will not always be the optimum MCS and such result can only be expected when the quality of all or most client STA links are very good. Now, the PREDICTED TX_PRR for each client station is known and one can proceed with the gene score computation.

For scoring the maximum transmit power gene, an adjusted SNR is computed for each STA. This adjusted SNR is simply the TX_SNR used in the MCS gene score above minus the proposed dB reduction in transmit power. From this adjusted SNR and the STA TX_MCS, the PRR vs SNR graph yields an adjusted TX_PRR. The gene score is then computed as the summation across all STA of the (ADJUSTED TX_PRR) x (TX_MCS). Although it is expected that the highest transmit power setting will get the highest score, one can set a margin of allowance for optimization of transmit power. For instance, if the gene score of two transmit power values are within approximately 5%, the lower of the two transmit power values can be given a higher score.

Finally, for the guard interval gene, the short GI of 400 nsec is only recommended if the downlink data rates toward the client STA are high. A rule of thumb from [17] will be used. According to their test measurements, a short GI leads to a 30% increase in error rates while boosting the throughput by 11% (from IEEE 802.11n standard). From this, the gene is scored as follows. For 800 nsec, the gene score is the summation across all clients of (TX_PRR) x

(TX_MCS). The gene score for the 400 nsec case is computed differently as the summation for all clients of (1 – 1.3 x (1- TX_PRR)) x (TX_MCS) x 1.11.

An overview of the multi-objective GA was outlined in Section 4 while a thorough discussion of the fitness function was given in Section 5. The next section compares the self-adaptive AP algorithm with the Automatic Channel Selection (ACS) algorithm used in `hostapd`. The operation and computations involved in ACS are not discussed in much detail and the reader is referred to [16] for a more complete discussion.

VI. EXPERIMENTAL RESULTS

A sample result of `iwlist wlan0 scanning` is summarized in Figure 9. Again a `bash` script is used to create this summary. It averages the values of the signal received from each AP to smooth out sudden spikes in the readings. Also, only the access points with the highest signals are considered – those with signals higher than -90 dBm. Other access points which are too close to the noise floor are ignored since they will not affect the interference noise floor computation in a significant way.

The output of the ACS algorithm and its recommended channel use is presented here. A complete scan from channels 1 to 11 is performed. For each channel, two readings are gathered spaced 5 seconds apart. From the raw data similar to Figure 5, a summary table is obtained (Table 2). From this computation, the unmodified ACS algorithm used by `hostapd` recommends using Channel 1 for HT 20 MHz and Channel 1+5 for HT 40 MHz. If one will check [16], the sample computation led to a choice of channel 13 HT 20 MHz. This is not surprising because the edge channels just summed up 3 values of interference factors versus 5 for the center channels. These results supports the seeming inadequacy of the ACS algorithm, particularly the formulas used to quantify interference. With a modified ACS, using average instead of sum for the interference factors, the recommended channels are channel 2 for HT 20 MHz and 4+8 for HT 40 MHz. Even before a full analysis

TABLE 2
RECOMMENDED CHANNELS OF OPERATION (IN BOLD) BASED ON THE ACS ALGORITHM

Channel prim+seC	setting	band (Mhz)	SUM oF interf factor	AVE oF interf factor
1	HT20	2402-2422	**0.1798**	0.0599
1+5	HT40+	2402-2442	**0.4814**	0.0688
2	HT20	2407-2427	0.2187	**0.0547**
2+6	HT40+	2407-2447	0.5184	0.0648
3	HT20	2412-2432	0.2779	0.0556
3+7	HT40+	2412-2452	0.5745	0.0638
4	HT20	2417-2437	0.3174	0.0635
4+8	HT40+	2417-2457	0.5695	**0.0633**
5	HT20	2422-2442	0.3389	0.0678
5+9	HT40+	2402-2442	0.6527	0.0725
6	HT20	2427-2447	0.3386	0.0677
6+10	HT40+	2407-2447	0.6153	0.0769
7	HT20	2432-2452	0.3558	0.0712
7+11	HT40+	2412-2452	0.5763	0.0823
8	HT20	2437-2457	0.3804	0.0761
9	HT20	2442-2462	0.3888	0.0778
10	HT20	2C447-2467	0.3137	0.0784
11	HT20	2452-2472	0.2767	0.0922

using the self-adaptive AP algorithm, the soundness of the result of the modified ACS specifically 4+8, is supported by the raw data in Figure 9.

```
AP CHANNEL_FREQ SIGNAL SECONDARY_CHANNEL
XX:XX:XX:B6:52:3F 2412 -52.00 no
XX:XX:XX:D4:D9:68 2462 -57.00 below
XX:XX:XX:06:ED:7E 2412 -77.00 above
XX:XX:XX:31:F3:A4 2462 -79.00 below
XX:XX:XX:40:A5:3E 2462 -87.00 below
XX:XX:XX:0A:14:5F 2437 -85.00 no
```

Fig. 9. Sample summary of iwlist wlan0 scanning

Just by observation, the two most powerful interferer access points with signal levels of -52 and -57 dBm are situated at channels 1, and 7+11, respectively. Thus, if one is to choose a 20 MHz channel, channel 4 would be a sound choice indeed. It is now time to apply the algorithm used in the self-adaptive AP.

As discussed in previous sections, the AP will first use the raw data of interferer access points as shown in Figure 9. The resulting interference + noise floor is shown in Figure 10. The AP signal readings in Figure 9 and plotted in Figure 10 are just that – signal strengths. They do not tell what percentage of time that signal strength is present in the air. Thus, the average powers of the interferers are overestimated. Theoretical calculations of packet reception rates (PRR) are found to be too high compared to real measurements when the uplink signal-to-noise ratios are used to get the corresponding PRR from the graph using the interference + noise floor in Figure 10. Thus, the busy time/active time ratio is used as a correction factor to generate a lower interference + noise floor (Figure 11). The signal level received from interferer access points are only those of beacon transmissions which are typically broadcasted by an AP every 100 msec and occupying the medium only for a brief 50 bytes at 1 Mbps data rate. After computing the interference noise floor, the busy time/active time ratio for the chosen channels are expressed in dB and are subtracted from the interference noise floor for those channels resulting to reduction to more reasonable values. After this correction, the uplink signal-to-noise ratios will be higher than before the correction and the theoretical PRR estimates decrease and become closer to real measurements. Note that the uplink signal-to-noise ratio from a client STA is the gathered RX_SIGNAL minus the average interference present in the gene channel frequency-channel setting combination.

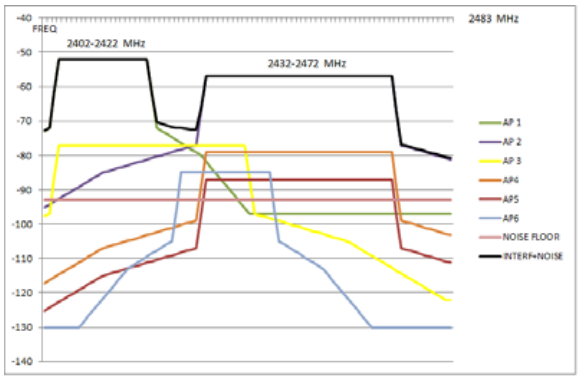

Fig. 10. Interference + Noise Floor (in **black line)** sums up all the interference caused by all the interferer access points in Figure 9 to an initial noise floor of -93 dBm

TABLE 3
CORRECTION FACTORS VERSUS BAND OF FREQUENCIES

Band of frequencies	Chanenl	Correction in dB
2400-2422	1	-10.51
2422-2442	5	-12.28
2442-2462	9	-12.51
2462-2472	11(upper half)	-11.65

The correction factor that will be used to lower the interference + noise floor will use the busy time/active time ratios of channels 1, 5, 9, and 11. The reading at channel 11 is divided by 2 to compensate the fact that the channel 9 scan already covered half of channel 11. The interference factors of these channels are converted into dB using the formula 10log(interference factor). It is actually more proper to call these busy time/active time ratio rather than interference factor since the latter is a terminology used by ACS. The essence of this ratio is that it indicates the percentage of time the channel is occupied or busy. Thus, subtracting this ratio (in dB) from the initial power estimate (in dBm) as shown in Figure 10 gives the corrected interference + noise floor. Table 3 shows the correction factor (in dB) over the band of frequencies and Figure 11 gives the corrected interference + noise floor.

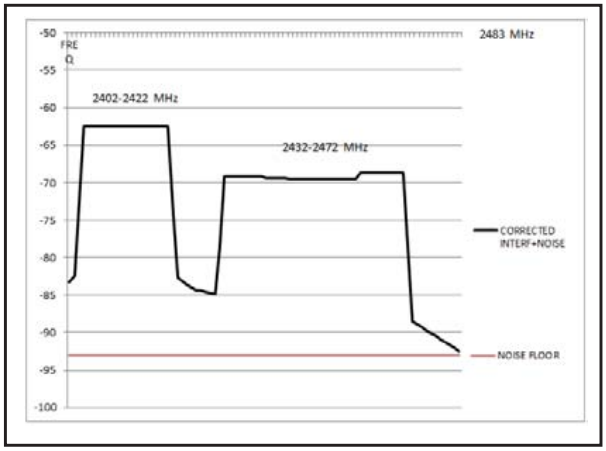

Fig. 11. Corrected Interference + Noise Floor using busy time/ active time ratios of Channels 1,5,9 and 11

The corrected or adjusted interference + noise floor will be the basis for the first series of runs of the GA. At this point, the self-adaptive AP is just exiting STA mode. It has not operated as an AP yet and there are still no connected clients. After initializing the 1st generation of population, the fitness function will evaluate 50 randomly-generated chromosomes with the following objectives: minimize interference, maximize power, and maximize the MCS data rate. The default channel setting of HT 20 MHz and the guard interval of 800 nsec will also be given higher scores. This way, the device can immediately start operating as an AP and serve wireless clients. In the context of the overall program flow, the function objective_channel() in the C++ code has finished its job, that is, to construct the interference + noise floor (Figure 11) including the correction provided by the busy time/active time ratio. At this stage of the code, and for simplicity, PRR-MCS has not yet been introduced into the fitness calculations since the AP has not yet gathered client STA statistics. The channel frequency and channel setting configurations are initially scored using the average interference in their band of operation. The average interference is equal to the area under the curve in Figure 11 over the band of operation (e.g. 2402-2422 for channel 1 at HT 20 MHz) divided by the channel setting bandwidth (e.g. 20 or 40 MHz). The use of a simpler fitness scoring for the initial GA run does not devalue the concept of PRR-MCS. One can assume an RX_SIGNAL and an RX_MCS from a hypothetical wireless client STA and get a corresponding SNR by subtracting the average interference from the RX_SIGNAL. Then the PRR vs SNR graph can be used to predict a RX_PRR and multiplying this by the RX_MCS yields a PRR-MCS metric which can be used for fitness scoring. However, it is obvious that such fitness scoring will lead to the same solution because the variables are held constant except for the average interference, which varies with the channel band. Table 4 summarizes the result of the initial set of GA runs using the average interference fitness scoring scheme. Note that the fitness score is not yet in terms of PRR-MCS.

The result in Table 3 clearly showed that the solution converged to a channel frequency of 5 and channel setting of HT 20 MHz. This band covers 2422 to 2442 MHz. Figure 12 compares the recommendations of the self-adaptive GA versus the best recommendation of ACS (4+8 or 2417-2457MHz) and clearly demonstrates that the former outperforms the latter in interference mitigation via channel selection. ACS clearly missed channel 5 which sits in a region of lowest interference. There are also other recommendations from the self-adaptive GA, with fitness scores of 138, to use channels 7 to 11 using 20 or 40 MHz but these chromosomes were removed by the 5th generation. Lastly, channels 12 and 13 were not included in the calculations since the AP hardware used does not support those bands.

TABLE 3
MOST FIT CHANNEL CONFIGURATIONS USING INITIAL SET OF GA RUNS (6 GENERATIONS)

LAST SEEN IN generation	channel freq	channel setting	FITNESS SCORE/ REMARKS
5th	6	HT20	140
5th	9	HT40-	140
6th	5	HT20	144(CONVERGED SINGLE SOLUTION)

At this point, the AP is serving wireless client stations and it will continuously gather wireless client statistics. Again a `bash` script is used outside of the C++ code. The code can access the `bash` script using a system() call and it will parse a text file generated by the `bash` script. The script will also handle averaging the readings, specifically signal and MCS, in order

to smooth out any variations. For the succeeding discussion, the associated client STA statistics are those shown in Figure 7.

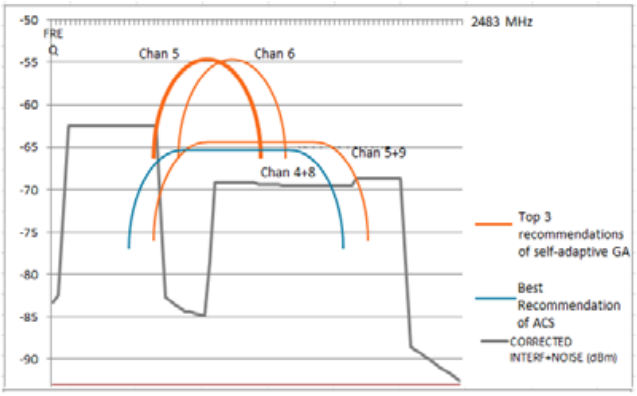

Fig. 12. Top 3 recommendations of self-adaptive GA versus the best recommendation of ACS algorithm

In the context of the program flow, the function objective_station_dump() will take over in a way similar to what objective_channel() did with the scan of interferer access points. The objective_station_dump() function will process the gathered wireless client statistics and most importantly, derive the PRR-MCS values for the 5 chromosome genes. Only after this function is done with these computations will evaluate_fitness() be called again using the revised objectives of minimize interference, optimize transmit power, and optimize data rate. The details of objective_station_dump() was already discussed extensively in the previous section. For this paper, the fitness score of a chromosome is computed as just the sum of the fitness scores of each gene and all are in units of PRR-MCS (% x Mbps). Table 4 shows the top 10 solutions of a sample run by the 6th generation.

Table 4 serves to illustrate the variation in the most likely candidates from the whole search space. By the 10th generation of the sample run, most of the 50 chromosomes in the population have either 5 or 5+9 as channel frequencies, and only 8% of the chromosomes have channel 6. Transmit power reductions are either 0 or 1 dB with 72% of the chromosomes recommending a reduction of 1 dB from the maximum transmit power. Thus optimization of transmit power can be achieved by the multi-objective GA and is often recommended as a better option than simply setting the transmit power at maximum. The more aggressive guard interval of 400 nsec is only selected only 18% of the time. Finally, the MCS data rate is more diverse. This is a good indication that the multi-objective GA (MOGA) is adapting to the wireless conditions of the client stations. The advantage of a lower data rate in downlink is that stations can connect at lower error rates. From the preceding discussion, it is evident that the MOGA for the self-adaptive Access Point is well suited for such interplay of wireless parameters and network

TABLE IV
MOST FIT CHROMOSOMES BY THE 6TH GENERATION

chan freq	Chann setting	band (Mhz)	max data rate mbps	less tx pow (db)	GI	FIT score
5+9	HT40+	2422-2462	52x2	0	800	430
5+9	HT40+	2422-2462	52x2	0	800	430
6	HT20	2427-2447	39	**0**	400	424
5+9	HT40+	2422-2462	6.5x2	0	400	423
6	HT20	2427-2447	39	1	800	422
5+9	HT40+	2422-2462	52x2	1	400	416
5+9	HT40+	2422-2462	39x2	1	400	416
5+9	HT40+	2422-2462	52x2	**1**	400	416
5+9	HT40+	2422-2462	39x2	1	400	416
5	HT20	2422-2442	52	2	400	410

conditions. Figure 13 closes this section with a graph of the distribution of maximum MCS data rate for the 50-chromosome population by the 10th generation.

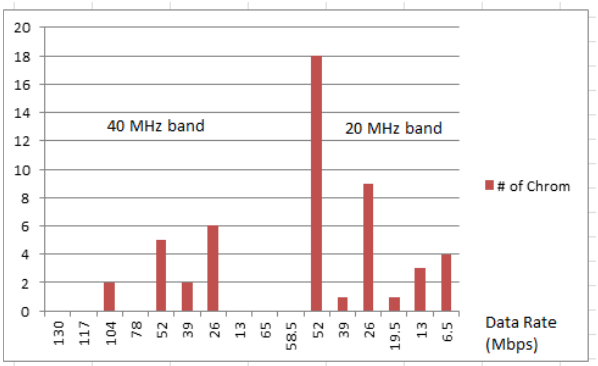

Fig. 13. Distribution graph of instances of certain MCS data rates across a population of 50 chromosomes by the 10th generation

VII. Conclusion and Future work

Variations on the fitness score or the GA operations are possible extensions to this work. A weighted sum approach for the fitness function or a tournament approach in the GA selection are just some of the enhancements worth exploring in the future. Such enhancements are well supported by the most important contributions of the current paper, namely: (1) the single-metric of PRR-MCS for scoring the different genes, (2) the normalization across multiple objectives or dimensions of interference mitigation and optimization of bandwidth, data rate, power, and guard interval, and (3) the implementation of multi-objective genetic algorithm (MOGA) to make a WLAN access point self-adaptive to dynamic wireless network conditions and to multi-radio ecosystems (e.g. HetNets).

Another important next step for this research is the actual compiling of the C++ code into a Linux-based WiFi Access Point. Important requirements for such endeavor have already been identified and discussed in this work. In order to fully implement a stand-alone daemon based on the C++ code, thresholds should be identified such as what level interference, error rates, or PRR-MCS will trigger a restart of the GA or the program. Finally, possible use of Heuristic Search Technique or Multi-Mode Self-Adaptive (MMSA) algorithm can be explored.

Acknowledgment

The authors would like to thank the Linux and open-source community whose programs were used as cited in different parts of this paper. Thank you for powering not only the appliance used for the experiments but for powering the Internet as well.

References

J. G. Andrews, "Seven Ways that HetNets Are a Cellular Paradigm Shift" IEEE Communications Magazine, vol. 51 no. 3, March 2013. pp. 136—144.

A. Zubow, and R. Sombrutski. "Reinvestigating Channel Orthogonality - Adjacent Channel Interference in IEEE 802.11n Networks," Tech. Republic, 2011.

T. W. Rondeau, B. Le, CJ. Rieser, and C. W. Bostian, «Cognitive Radios with Genetic Algorithms: Intelligent Control of Software Defined Radios," Proceeding of the SDR 04 Technical Conference and Product Exposition, SDR Forum 2004.

A. Garcia-Saavedra, B. Rengarajan, P. Serrano, and X. Costa-Pérez, «SOLOR: Self-Optimizing WLANs with Legacy-Compatible Opportunistic Relays,» IEEE/ACM transactions on Networking, vol. 20 no. 10.

H. B. A. Sidi, Z. Altman, and A. Tall, «Self-Optimizing mechanisms for EMF reduction in heterogeneous networks,» 2014 12th International Symposium and Workshops on Modeling and Optimization in Mobile, Ad Hoc and Wireless Networks (WiOpt), Hammamet, Tunisia, May 2014.

R. Pries, D. Staehle, B. Staehle, and P. Tran-Gia, «On Optimization of Wireless Mesh Networks using Genetic Algorithms,» International Journal on Advances in Internet Technology, vol. 3 nos. 1 & 2, 2010.

Y. S. Chia, Z. W. Siew, H T. Yew, S. S. Yang, and K. T. Z Teo, «An Evolutionary Algorithm for Channel Assignment in Wireless Mobile Networks,» ICTACT Journal on Communication technology, vol. 3 no. 4, December 2012.

X. Fu, A. G. Bourgeois, P. Fan, and Y. Pan, «Using a genetic algorithm approach to solve the dynamic channel-assignment problem,» International Journal of Mobile Communications, Vol. 4, No. 3, 2006, pp. 333-352.

Y. Ding, Y. Huang, G. Zeng, and L. Xiao, «Channel Assignment with Partially Overlapping Channels in Wireless Mesh Networks,» Proceeding WICON '08 Proceedings of the 4th Annual International Conference on Wireless Internet, Article No. 38, 2008.

B. Jalili, and M. Dianati, «Application of Taboo Search and Genetic Algorithms in Planning and Optimization of UMTS Radio Network,» Proceeding IWCMC '10 Proceedings of the 6th International Wireless Communications and Mobile Computing Conference, pp. 143-147.

D. Cacciani, F. Garzia, A. Neri, and R. Cusani, «Optimal Territorial Resources Placement for Multipurpose Wireless Services Using Genetic Algorithms,» Wireless Engineering and Technology, vol. 2 no. 3, July 2011, pp. 184-195. Available: http://www.SciRP.org/journal/wet

B. Paikaray, "Vertical Handoff Decision Based On Genetic Algorithm in 4G Network," CoRR abs/1209.4968, Cornell University Library, Ithaca, NY, 2012. [Online]. Available: http://arxiv.org/pdf/1209.4968v1.

"The Effects of Adjacent Channel Rejection and Adjacent Channel Interference on 802.11 WLAN Performance," Texas Instruments Whitepaper SPLY005, November 2003.

J. Zhang, K. Tan, J. Zhao, H. Wu, and Y. Zhang, "A Practical SNR-Guided Rate Adaptation," INFOCOM 2008. The 27th Conference on Computer Communications. IEEE, pp. 13-18 April 2008.

D. Halperin, W. Hu, A. Sheth, and D. Wetherall, "Predictable 802.11 packet delivery from wireless channel measurements," ACM SIGCOMM, 2010.

"ACS - Linux Wireless," The Official Linux Wireless Wiki. Web. <http://wireless.kernel.org/en/users/Documentation/acs>.

"Wireless Reliability - Guard Intervals," The InterOp Insider. University of New Hampshire InterOperability Laboratory. Web. <https://www.iol.unh.edu/blog/2014/6/16/>.

R. Ligeiro and H. Miranda, "An analysis to the deployment of access points using genetic algorithms." [Online]. Available: http://www.di.fc.ul.pt/~hmiranda/papers/ligeiro06-slides.pdf

K. Ohnishi, K. Tsukamoto, S. Kashihara, & Y. Oie. "Self-configuration of wireless access points based on mechanisms of biological development and evolution," Self-Adaptive and Self-Organizing Systems Workshop (SASOW), 2010 Fourth IEEE International Conference, pp. 17-25.

T. Vanhatupa. Wi-Fi Capacity Analysis for 802.11 ac and 802.11 n: Theory & Practice. Ekahau Inc, 2013.

A. Riedl, "A Versatile Genetic Algorithm for Network Planning," Proceedings of EUNICE, vol. 98, September 1998, pp. 97-103.

J. Kim and J. Lin, "Comparison of self-adaptive wireless networks using mobile base stations and mobile access points," Wireless and Microwave Technology, 2005, pp. 108-110.

D. Turner, S. Savage, and A. C. Snoeren, "On the empirical performance of self-calibrating wifi location systems," 2011 IEEE 36th Conference on Local Computer Networks (LCN), October 2011, pp. 76-84.

A. Zubow, and R. Sombrutzki, "Adjacent channel interference in IEEE 802.11n," IEEE Wireless Communications and Networking Conference (WCNC), April 2012, pp. 1163-1168.

P. Miklavcic, "On the number of non-overlapping channels in the IEEE 802.11 WLANs operating in the 2.4 GHz band," Elektrotehniski Vestnik, 2014, 81(3): 148.

S. Vigneshwaran, and C. Selvaraj, "Implementation of WLAN N and Estimation of Co Channel and Adjacent Channel Interference," J Comput Eng Inf Technol 5: 2, http://dx.doi.org/10.4172/2324, 9307, 2.

G. K. Audhya, K. Sinha, S. C. Ghosh, and B. P. Sinha, "A survey on the channel assignment problem in wireless networks," Wireless Communications and Mobile Computing, 11(5), 2010, pp 583-609.

J. Cheeneebash, J. Antonio Lozano, and H. Coomar Shumsher Rughooputh. "A survey on the algorithms used to solve the channel assignment problem," Recent Patents on Telecommunication, 1(1), 2012, pp. 54-71.

I. Amro and W. Ghanem, "GSM Automatic Frequency Planning with the Aid of Genetic Algorithms," Fifth International Conference on Genetic and Evolutionary Computing (ICGEC), August 2011, pp. 73-76.

S. L. V. S. Jyothi, and S. S. Gowri, "Modified Genetic Algorithm for Channel Allocation Problem."

The Contributors

Argel A. Bandala is an Associate Professor and Research Faculty of the Electronics Engineering Department at De La Salle University. He received his Master of Science in Electronics and Communications Engineering in year 2012 and Doctor of Philosophy in Electronics and Communications Engineering in year 2015 at De La Salle University. He is the current Vice-Chair, The Institute of Electrical and Electronics Engineers (IEEE) Philippines Section and secretary of Computational Intelligence Society Philippine Chapter. He is also a member of IEEE Robotics and Automation Society. His main works are "Implementation of Varied Particle Container for Smoothed Particle Hydrodynamics-Based Aggregation for Unmanned Aerial Vehicle Quadrotor Swarm" and "Swarming Algorithm for Unmanned Aerial Vehicle (UAV) Quadrotors – Swarm Behavior for Aggregation, Foraging, Formation, and Tracking.

Lemuel F. Banal has a BS in Aeronautical Engineering from Philippine State College of Aeronautics and is currently taking up MS in Mechanical Engineering at De La Salle University. He is also a faculty member of the Department of Aeronautical Engineering and Aircraft Maintenance Technology of FEATI University.

Alvin B. Culaba is a University fellow, and Full Professor of the Mechanical Engineering Department at De La Salle University, Manila, Philippines. He is also an Academician of the National Academy of Science and Technology, Department of Science and Technology, Philippines. His areas of specialization include: energy technology and management, life cycle assessment, management of technology, manufacturing and environmental system engineering, and cleaner production technologies. He has published more than 40 Scopus-indexed papers in the field of environment and energy engineering with an h-index of 15.

Elmer Dadios is a University Fellow and Professor at De La Salle University. He is also the president, Neuronemech, Inc. In 1996, he received his Doctor of Philosophy from Loughborough University. In 1997, he was an Exchange Scientist in Japan Society for the Promotion of Science, Tokyo Institute of Technology. He served as the Director of Engineering Graduate School, De La Salle University in 1998-1999 and Director of School of Engineering, De La Salle University in 2003-2004. He is also the General Chair for HNICEM in 2003, 2005, 2007, 2009, 2011, 2013. His main works are "Fuzzy Logic – Controls, Concepts, Theories and Applications," ISBN: 978-95351-0396-7, 2012. "Fuzzy Logic – Algorithms, Techniques and Implementations," ISBN: 978-953-510393-6, 2012. "Fuzzy Logic – Emerging Technologies and Applications," ISBN: 978-953-51-03370, 2012. His research interests includes; Robotics, Mechatronics, Automation, Intelligent Systems, Neural Networks, Fuzzy Logic, Genetic Algorithms, Evolutionary Computation and IT. He is a Senior Member in The Institute of Electrical and Electronics Engineers (IEEE) and founder and current of Chair of IEEE Computational Intelligence Society, Philippines. He is a member of IEEE Region 10 Executive Committee and founder and President of The Mechatronics and Robotics Society of the Philippines

Joel C. Delos Angeles graduated in 1999 with a bachelor of science degree in Electronics and Communications Engineering from the University of the Philippines in Diliman. He has more than a decade of experience and pioneering work in the area of Internet technologies, broadband wireless access, and telecommunications in the Philippines. He has 2 patent grants and 3 patent publications from the United States Patent and Trademark Office (USPTO) in the areas of Quality of Service (QoS), network management, and

real-time traffic services. He recently got his Master of Science degree in Electronics and Communications Engineering from De La Salle University Manila where he published several papers in using Artificial Intelligence (AI) to solve problems in communications. He is currently an Assistant Professor in De La Salle University Dasmarinas while designing high-power GSM/LTE coaxial cavity diplexers for CIRTEK Advanced Technologies and Solutions Inc.

Laurence A. Gan Lim is an Full Professor of the Mechanical Engineering Department at De La Salle University. He obtained his Doctor of Philosophy in Computer Science at Coventry University. He is the Chair of the Institute of Electrical and Electronics Engineers (IEEE, Philippines). He is also a member of the Philippine Society of Mechanical Engineers (PSME). His main work is "Implementatio of GA-KSOM and ANFIS in the classification of colonic histopathological images".

Rodrigo S. Jamisola Jr. received his B.S. degree in Mechanical Engineering from the University of the Philippines-Diliman, M.E. degree (research-based) in Mechanical Engineering from the National University of Singapore in 2001, M.Sc. degree in Electrical and Computer Engineering from Colorado State University in 2006, and Ph.D. degree in Electronics and Communications Engineering from De La Salle University-Manila in 2009. He joined De La Salle University as an Asst. Professor in 2008 and Toyota Motor Philippines as R&D Manager in 2011. He was a Post-doctoral Research Fellow at Daegu-Gyeongbuk Institute of Science and Technology in South Korea, and then at Istituto Italiano di Tecnologia in Genova, Italy. He is currently a Sr. Lecturer at Botswana International University of Science and Technology. His research interest includes control of combined manipulators, machine learning, numerical optimization, and human–machine interfaces.

Andres Philip Mayol is a graduate student and a research assistant of the Mechanical Engineering Department at De La Salle University, Manila, Philippines. He is a Magsaysay Young Engineers and Technologist awardee given by the National Academy of Science and Technology, Department of Science and Technology Philippines. His research interest are photobioreactor design, Computational fluid dynamics, and algal biofuels and bioproducts. He has published 4 Scopusindexed papers in the field of environment and energy engineering.

Analene Montesines Nagayo earned her B. Sc. and M. Eng. degree in Electronics and Communications Engineering (ECE) from De La Salle University-Manila. She is currently pursuing her PhD studies in Mechanical, Energy and Industrial Engineering at Botswana International University of Science and Technology. She worked in De La Salle University as an assistant professor from 1992 to 2009, Don Bosco Technical College as Assistant Professor from 1996 to 2002 and as Program Head of ECE department in 2010 to 2011, Future University (formerly Computer Man College) in Sudan as an Assistant Professor and Head of Computer Engineering department in 2009 to 2010, and Mapua University (formerly Mapua Institute of Technology) as a Professor from 2010 to 2011. From 2011 to present, she is working as full-time Lecturer at Al Musanna College of Technology in Sultanate of Oman. Her research interest includes Analog and Digital Electronics System Design, Embedded Systems, Control and Automation, Biomedical Informatics and Instrumentation, Data Communication and Power Electronics.

Ronnie O. Serfa Juan received his BSc in Electronics and Communications Engineering from the Technological University of the Philippines-Manila, and he earned his MSc in Information and Telecommunications Studies, majoring in Computer Systems and Network Engineering, at Waseda University in Tokyo, Japan in 1999 and 2007, respectively. He is currently working toward his Ph.D., majoring in Computer and Control, at Cheong-Ju University in Cheong-Ju City, South Korea. He passed the ASEAN Electronics Engineering evaluation examination last November 2016. His research interests include radio frequency identification (RFID), advanced driver assistance system (ADAS) technology, Controller Area Network (CAN) and FlexRay Technology.

Edwin Sybingco received the B.S. and M.S in Electronics and Communications Engineering from De La Salle University in 1990 and 1993, respectively. He is currently a Faculty Member in Electronics and Computer Engineering Department, De La Salle

University, where he teaches courses related to signal processing, machine vision, and control systems. His principal research interests include various topics in signal processing, intelligent transport system, and Big Data.

Aristotle Ubando is an Associate Professor and a Research Fellow of the Mechanical Engineering Department at De La Salle University, Manila, Philippines. He is a recipient of the Fulbright Philippine Agriculture Scholarship Program for Doctoral Dissertation Award at the University of Arizona addressing climate change and energy production through algal systems in 2013. His research interests are optimization of energy systems, life-cycle assessment, and processing of algal biofuels and bioproducts. He has published more than 20 Scopus-indexed papers in the field of environment and energy engineering with an h-index of 4. He currently works on multiple projects in improving the agriculture and aquaculture industry in the Philippines.

Ira C. Valenzuela received her Bachelor of Science in Electronics Engineering from Technological University of the Philippines in 2012 and Master of Science in Electronics and Communications Engineering from Mapúa Institute of Technology in 2015. She is currently working towards her Doctor of Philosophy in Electronics and Communications Engineering at De La Salle University in the area of computational intelligence. Her research interests are materials design, IC design, microelectronics, artificial intelligence, and evolutionary computing. Krister Ian Daniel Z. Roquel is currently taking his PhD in Civil Engineering at De La Salle University Manila. He worked at De La Salle University – Manila as a part-time lecturer in the Civil Engineering Department shortly after earning his Masters in Civil Engineering at the same University. He specializes in Transportation Engineering and focuses his research on discrete choice modeling and transportation economics.

Ryan Rhay P. Vicerra is an Associate Professor of the Manufacturing Engineering and Management Department at De La Salle University. He received his Master of Science in Electronics and Communications Engineering in year 2008 and Doctor of Philosophy in Electronics and Communications Engineering in year 2015 at De La Salle University. He is a member of The Institute of Electrical and Electronics Engineers (IEEE) Philippines Section and Computational Intelligence Society Philippine Chapter. His main works are “Swarm intelligence for underwater swarm robot system”, “Development of an underwater swarm robot system”, and “Simulation of slime mold swarm intelligence”.

Guidelines for Contributors

1. The Journal on Computational Innovations and Engineering Applications (JCIEA) aims to promote the development of new and creative ideas on the use of technology in solving problems in the field of computational applications, computational intelligence, electronics and information and communications technology (ICT), manufacturing engineering, energy and environment, robotics, control and automation, and all their related fields. Manuscript submissions should, therefore, be in pursuit of the same goal and within the related fields.
2. JCIEA only accepts manuscripts written in English. The responsibility for copy-editing manuscripts, as well as obtaining reproduction permissions for the use of graphics and other materials from their references, will fall on the author.
3. Authors must also remember to cite all references and ensure that their paper submission has not been previously published or is undergoing peer review for another publication.
4. Manuscripts should include a unique title, an abstract, some keywords, an introduction and discussion of the study, a presentation and discussion of results, and a conclusion. Authors may also include an acknowledgement of funding organizations or consultants, if needed.
5. Manuscripts may be sent to *jciea.dlsu@gmail.com* or *jciea@dlsu.edu.ph* as either an MS Word file (*.doc or *.docx) or a LaTeX file (*.tex), including its supporting files or submit to www.jciea.com.
6. Manuscripts in either file format should have the following features:

- Single-spaced, two-column format with 1-inch margin on all sides on letter-sized template
- Font to be used is Times New Roman, size 11
- Graphs (*.eps, *.svg), tables (*.csv), and images (*.jpg, *.png) should be saved and sent apart from the MS Word file.
- Citations and references should be submitted in IEEE format.
- Submission of these references in a BibTeX format is preferred.

7. Manuscript should be eight to twelve (8–12) pages long, including all figures, tables, and references. Manuscripts exceeding the 12-page limit will require permissions from the editors.
8. Authors must include their full names and affiliations in the manuscript. They may include a 150- to 200-word biography to be included in the back portion of the journal.

Call for Papers

SCOPES AND TOPICS

Artificial Intelligence

Agents and Multi-agent Systems
Computational Intelligence
Genetic and Evolutionary Algorithms
Data Mining
Expert Systems
Fuzzy Logic
Machine Learning
Machine/Computer Vision
Natural Language Processing
Neural Networks

Emerging Technology Trends

Big Data Analytics
Biomedical, Health Care and Assistive Technologies
Cloud Computing
Human-to-Machine Interfaces
Internet of Things
Intelligent Transport Systems
Smart Cities
Smart Grids
Smart Farm Technologies
Virtual/Augmented Reality
Wireless Sensor Networks

Energy and Environment

Environmental Informatics
Environmental Systems Management
Green Technology
Industrial Ecology
Life Cycle Assessment and Material Flow Analysis
Nanotechnology and Nanomaterials
Renewable and Non-renewable Energy Sources
Solid Waste Management
Sustainability Models

Engineering, Information, and Communications Technology

Bioinformatics and Bioengineering
Biomedical Engineering
Biometrics
Business Intelligence
Computer-Aided Network Design
Computing Architectures and Systems
Cyber/Internet Security
Data Analytics
Decision Support Systems
Digital/Analog Signal Processing
E-Commerce Application Fields
E-Learning and Mobile Learning Tools
Electronic Circuits and Systems Engineering
Electronic Waste
Gamification
Image and Video Processing
Information and Communications Technology
Mechatronics Engineering
Power and Energy
Robotics, Control, and Automation
Sensing and Sensor Networks
Virtual Learning Environments
Web Analytics

IMPORTANT DATES

JCIEA Vol.2 No.2, January 2018
September 15, 2017 - Deadline for Submission of Full Paper
October 30, 2017 - Notification of Acceptance
November 30, 2017 - Deadline for Submission of Final Paper

For inquiries and paper submissions, email us at **jciea@dlsu.edu.ph**
or visit at www.dlsu.edu.ph/offices/publishing-house/journals/jciea
www.jciea.com